2015

Thermal Energy Storage with Encapsulated Phase Change Materials for High Temperature Applications

Ying Zheng
Lehigh University

Follow this and additional works at: http://preserve.lehigh.edu/etd

Part of the Chemical Engineering Commons

Recommended Citation

Thermal Energy Storage with Encapsulated Phase Change Materials
for High Temperature Applications

by

Ying Zheng

Presented to the Graduation and Research Committee
of Lehigh University
in Candidacy for the Degree of
Doctor of Philosophy

in

Chemical Engineering

Lehigh University
January 2015

Copy Right

DISSERTATION SIGNATURE SHEET

       Approved and recommended for acceptance as a dissertation in fulfillment of the requirements for the degree of Doctor of Philosophy.

_____
Date

                                         _____
                                         Dissertation Director

_____
Accepted Date

                                         Committee Members:

                                         _____
                                         Mark A. Snyder, Ph.D., Committee Chair

                                         _____
                                         Kemal Tuzla, Ph.D., Advisor

                                         _____
                                         Sudhakar Neti, Ph.D., Committee Member

                                         _____
                                         Alparslan Oztekin, Ph.D., Committee Member

ACKNOWLEDGEMENT

I would like to express my sincere gratitude to my advisor Professor Kemal Tuzla for his continuous guidance and patience throughout the course of my Ph.D. study and research. I thank him for the professional knowledge that he taught me patiently all the way through my study, but also the skills of relationship management and communications, which make me really enjoy the study and life at Lehigh. I am also greatly thankful to my co-advisor Professor John C. Chen for his guidance on my Ph.D. research, and his great advice on how to present and interact with the industrial professionals. It is an honor for me to be a student of these two professors and obtain my doctoral training under them.

I would like to acknowledge my thanks to Prof. Sudhakar Neti, Prof. Alparslan Oztekin, and Prof. Wojciech Z. Misiolek for their valuable advice and guidance during this multidisciplinary project. We worked together and shared many ideas with my colleagues Weihuan Zhao and Joseph C. Sabol, who were always cooperative and helpful – I thank to both of them. It is a great pleasure to work in a cross-functional team to have diverse perspectives, refine understanding through discussions and explanations.

I would like to express my thanks to the other member of my committee Prof. Mark A. Snyder for his invaluable advice in my dissertation, and his great teaching in Transport Processes which turned out to be my favorite class at Lehigh. I would like to acknowledge the technicians John Caffrey, Paul N. Bader, William Maroun and Michael Rex, the undergraduate students John L. Barton, Matthew V. Bernstein - without their generous help

TABLE OF CONTENTS

LIST OF FIGURES

xii

xiii

LIST OF TABLES

ABSTRACT

The objective of this research is to develop a storage technology for thermal energy utilizing phase change material (PCM) for high-temperature concentrating solar plant (CSP) applications. The project involves:

- Development of an experimental measurement technique to select and characterize EPCM candidates;

- Design and testing of a thermal energy storage (TES) system with selected EPCM capsules to demonstrate the technical feasibility of the technology;

- Development of a computational model to analyze the dynamic heat transfer performance of TES systems, and compare it with experimental data to verify and improve the model for further applications.

From initial explorations of candidate media, the two salts $NaNO_3$ and eutectic $MgCl_2$-NaCl are selected as storage media with phase change. A specialized calorimeter with requisite size and temperature capability is designed and built to obtain enthalpy values of the phase change materials (PCMs) at temperatures below and above their melting points. The calorimeter tests prove that the salts and the encapsulation methods chosen here can store thermal energy effectively while taking advantage of the latent heat of phase change. Repeated thermal-cycles show sustained performance of the EPCM, with no discernible

diminishment in storage capacity.

Stainless steel capsules containing the PCMs are fabricated then and installed in a pilot-scale TES system for performance tests. The test section is first tested using solid copper capsules in place of the EPCM capsules. The results of the testing verify that the current instrumentation is capable of measuring the energy stored or extracted from the EPCM capsules with an error of +/- 5%. The test section is then loaded with EPCM capsules and subjected to thermal cycles with phase change in each cycle. The test section with EPCM capsules successfully demonstrate its ability to transfer thermal energy to and from a transport fluid, achieving energy storage and retrieval in multiple charging and discharging cycles.

Meanwhile a simulation model is developed for the thermal energy storage system and its predictions are found to agree with experimental measurements within +/- 8% in stored energy. The dynamic performance of charging and discharging rates are also well predicted by the simulation model, giving confidence to engineering design capabilities in future applications using encapsulated phase change materials for energy storage.

1 INTRODUCTION

1.1 Phase Change Materials

Phase change material is a name for a substance when it is capable of transformation from a phase or a state (i.e., solid, liquid, gas) to another phase (i.e., solid, liquid, gas) at a specific temperature and pressure. Phase change is common in nature, and used to describe the transitions between solid, liquid and gaseous states as shown in Table 1-1.

Table 1-1. Phase change between solid, liquid and gaseous states [1].

From \ To		Solid	Liquid	Gas
	Solid	solid-solid transformation	melting	sublimation
From	Liquid	solidification	—	evaporation
	Gas	desublimation	condensation	—

A phase of a thermodynamic system has uniform physical properties. During a phase change, the bonding energy between the particles changes, and as a result, certain properties of the materials change. Latent heat is defined as the enthalpy change (usually noted as ΔH) of a thermodynamic system when it changes from one phase to another. For example, when ice (solid) melts to water (liquid) at 0 °C, 1 atm, the enthalpy change is 334 kJ per unit mass of the ice [2], which is also known as the heat of fusion. Because of the

significant enthalpy changes during the phase transitions, phase change materials are commonly used in many technologies in regard to their thermal energy, in which the thermal energy is stored and retracted at a targeted temperature by phase change of storage media, called as latent energy storage.

1.1.1 Desired Properties of Phase Change Materials

Technically speaking, any substance can be used as phase change materials in thermal energy storage applications, since it can go through the phase transitions as long as the external conditions are satisfied. However, for employment as latent heat storage medium, the material must possess certain desirable thermodynamic, kinetic and chemical properties for specific applications; moreover, economic consideration and its availability are quite important factors when transferring the technology to the markets. The various criteria that govern the selection of phase change materials are summarized [3-8] and explored as follows:

- Thermal properties.

Desired thermal Properties of the PCM includes: (i) suitable phase change temperature; (ii) high latent heat of transition; (iii) suitable thermal conductivity. For a specific application, the phase change temperature of PCM should be in the targeted operating temperature range for the thermal energy storage system. For example, in the solar power plant applications, many researchers have been focusing on the phase change materials with high melting temperatures, especially in the range of 300 °C – 900 °C considering the

advantages in turbine efficiency in the downstream for power generation [9-13]. Besides the suitable phase change temperature, the latent heat of fusion is another important factor in selecting the phase change materials. Latent heat is the amount of energy that the PCM can store or retrieve per unit mass or volume of material during its phase change. Especially the value on a volumetric basis, it directly determines the size of containments for the PCM. It is desirable for the chosen PCM to possess high latent heat since the higher storage capacity of the PCM, the smaller containment is required, which thus could reduce the capital cost of storage facilities and mass of the materials. While the storage capacity of the PCM determines the total amount of energy storage, the power of energy storage, or the rate of energy storage is another essential factor for the TES system considering it defines how fast the energy can be charged or discharged. The rate of energy storage is determined by the heat transfer performance between the heat transport fluid (HTF) and the PCM, and the conduction in the PCM. The former is mostly the convective heat transfer which is determined by the properties of the HTF, surface geometries of PCM and temperature difference between the HTF and the surface of PCM. The latter one is mostly determined by the thermal conductivity coefficient of the PCM and potentially some convection within the liquid PCM. The higher thermal conductivity coefficient of the PCM, the faster the heat could transfer to overall PCM and reach thermal equilibrium. Since the power of the TES will greatly depend on the specific applications with different time basis (seasons, hours, or seconds), the PCM should be carefully screened in regards to its thermal conduction and heat transfer performance of the overall TES system.

- Physical properties.

Desired physical properties of PCM includes: (i) high density; (ii) small volume change; (iii) low vapor pressure. As discussed previously in the section of thermal properties, it is favorable to have a high storage capacity of PCM especially on a volumetric basis. Thus higher density of the PCM is desirable since in one hand it reduces the mass of the PCM required, and in the other hand, it allows a smaller size of the storage container. Both of them could reduce the cost of the TES system. When packing the PCM in the storage system, or encapsulating the PCM in single capsules [13], the volume change of the PCM has drawn a lot of attentions because of the significant thermal expansion during the phase transitions [14,15] which could risk the explosion of the capsules or containments. It is favorable for the PCM to have a small volume change and low vapor pressure at operating temperatures, which could reduce the risk for breaking the containments.

- Kinetic properties.

Desired kinetic properties of the PCM include: (i) no supercooling; (ii) sufficient crystallization rate. Supercooling, also known as undercooling, is the process of lowering the temperature of a liquid or a gas below its freezing point without it becoming a solid. When PCM suffers supercooling, there is no expected latent heat because no phase transition happens, which will significantly interfere with proper heat extraction from the storage system. Supercooling has been a troublesome aspect in PCM development, especially for salt hydrates [3,4,7,8] which will be introduced in details later.

- Chemical properties.

Desired chemical properties of the PCM include: (i) long-term chemical stability; (ii) compatibility with materials of construction; (iii) no toxicity; (iv) no fire hazard. As reported by IRENA in the technology brief of thermal energy storage [16], the typical current international values for the economic lifetime is 20 years for the storage in phase change. The chemical stability of PCM is essential in terms of the stable chemical composition and sustained physical chemical properties for the reliable storage performance of overall TES system. PCM, especially for the salt hydrates, it can suffer from degradation of loss of water, which will significantly affect its storage capacity and phase change temperature. Compatibility with materials of construction is another important issue which needs significant attentions when packing the PCM in either a large containment or in single capsules. The interaction between the PCM and construction material is due to material diffusion or chemical reactions, and eventually changes the chemical and thermal properties of PCMs, and affects the overall storage performance of the TES system. Another issue which always needs the most considerations is the safety. PCM should be non-toxic, non-flammable and non-explosive for safety in applications.

- Economics.

The storage of thermal energy, typically from renewable energy sources, is the heat or surplus energy product, which can replace heat from fossil fuels, reduce CO_2 emissions and lower the need for costly peak power and production capacity. The cost of TES system

7

will determine the viability of the technology in markets. The investment required for a TES system includes material cost (\$/kWhth), manufacturing cost (\$/kWhth), the cost of the tank and associated control facilities (\$/kWhth). It has been reported that the material could cost about 42% of the overall investment (~ \$26/kWhth) [17]. Therefore it is important for the PCM to be low-cost and have availability in large quantities.

1.1.2 Classification of Phase Change Materials

As discussed in Table 1-1, seven phase transitions exist for a substance changing from one phase to another when external conditions are satisfied (i.e., temperature and pressure). In the applications of the latent heat, more attention has been paid for the solid-liquid and solid-solid transitions [3-5] considering the associated small volume change. Typical phase change materials well-known to all of us are ice, paraffin and Glauber Salt $(Na_2SO_4 \cdot 10H_2O)$[4]. For a liquid-gas, or a solid-gas phase transition, although the latent heat associated with the phase change is on the same magnitude, or even higher than the cases in solid-solid and solid-liquid transitions, the practical problems of storing a gaseous phase with abrupt volume change and the requirements of pressurized containers rule out their potential utility.

In 1983 Abhat reviewed the phase change materials for low temperature latent heat storage in the temperature range 0 °C - 120 °C[4] and classified the PCMs by chemical properties as shown in Table 1-2, in which the heat storage materials are classified as organic and

inorganic substances. Organic and inorganic heat storage materials that have been considered include paraffins, fatty acids, inorganic salt hydrates and eutectic compounds. This classification has been widely used in many recent publications for phase change materials [5,7,18] for a larger temperature ranges, including elevated temperatures to ~ 800 °C. The important heat storage material groups are examined in details below.

Table 1-2. Classification of the phase change materials for thermal energy storage[4].

-
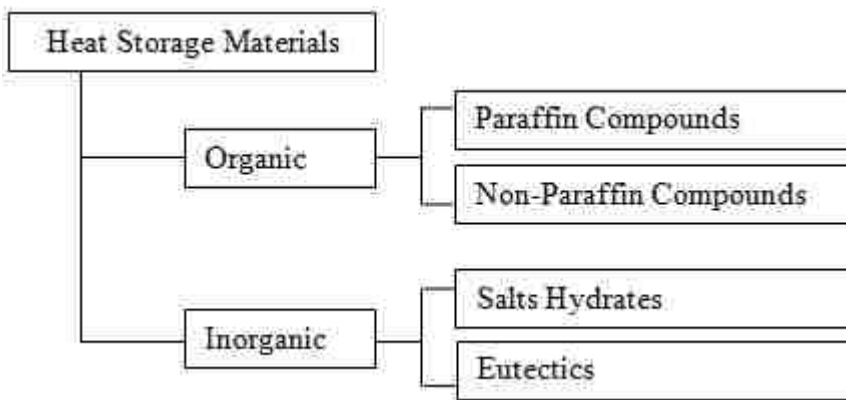
- Paraffins.

As we normally understand, paraffins are substances having a waxy consistency at room temperature. Chemically speaking, they are a white or colorless soft solid derived from petroleum that consists of a mixture of straight-chain hydrocarbon molecules with only a small amount of branching [19]. Paraffins contain in them one major component, called

9

alkanes, of which the general formula is C_nH_{2n+2}. The n-alkane content in paraffin waxes usually exceeds 75% and may reach 100% [20]. Pure paraffins contain only alkanes in them, such as the paraffin octadecane $C_{18}H_{18}$. The phase change temperatures of the alkanes increase with the increasing number of carbon atoms in them as indicated in Table 1-1. Generally, alkanes containing 14 - 40 atoms possess melting points between 6 °C − 80 °C as shown in Table 1-3. And the commercial waxes may have a range of 8 − 15 carbon atoms [20].

Table 1-3. Melting point and latent heat for paraffins with different number of carbon

atoms.

No. of Carbon Atoms	Melting Point (°C)	Latent Heat (kJ/kg)
14	5.5	228
15	10	205
16	16.7	237.1
17	21.7	213
18	28	244
19	32	222
20	36.7	246
21	40.2	200
22	44	249
23	47.5	232
24	50.6	255
25	49.4	238
26	56.3	256
27	58.8	236
28	61.6	253
29	63.4	240
30	65.4	251
31	68	242
32	69.5	170
33	73.9	268
34	75.9	269

Paraffins qualify as heat storage media due to their large availability, fairly high latent heat

(~ 200 kJ/kg, or ~ 250 kJ/dm^3), and solidification without supercooling [4] However, only

technical grade paraffins may be used as storage media in the thermal energy storage

applications, which brought an attention to the cost of materials [4,21,22]. Physical properties

for some paraffins are tabulated in Table 1-4.

Table 1-4. Physical properties of some paraffins

Materials	Melting Point (°C)	Latent Heat (kJ/kg)
paraffin 5913	22-24	189
Octadecane	28	244
paraffin 6106	42-44	189
paraffin P116	45-48	210
paraffin 5838	48-50	189
paraffin 6035	58-60	189
paraffin 6403	62-64	189
paraffin 6499	66-68	189

- Non-paraffins.

The non-paraffin organics are the most numerous of phase change materials with highly varied properties. Unlike paraffins possessing very similar properties, each of these materials will have its own properties as shown in Table 1-5 . Abhat [4,21] and Buddhi et.al. [23] have conducted extensive surveys of organic materials and indentified a number of esters, fatty acids, alcohol's and glycol's promising for latent heat storage. The non-paraffins are further classified as fatty acids and other non-paraffin organics considering the fatty acids have fairly high heat of fusion as tabulated in Table 1-6. As for safety these non-paraffin organics require more attention because these materials are flammable and should not be exposed to excessive high temperatures, flames or oxidizing agents.

Fatty acids are organic compounds characterized as $CH_3(CH_2)_{2n}COOH$ with latent heat values comparable to those of paraffins. They are known to have a sustained melting and freezing behavior with no or minor supercooling [4,24-26], therefore they qualify as good phase

12

change materials. Their major drawback is their cost, which is twice higher than that of

paraffins[21].

Table 1-5. Melting points and latent heat of non-paraffin substances.

Materials	Melting Point (°C)	Latent Heat (kJ/kg)
Formic acid	7.8	247
Glycerin	17.9	198.7
Caprylone	40	259
Phenol	41	120
Methyl eicosanate	45	230
O-Nitroaniline	50	93
Heptaudecanoic acid	60.6	189
Phenylacetic acid	76.7	102
Thiosinamine	77	140
Methyl brombrenzoate	81	126
Alpha napthol	96	163
Glautaric acid	97.5	156
Quinone	115	171
Stibene	124	167

Table 1-6. Melting point and latent heat of fatty acids.

Materials	Melting Point (°C)	Latent Heat (kJ/kg)
Caprilic acid	16.5	149
Capric acid	31.5	153
Lauric acid	42-44	178
Myristic acid	54	187
Palmitic acid	63	187
Stearic acid	70	203
Acetic acid	16.7	184
Polyethylene glycol 600	20-25	146
Pentadecanoic acid	52.5	178
Tristearin	56	191
Acetamide	81	241
Methyl fumarate	102	242

- Salt – hydrates.

Salt hydrates, characterized as $M \cdot nH_2O$, where M is an inorganic compound, are an important class of heat storage materials due to their high volumetric storage capacity (~ 350 kJ/dm^3). In fact, their use as PCMs could be dated back to as early as 1947 [27]. The major problems in using salt hydrates as PCMs are incongruent melting and significant supercooling. Most of the salts hydrates melt incongruently, that is, they melt to a saturated aqueous phase and a solid phase which is generally a lower hydrate of the original salts. Due to the density difference, the solid phase settles down and collects at the bottom of the container, a phenomenon also called decomposition. Unless additional processing conditions are taken, this phenomenon is irreversible. Then during the solidification process, the solid phase will not combine with the saturated solution to form the original salt hydrate, and the overall properties of the material changes with the heating and freezing cycles. Another important issue with salt hydrates is their poor nucleating properties resulting in supercooling of the liquid salt hydrate prior to solidification. Typical techniques, which are suggested in the literature to reduce the supercooling, are (1). addition of nucleating agent that possesses a similar crystal structure to that of the parent substance [28]; (2). using a "cold finger" in the PCM [22]; (3). promoting heterogeneous nucleation through contacting metallic heat exchanger surface[21]. The effects and influence of these techniques should be examined for various melting and freezing characteristics of salt hydrates.

- Eutectic.

An eutectic is a minimum-melting composition of two or more components, each of which melts and freeze congruently forming a mixture of the component crystals during crystallization[29]. Eutectics of organic or inorganic compounds raise a lot of attention as phase change material in thermal energy storage, since they possess a fixed melting/solidification point, and acceptable values for the heat of fusion [4,5,30].

- Metallics.

In the class of inorganic heat storage materials, it is worthy to mention the metallics group. This category includes metals and metal eutectics. They are likely to be heat storage candidates because of their high heat of fusion (~ 500 kJ/kg) [7,11,31] in a wide temperature range from 28°C up to 950 °C. They also offer a good thermal conductivity for heat transfer, and high density which contributes to a large storage capacity on a volume basis. However, these metallics have not yet been seriously considered for PCM technology because of weight penalties.

1.2   Storage of Thermal Energy

Thermal energy storage is a technology that store thermal energy by heating a storage medium so that the stored energy can be used at a later time for various heating applications and power generation, in which the TES system can help balance energy demand and

supply on a daily, weekly and even seasonal basis. It can also reduce peak demand, CO_2 emissions and energy consumption while increasing overall efficiency of the energy system. It has been very popular for the conversion and storage of variable renewable energy, such as solar energy, in the form of thermal energy, which has greatly increased the share of the renewable energy in the energy markets. The TES has became particularly important to be integrated in concentrating solar power plants where the solar heat can be stored when the solar energy is most available during the daytime, and retrieved to continuously produce electricity after the sunset when the sunlight is not available.

1.2.1   Key Properties of Thermal Energy Storage System

The storage technology for thermal energy can be classified by its mechanism as (i).sensible heat storage by sensible heating or cooling a liquid or solid storage medium such as water, sand, molten salts, rocks, etc.; (ii). latent heat storage utilizing the latent heat of the phase change material at its transition temperature; (iii). thermo-chemical storage using endothermal and exothermal chemical reaction to store and release thermal energy.

Thermo-chemical energy storage is utilizing the endothermic chemical reaction to store the heat while extracting the heat through reversible exothermic process. The common advantages of this mechanism is its high storage capacity in a magnitude of ~ 4 GJ/m^3 and high operation reaction temperature (~ 500 - 2000 °C), which offers relatively low costs for energy storage through thermo-chemical conversion paths and considerate efficiency

for power generation. The chemical storage materials have been investigated including ammonia, metal oxide/metal (SnO_x/Sn) and calcium carbonate. The critical issue of chemical system is the kinetic behavior of the reactions, and the development of the technology is at a very early stage [32].

Sensible heat storage, associated with temperature increase of the storage medium, is the most common approach for thermal energy storage and the only storage technology used in commercialized solar electric generating plants up to now. Materials that have been used for sensible heat storage include water, rocks, graphite, oil based fluids, and some salts with low melting points [32]. However, large-scale storage (~ 500 MWth) will require a volume in the order of 2×10^5 m^3, too large for cost-competitive containment and heat transfer. An improvement over sensible heat storage can be obtained by utilizing latent heat of phase change. With a judicious choice of melting temperature, this will achieve a greater increase in enthalpy per unit mass of storage material with the same temperature swing.

For a given application, the thermal energy storage system is designed to accumulate energy when production exceeds demand and to make it available at the users' request. The key properties of the thermal energy storage system are described below[16].

- Capacity: the capacity defines the total energy that can be stored in the system, which depends on properties of the medium, the size of the system and operating conditions.

- Power: the power defines how fast the energy can be stored into the system and can be extracted from the system when the energy is needed.

- Efficiency: the efficiency is the ratio of the energy provided to the user to the total energy needed to charge the storage system. It accounts for the efficiency of the transformation between the different forms of the energy as well as the energy loss during the storage period and charging/discharging period.

- Storage period: it defines the time period for the energy storage, i.e., hours, days, weeks, and months for yearly storage.

- Charge and discharge time: it defines how much time is needed to charge the system for energy storage and how long the energy can be extracted from system in discharging process. It is closely related with the thermal properties of the storage medium and heat transfer fluid, as well as the operating conditions of the TES system.

- Cost: the cost usually refers to the capacity in $/kWh of the storage system, which includes the capital cost, operation and maintenance cost over its lifetime.

As introduced previously, thermal energy can be stored as sensible heat in heat storage media, as latent heat using phase change materials or as thermo-chemical energy associated with chemical reactions. The general values of the key properties for each of the storage

technology are summarized in Table 1-7.

Table 1-7. The values of the key properties for the thermal energy storage technology.

Key Properties	Storage Technology		
	Sensible Heat Storage	Latent Heat Storage	Thermo-chemical Storage
Capacity (kWh/tonne)	10 -50	50 - 150	120 - 250
Power (MW)	0.001 - 10	0.001 - 1	0.01 - 1
Efficiency (%)	50 - 90	75 - 90	75 - 100
Storage Period (h, d, m)	d, m	h, d, m	h, d
Cost ($/kWh)	0.2 – 20	20 – 100	15 - 180

1.2.2   Thermal Energy Storage with EPCM

Renewable energy is of considerable current interest due to increasing demands on the world's supply of fossil fuels, and world-wide attention on global warming associated with the increasing amount of CO_2 in our atmosphere, as noted by latest declarations from the Intergovernmental Panel on Climate Change [33]. To date, renewable sources have only been minor contributors to the worlds energy supply. In 2011, approximately 13% of the total electricity generation in U.S. is derived from renewable energy sources, with solar energy accounting for ~1% [34].

One disadvantage of most renewable sources, including solar energy, is their intermittent and variable nature as governed by locations and weather conditions. Even in locations with favorable solar incidence, the diurnal cycle provides only about 3,000 hours of significant irradiance in a year. Consequently, current solar power plants have average

capacity factors of barely 20%, in comparison to capacity factors of 85% for conventional

coal plants and 90% for advanced nuclear power plants [35]. One way to improve the capacity

factor of solar plants is to integrate a thermal energy storage system in the power plants.

Such systems enable the storage of energy when the solar incidence is strong, and then

release that energy for power generation during cloudy or nocturnal periods of low or no

solar incidence. It has been reported that the use of storage systems can double the capacity

factor of the solar thermal/electric power plants to ~40% or greater [18].

Of the CSP storage methods, molten-salt storage is the only storage currently used in

commercial concentrating solar plants [36], where the energy is stored by sensible heating of

molten salt and the molten salt is stored and circuits between a cold tank and a hot tank. In

daytime with excess sunshine, the molten salt is pumped to a heat exchanger to capture the

energy from a heat transfer fluid, such as oil, and store the energy in the hot tank. Then

when the energy is needed, the molten salt is pumped from the hot tank to relieve the energy

to the HTF, and then circuit back to the cold tank. A one-tank TES system with hot fluid

at the top and cold fluid at the bottom of the tank, is developed by Sandia National

Laboratories, using quartzite rock and silica sand as the storage medium [9]. Such one-tank

TES system using sensible heating of the storage medium is predicted to reduce the

investment of the storage system by ~ 32% compared to the two-tank system [36]. However,

large solar plants will need TES components of 500 MWh thermal, or greater, requiring

large volumes of storage medium, of the order ~ $5 \times 10^5 \, \text{m}^3$. Latent heat storage, utilizing

latent heat of phase change to complement sensible heat storage, can achieve significantly

higher storage densities [16], thus reducing the required volume of storage medium and its containment vessel. This promises to significant reduction in the capital cost of TES, and the total cost of solar electric generating plants.

A few research and development efforts have pioneered the use of latent heat storage technology at temperatures suitable for CSPs. Several reports has been focused on a shell-and-tube system, with the phase change materials, such as KNO_3, placed in a large container and a heat transfer fluid flowing in the embedded tubes in the PCM [18,37,38]. A difficulty of such shell-and-tube system is its slow charging and discharging rates, which are due to the low thermal conductivity of most PCMs and the limited heat transfer area of the immersed tubes. This is of special concern during the heat extraction (discharging) phase when liquid PCM will form a frozen layer on the heat transfer surfaces, hampering further energy transfer between PCM and the heat transfer fluid (HTF).

To address this issue, the approach investigated in the current development is to reduce the dimensional scale of the PCM by containing measured amounts of the PCM in individual capsules, of which the approach has been proposed in early 1988 by Luz International [39]. By placing limited amounts of the PCM in individual capsules, one minimizes the dimensional scale for conduction within the PCM, and simultaneously increases the total contact area of the capsules for convective heat transfer with the HTF. With appropriate selection of the capsules' dimensions, the physical scale for heat transfer can be optimized to reduce conduction resistance within the PCM and to enhance external convective heat

transfer between the capsules and the HTF. The ideal dimensions for the capsules can be optimized for various PCMs and HTFs with different thermal properties. In plant applications, this beneficial improvement of heat transfer will be balanced against fabrication cost of encapsulation. Initial cost estimates indicated that these types of EPCM based TES system can be implemented with a less expensive investment than currently used two-tank system for storage of thermal energy [17].

1.3   Objective of this Research

The objective of this research is to develop a storage technology for thermal energy using encapsulated phase change materials (EPCM) for high temperature applications in concentrating solar power plants. Several issues need to be resolved for the proposed use of encapsulated PCMs for thermal energy storage:

- Selection of PCMs for operating temperatures up to 550 °C.

- Characterization of the encapsulated PCM, and evaluation of its storage performance in long-term melting/freezing cycles.

- Design and test of a pilot-scale thermal energy storage system with EPCMs.

- Development of a simulation model for the EPCM based TES system.

The research in this project covers experimental development of encapsulated phase

23

change materials, suitable for high temperature applications in the range of 300 °C – 550 °C. Calorimetry is utilized to characterize the proposed ECPMs, with attention on energy storage capacity and sustained storage performance over multiple thermal cycles and after long-term exposure to high temperatures. $MgCl_2$-NaCl eutectic and $NaNO_3$ are found to be two candidates for thermal energy storage at high temperatures with phase changes at 444 °C [30]and 308°C [40] respectively. To demonstrate the storage technology, a pilot-scale TES system is actually designed, operated and tested with encapsulated phase change materials. To verify that such a system can be successfully engineered, a computational model of the test TES system also has been developed and its predictions are compared to actual performance measurements.

2 CHARACTERIZATIONS OF EPCM BY CALORIMETRY

2.1 Encapsulated Phase Change Materials

After consideration of many candidates, two salts are selected for investigation as phase change materials: sodium nitrate ($NaNO_3$) and eutectic of magnesium chloride and sodium chloride ($MgCl_2$-$NaCl$, 57% mole fraction for $NaCl$). These are chosen as PCM candidates for CSP applications because of their desirable melting points, 308 °C and 450 °C, respectively.

After experimenting with various encapsulating materials and capsule geometries [41], a decision is made to use cylindrical steel shells to encapsulate the PCM. Thermal cycling tests have found that carbon steel 1018 and stainless steel 304 withstood thermal cycling with the two selected PCMs, without significant deterioration. As anticipated from published reports [42-44], no corrosion has been detected in the $NaNO_3$ capsules. Literature reports regarding $MgCl_2$-$NaCl$ imply that corrosion of stainless and carbon steels could be a problem [45]. While no deterioration in performance is observed in the tests described below, longer corrosion test for $MgCl_2$-$NaCl$ should be considered.

From analyses using finite-element models, the cylindrical geometry has been found to have both adequate containment strength and good transient heat transfer characteristics for anticipated CSP operating conditions [41,46]. To obtain reasonable response times for

internal heat transfer during thermal charging or discharging, a simulation model has been developed for a single cylindrical encapsulated phase change materials as indicated in eqn. 2-1 and eqn. 2-2 shown below. The temperature in the PCM depends on the radial location and time only. With the thermal properties of $NaNO_3$ [40], the time needed to heat up the $NaNO_3$ from 250 °C to 350 °C is calculated for a $NaNO_3$ capsule with a 400 °C Therminol VP-1 as heat transfer fluid. Sensible heat as well as phase change are considered in this case, assuming only radial conduction in the PCM and a convective heat transfer coefficient on the outside surface of the EPCM is calculated using Zhukauskas's correlation[47]. The heat transfer time has been calculated for the $NaNO_3$ capsules with different diameters and the results are shown in Figure 2-1. For a storage time of 8 hrs, it has been determined that the characteristic dimension of the capsules should be less than 20 cm. In the encapsulation procedure, the steel capsules are filled with measured amounts of either $NaNO_3$ or $MgCl_2$-NaCl, and sealed by welded end caps. Sufficient void volume, typically in range of 25-30 % [48,49], is left in each capsule to accommodate volume change of the PCM with phase change.

$$\rho_{PCM} C_{p,PCM} \frac{\partial T_{PCM}}{\partial t} = k_{PCM} \frac{1}{r_{PCM}} \frac{\partial}{\partial r_{PCM}} \left(r_{PCM} \frac{\partial T_{PCM}}{\partial r_{PCM}} \right)$$

eqn. 2-1

$$\left(k_{PCM} \frac{\partial T_{PCM}}{\partial r_{PCM}} \right)_{r_{pcm}=R} = \left[h_s A_s (T_f - T_s) \right]_{r_{pcm}=R}$$

eqn. 2-2
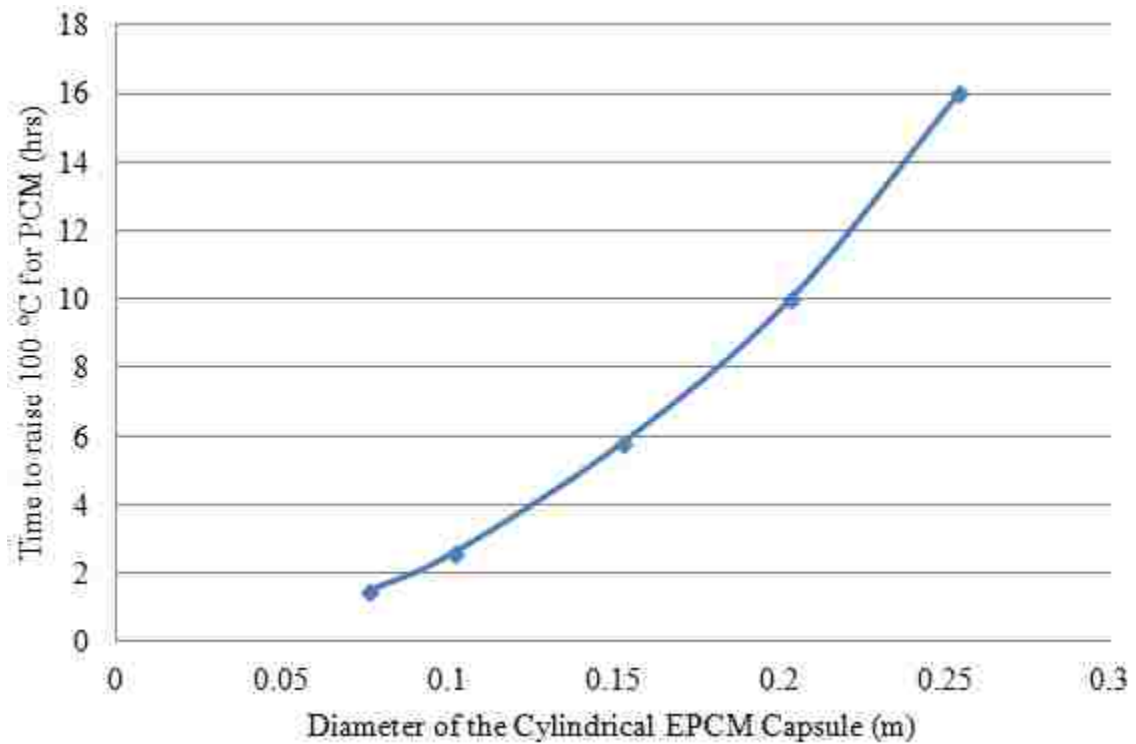
Figure 2-1. The heat transfer time for the encapsulated NaNO$_3$ with 100 °C temperature increase and phase change in various size of the capsules.

Figure 2-2 shows a cut-away photograph of a capsule, after multiple thermal cycles through the melting/freezing sequence. In this photograph, the light colored regions are the PCM, dark regions are voids, and grey boundaries are the capsule walls. It is seen that the capsule maintains integrity and original geometry after multiple thermal cycles of melting and freezing.
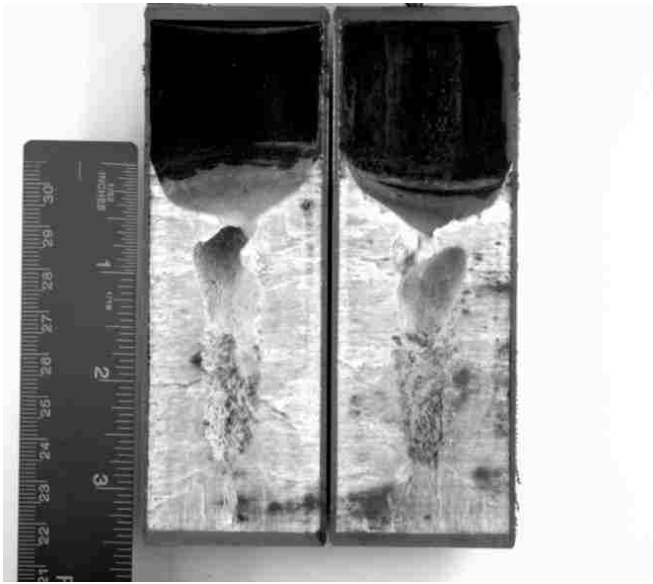
Figure 2-2. Cut-away photo of EPCM (MgCl$_2$-NaCl eutectic) after thermal cycling.

For use as storage media, specific enthalpies of EPCM capsules are required over the temperature ranges of interest, for both solid and liquid phases. To determine their enthalpies, calorimetric measurements with encapsulated bulk PCMs are desired. Unfortunately, no commercially available calorimeter is found to be suitable, due to the elevated temperature ranges and dimensional scale required in this investigation. A special drop calorimeter is developed and built for our purpose. The design described by Southard, J.C. [50], and Yamaguchi, K. and Itagaki, K. [51], is revised to use silicon oil as the immersion fluid, and the dimensions are optimized for accurate temperature measurements during drop experiments. Selection of the silicone oil is especially important since it has to accommodate samples at temperatures up to 550 °C, without undesirable bubbling or vaporization. The dimensions of the calorimeter are optimized to be small enough for sufficient temperature change during the drop experiments (for measurement accuracy),

28

and large enough to avoid large temperature changes during heat loss measurements. Details are described below.

2.2   Calorimeter Design, Operation and Calibration

The key component of the calorimeter is an insulated vessel containing a measured amount of silicone fluid. The silicone oil selected (Dynalene 600) has a high flash point (315 °C), fairly good thermal conductivity, and low vapor pressure – thus avoiding bubble nucleation and evaporation when contacted by hot samples of EPCM. To handle the sizes of our samples, some 4.5kg of the silicone oil is required. This amount of silicon oil and the corresponding dimensions of the calorimeter are selected to optimize accuracy of temperature measurements. A larger mass of silicone oil will reduce temperature rise of the calorimeter during the sample-drop phase, while a smaller mass will increase the effect of heat loss to ambient air - either of which will reduce accuracy of the calorimeter measurements just as shown in Figure 2-3. In this research, the temperature increase of the calorimeter is chosen to be higher than 5 °C considering that the temperature measurement errors is ~ 0.1 °C by thermistor. With a desirable small ratio of the heat losses to the total energy increase of the calorimeter, the mass of the silicon oil in the calorimeter is chosen to be ~ 5 kilograms. The vessel is constructed with thin stainless steel sides and bottom, insulated with an externally layer of polymer foam. Thermal isolation of the vessel from laboratory environment is further improved by placing the vessel within a concentric, guard cylinder, as illustrated in Figure 2-4. A mechanical stirrer is mounted in the vessel to

29

achieve uniform temperature in the silicone fluid. A wire rig is used to suspend the test sample of EPCM in the silicone oil during tests. Thermistors are submerged in the silicone fluid within the vessel, and between the vessel and external guard cylinders to accurately monitor temperatures during the tests. All measurements are recorded by a computerized data acquisition system.
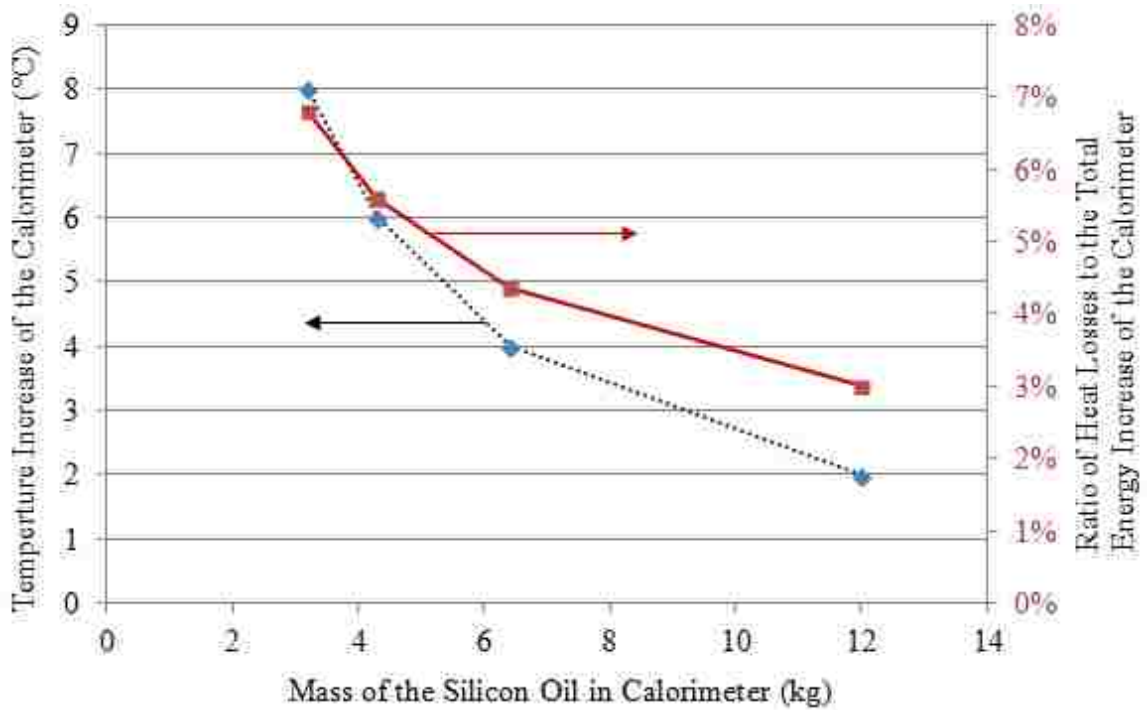
Figure 2-3. Optimization of the mass of the silicon oil in the calorimeter.
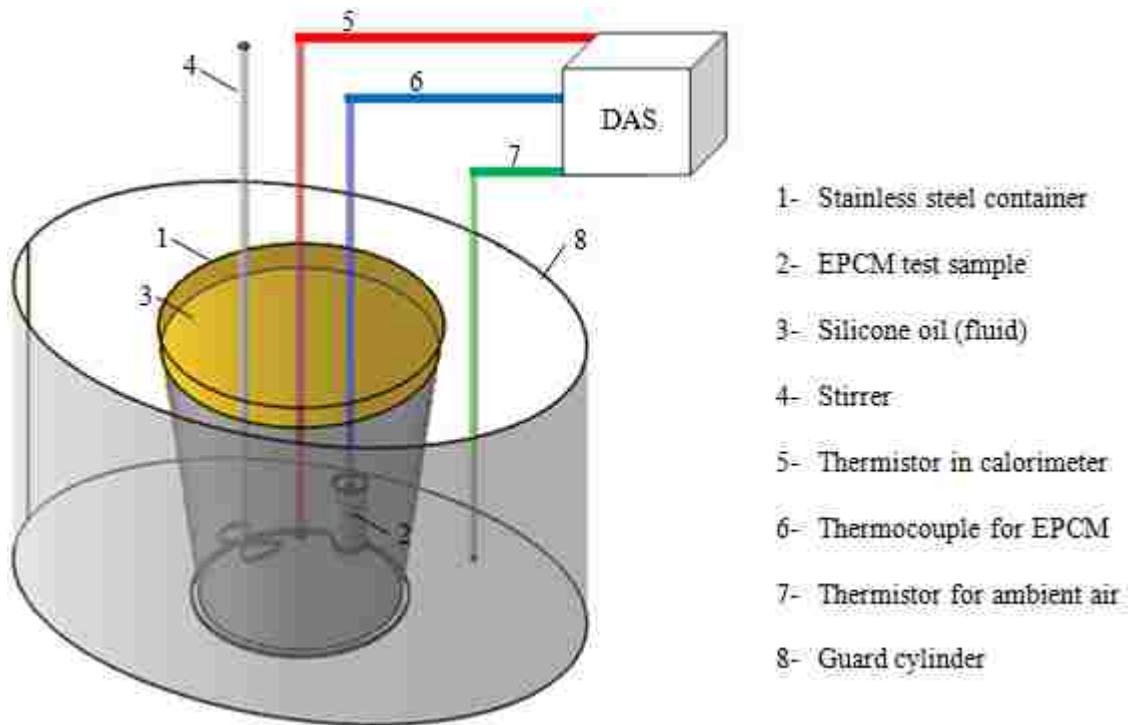
Figure 2-4. Schematic drawing of calorimeter.

In each experiment, the test sample of encapsulated phase change material is thermally charged by heating to a selected high temperature (in range of 250 - 500 °C) in an external furnace. To achieve a uniform temperature throughout the sample, it is enclosed in insulation material and the entire assembly kept in an isothermal zone of the furnace till steady state is obtained. Three thermocouples placed around the circumference of the sample to measure its temperatures, and an average reading is taken to represent the temperature of sample. Meanwhile, the calorimeter (vessel, stirrer, silicone oil fluid, and guard cylinder) will be maintained at the laboratory temperature. When steady states are achieved for both the calorimeter and test sample, the sample will be thermally discharged by rapid submersion into the fluid in the calorimeter. Temperature of the fluid is recorded

as heat transfer occur between the sample and the calorimeter, providing the data needed to determine enthalpy change of the sample as it discharges its stored thermal energy into the calorimeter.
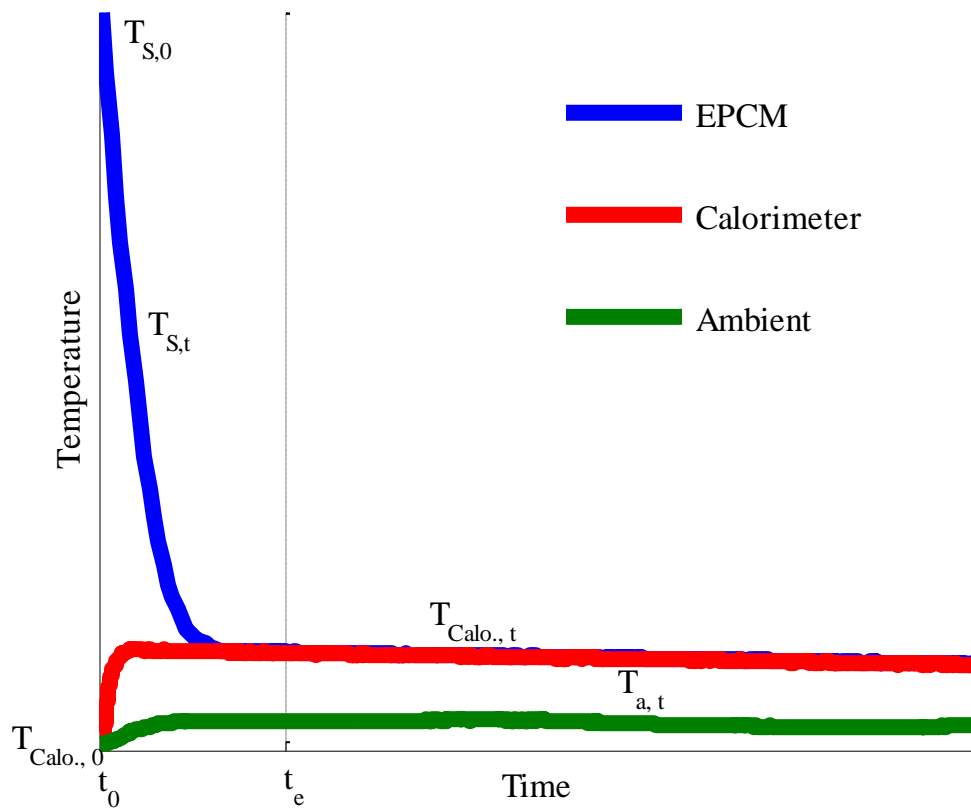
Figure 2-5. Example of temperature transients in calorimetric experiments.

Figure 2-5 shows a typical record of the transient energy transfer process between the sample and the calorimeter, where

$T_{S,t}$ = sample temperature

$T_{Calo.,t}$ = temperature of the oil-filled calorimeter

$T_{a,t}$ = outside air temperature between vessel and guard cylinder

At time t_0, the preheated sample is immersed into the silicone fluid and start to cool, transferring its thermal energy to the fluid and calorimeter vessel. As the sample temperature ($T_{S,t}$) decrease, the calorimeter temperature ($T_{Calo.,t}$) rise, until the two temperatures equilibrate at time t_e. This time-to-equilibration (t_e) vary significantly with thermal diffusivity of the PCM and capsule size. For each capsule sample, the magnitude of t_e is obtained by numerical analysis of the transient heat transfer process within the capsule, including effect of phase-change as discussed previously for optimization of the capsule sizes for heat transfer in eqn. 2-1 and eqn. 2-2. In the experiments, care is taken to obtain data at times greater than t_e to avoid errors from non-equilibration. At times greater than t_e, the combined temperature of sample and fluid decline slowly – corresponding to net energy loss from the calorimeter to its surroundings. Such a record of calorimeter temperatures provides the requisite information for an energy balance on the calorimeter. It is then possible to determine the thermal energy stored in the sample (Q_{EPCM}) at preheat temperature $T_{S,0}$. The following equations represent the energy change for various quantities from initial states (at time of sample immersion) to any time t.

$$Q_{EPCM} = Q_{Calo.} - Q_{Loss}$$

$$Q_{Calo.} = m_{Calo.}C_{p,Calo.}(T_{Calo.,t} - T_{Calo.,0})$$

$$\dot{Q}_{net} = \left[\sum_{Calo.+EPCM} mC_p \frac{dT}{dt}\right]_{after\ t_e} = UA\big(T_{a,t} - T_{Calo.,t}\big) + \dot{Q}_{mixer}$$

eqn. 2-5

$$Q_{Loss} = \int_{t_0}^{t} \dot{Q}_{net}dt = \int_{t_0}^{t}\big[UA\big(T_{a,t} - T_{Calo.,t}\big) + \dot{Q}_{mixer}\big]dt$$

eqn. 2-6

$$Q_{PCM} = Q_{EPCM} - Q_{Capsule}$$

eqn. 2-7

$$Q_{Capsule} = m_{Capsule}\int_{T_{S,t}}^{T_{S,0}} C_{p,Capsule}dT$$

eqn. 2-8

To use eqn. 2-3 to eqn. 2-8, it is necessary to know values for the heat loss to surroundings, Q_{Loss}, and the effective heat capacity of the calorimeter (including vessel, silicone oil fluid, etc.), $Cp_{Calo.}$.

Calibration for the heat capacity of the calorimeter (including vessel, silicone oil, etc.) is accomplished by using standard capsule samples of known properties. Two such samples are fabricated using solid stainless steel 304, with different masses and dimensions, as listed in Table 2-1. The thermal properties of stainless steel 304 are listed in Table 2-2. Since the heat capacity of the calorimeter varied with temperature, integration over the applicable temperature range is needed in order to obtain the thermal energy stored in a stainless steel sample.

34

Table 2-1. Standard capsule samples

	Material of Sample	Mass of Sample (g)	Size
Stainless Steel Sample A	Stainless Steel 304	834.3	38.1 mm Diameter × 101.6 mm Height
Stainless Steel Sample B	Stainless Steel 304	185.1	25.3 mm Diameter × 46.4 mm Height

Table 2-2. Thermal properties of stainless steel 304[52]

	Melting Point (°C)	Heat Capacity (J/kg K)						
		300 K	400 K	600 K	800 K	1000 K	1200 K	1500 K
Stainless Steel 304	1397	477	515	557	582	611	640	682

By preheating these samples of different masses to various temperatures, it is possible to obtain calibration of the heat capacity of the calorimeter over a range of calorimeter temperatures. The result is well represented by the following dimensional equation, eqn. 2-9, in the operational range of 25 - 60 °C.

$$C_{p,Calo.} = 2.05 \times T_{Calo.} + 1.39 \times 10^3$$

eqn. 2-9

where $Cp_{Calo.}$ is the effective heat capacity of calorimeter (vessel, silicone oil fluid, etc.) in J/kg K and $T_{Calo.}$ is its temperature in °C.

The net heat loss from calorimeter to surroundings (Q_{Loss}) has to be determined individually for each test, since its value varies with operating temperature, ambient air conditions, and power input to stirrer. In a given experiment, the transient temperatures are recorded as

illustrated in Figure 2-5. After equilibration of sample temperature and calorimeter temperature (after time t_e), the calorimeter temperature is seen to slowly decrease, representing the net energy loss from heat transfer to surroundings and energy input from the mixer. The rate of this decline measured from the transient temperature data, provides the information needed to determine the two coefficients UA and $\dot{Q}_{mixer}$ in eqn. 2-5. Knowing these coefficients, cumulative heat loss from the calorimeter (Q_{Loss}) can be calculated by integrating $\dot{Q}_{net}$ from initial submersion of the sample to any subsequent time t, as indicated by eqn. 2-5. After these calibrations for $Cp_{Calo.}$ and Q_{Loss}, the same procedure is used to obtain experimental measurements of thermal energy storage in the EPCM samples (Q_{EPCM}) in all tests with actual encapsulated PCMs. If desired, energy stored in the PCM material itself (Q_{PCM}) can be calculated by subtracting out the corresponding enthalpy changes of the capsule container ($Q_{Capsule}$).

An analysis of measurement uncertainty in this calorimetric procedure, indicates a maximum uncertainty (if all uncertainties error in the same direction) of 1.6% in final value of stored energy (Q_{EPCM}). The actual uncertainty in results reported below are expected to be less than this maximum uncertainty, as it is unlikely for all uncertainties to error in same direction.

2.3   Results of Calorimeter Tests

2.3.1   Verification of Energy Balances

Before experimenting with the encapsulated phase change materials, we wish to verify validity of the calorimetric measurements and analyses, by testing standard samples for which energy storage can be calculated directly from known thermal properties, enabling direct verification of energy balance. Four standard samples are utilized, two of solid stainless steel and two of encapsulated zinc. The steel samples store only sensible heat without phase change, while the zinc samples store both sensible heat and latent heat of fusion. The published properties of stainless steel are given above in Table 2-2, and properties of zinc are given in Table 2-3.

Table 2-3. Thermal properties of zinc [52,53]

Melting Point (°C)	Heat Capacity (J/kg K)					Latent Heat (kJ/kg)
	300K	400K	600K	693K	700K	
420	389	405	441	473	505	113

The preheat temperatures of these samples are measured by embedded or externally mounted thermocouples – thus providing direct measurement of sample temperatures at start of submersion into the calorimeter ($T_{S,0}$) for determination of enthalpy change during the drop tests. Figure 2-6 shows a representative record of such a run. This figure provides the information of temperatures needed to determine the energy stored in the sample capsule from eqn. 2-3 to eqn. 2-8 as experimentally measured in the calorimeter run Q_{EPCM}.
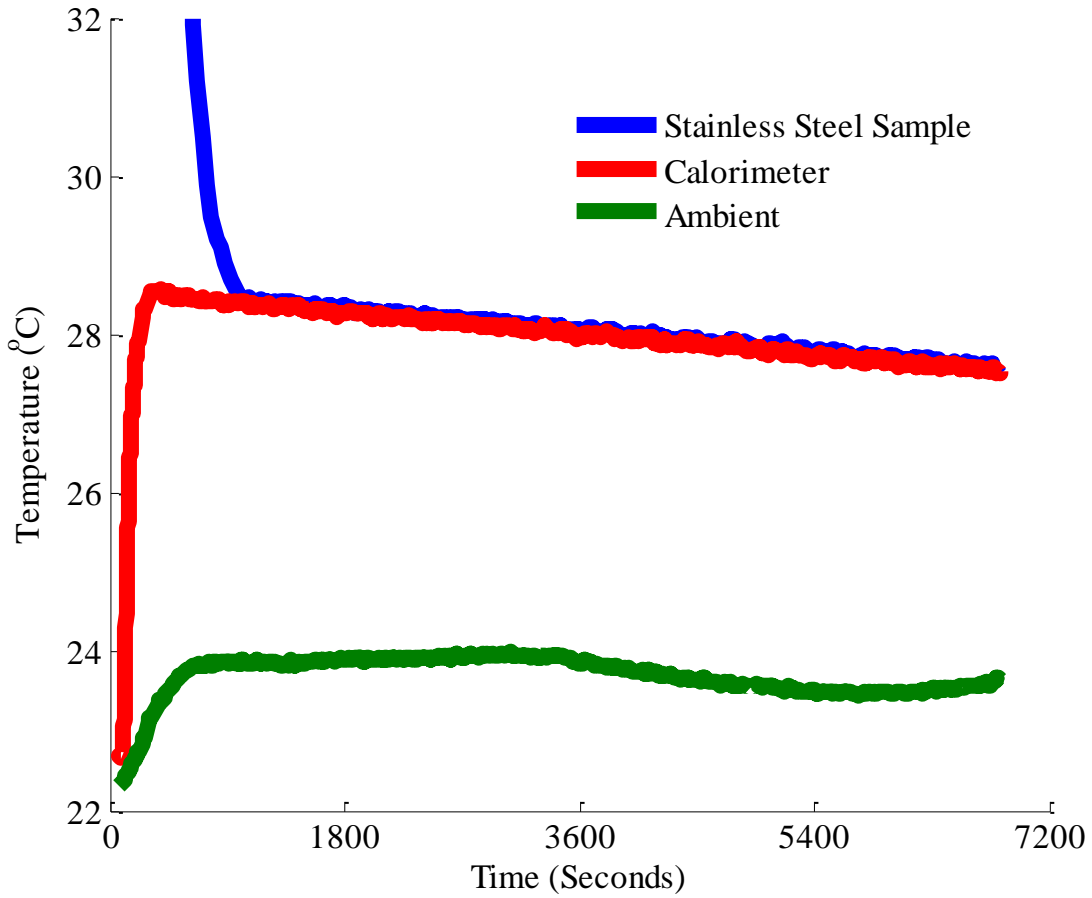
Figure 2-6. Example of transient temperature from verification test.

For these validation samples, each experimental value can be compared with an expected value directly calculated from the initial and end temperatures and known thermal properties.

$$Q_{EPCM,exp} = m_{PCM} \int_{T_{S,t}}^{T_{S,o}} \left(C_{p,Capsule} dT + H_m \right) + m_{Capsule} \int_{T_{S,t}}^{T_{S,o}} C_{p,Capsule} dT$$

eqn. 2-10

Results of this comparison can be expressed as percentage discrepancy between experimental and expected values of stored energy, expressed as:

38

$$Discrepency\ \% = \frac{Q_{EPCM,meas.} - Q_{EPCM,exp.}}{Q_{EPCM,exp.}} \times 100$$

<div align="right">eqn. 2-11</div>

Results of these verification tests for energy balance, with four different samples, at initial temperatures varying from 250 $^{\circ}$C to 490 $^{\circ}$C, are tabulated in Table 2-4. For both sensible heat storage (with steel) and phase change storage (with Zinc), it is seen that energy balances are satisfied with less than ±1.5% discrepancy, lending confidence to the experimental method and measurements.

Table 2-4. Verification tests

Sample (Initial Temperature)	$Q_{EPCM,meas.}$ (kJ)	Using Three Thermocouples around Sample		Using Internal Thermocouple	
		$Q_{EPCM,exp.}$ (kJ)	Discrepancy	$Q_{EPCM,exp.}$ (kJ)	Discrepancy
Stainless Steel Sample B Test 1 (490 $^{\circ}$C)	45.2	---	---	45.8	-1.3%
Stainless Steel Sample B Test 2 (250 $^{\circ}$C)	21.5	---	---	21.6	-0.5%
Stainless Steel Sample C Test 1 (280 $^{\circ}$C)	60.7	59.9	1.3%	60.6	0.2%
Zinc Sample A Test 1 (480 $^{\circ}$C)	45.9	46.2	-0.6%	---	---
Zinc Sample B Test 1 (490 $^{\circ}$C)	47.3	47.0	0.6%	---	---

2.3.2   Thermodynamic Properties of Candidate PCMs

For application as storage media, the following properties are needed for the two PCM salts ($NaNO_3$ and $MgCl_2$-NaCl eutectic): specific enthalpies over the temperature ranges of interest, for both solid and liquid phases, phase-transition temperatures, and latent heats of phase change. Only some of these properties are available from literature. Melting point for $NaNO_3$ is found from reference to be 308 $^\circ$C [40]. Additionally, this salt is reported to have a solid-phase transition around 275 $^\circ$C [40,49,54]. For $MgCl_2$-NaCl eutectic, the melting point is reported to be 450 $^\circ$C[45]. Enthalpy values reported in the literature for $NaNO_3$ [40,49,54] is measured with a very limited amount of material (~ 10 mg), while in this research, the enthalpy of bulk PCM is desired. No applicable enthalpy values are found in the literature for $MgCl_2$-NaCl eutectic. It is deemed necessary to obtain some additional enthalpy data for both PCMs in the temperature ranges of interest. This is accomplished using the calorimeter built in this investigation. A capsule with a known mass of PCM will undergo measurements in the drop calorimeter at several different preheat temperatures ($T_{S,0}$), selected to be both below and above phase transition temperature. Each calorimetric measurement, using eqn. 2-3 to eqn. 2-8 for data analyses, provides an enthalpy value at one temperature. A total of seven enthalpy measurements are obtained, four for the $NaNO_3$ and three for $MgCl_2$ – NaCl eutectic. Results are presented in Figure 2-7 and Figure 2-8, showing the data obtained here co-plotted with data deduced from available references. All enthalpies are taken relative to a base state at 20 $^\circ$C temperature and 1 atm. pressure. For $NaNO_3$ there is seen to be some differences (of order +/- 5%) between all values indicated. For eutectic $MgCl_2$-NaCl, no literature data are found and only the values determined in this project are shown.
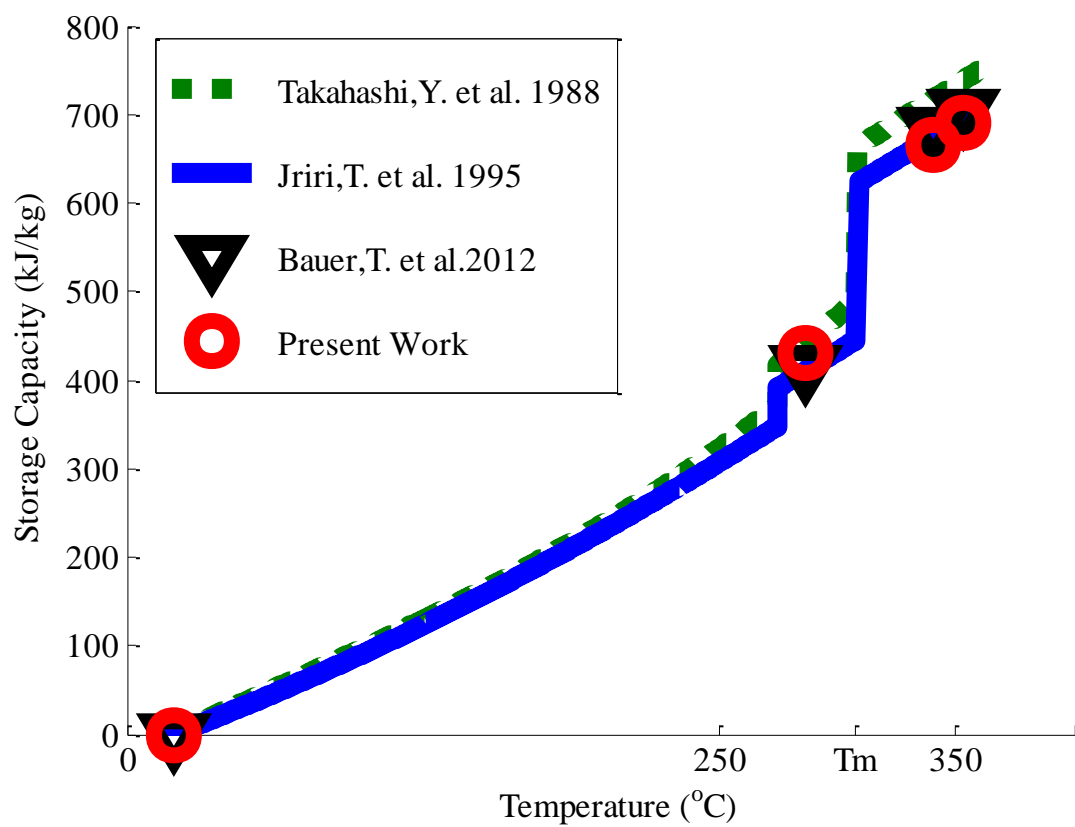
Figure 2-7. Specific enthalpy of $NaNO_3$.
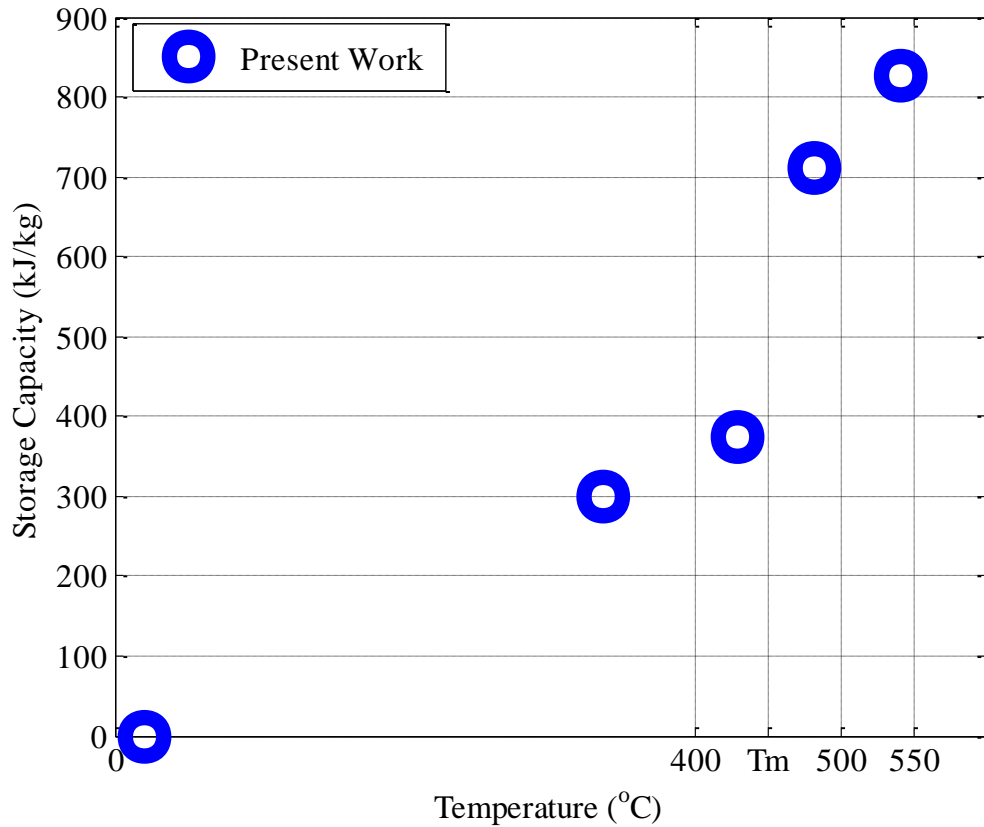
Figure 2-8. Specific enthalpy of MgCl₂-NaCl eutectic.

These thermodynamic properties enable calculation of an expected storage capacity for a given capsule in any calorimetric experiment assuming complete phase change of the PCM, using eqn. 2-12 and eqn. 2-13 written in terms of enthalpies. The actual storage capacities, measured in the calorimeter tests, can then be compared to these anticipated values.

$$Q_{EPCM,exp} = m_{PCM}\left[h_{PCM}(T_{S,0}) - h_{PCM}(T_{S,t})\right] + m_{Capsule}\int_{T_{S,t}}^{T_{S,0}} C_{p,Capsule}\,dT$$
<div align="right">eqn. 2-12</div>

$$Q_{PCM,exp} = Q_{EPCM,exp} - Q_{Capsule}$$

2.3.3 Performance of Encapsulated PCMs

Five samples of encapsulated phase change materials are fabricated and characterized in calorimeter experiments. Table 2-5 presents details of these samples, listing the phase change material, the capsule material, the capsule dimensions, and the mass of PCM in each sample.

Table 2-5. EPCM capsules

	PCM	Capsule	Size	Mass of PCM (g)
Sample 1	NaNO$_3$	Carbon Steel 1018	50.8 mm Diameter × 127 mm Height	269.6
Sample 2	MgCl$_2$-NaCl Eutectic	Stainless Steel 304	25.4 mm Diameter × 50.8 mm Height	28.8
Sample 3	MgCl$_2$-NaCl Eutectic	Stainless Steel 304	25.4 mm Diameter × 50.8 mm Height	23.9
Sample 4	MgCl$_2$-NaCl Eutectic	Carbon Steel 1018	50.8 mm Diameter × 127 mm Height	284.6
Sample 5	MgCl$_2$-NaCl Eutectic	Carbon Steel 1018	50.8 mm Diameter × 127 mm Height	282.5

These five samples of encapsulated phase change materials are characterized in calorimetric experiments as described above. An example of the temperature record obtained (for Sample 1 with NaNO$_3$) is shown in Figure 2-9 and Figure 2-10. Figure 2-9 displays the temperature history for the entire 1.8×10^4 seconds (~5 hours) of the experiment, including the preheat charging period when the sample temperature is raised from ambient to ~340 °C. At time of ~1.05×10^4 seconds, the hot sample is immersed into

the calorimeter fluid, equilibrated in temperature with the calorimeter, and thermally discharged. Figure 2-10 shows an expanded trace of the discharging process. These measurements of transient temperatures provide the requisite data for calculating energy balance for the EPCM capsule as it cools from its charged temperature (340 $^\circ$C) to the discharged temperature (~48 $^\circ$C), utilizing as described above.
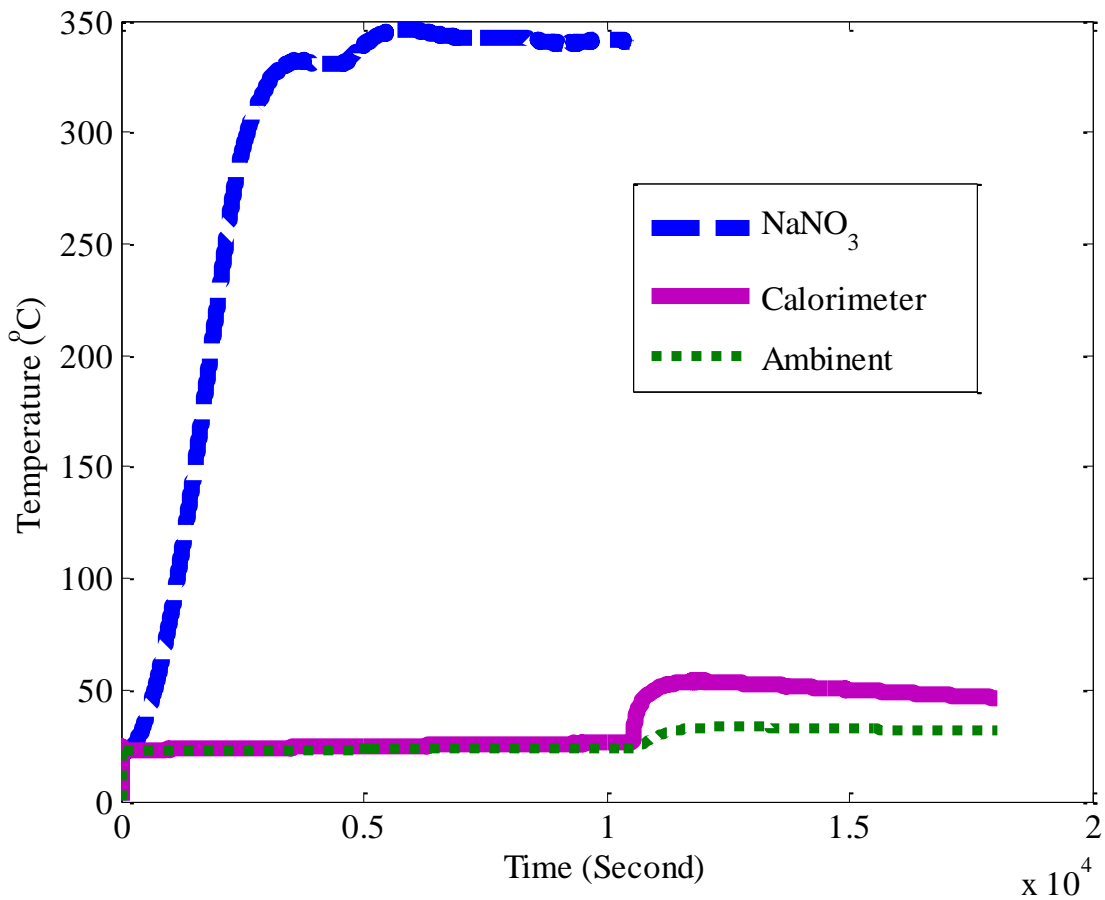
Figure 2-9. Example of temperature history for encapsulated phase change material in calorimeter experiment.

Data of this nature are obtained for all five EPCM samples in some 18 calorimeter

experiments under various test conditions. In examination of these results, the first question to address is whether or not the phase change material behaves as designed, storing energy in a thermal cycle with complete phase change. The data from the calorimeter run are analyzed by eqn. 2-3 to eqn. 2-8 to obtain an experimental value for energy stored in the EPCM $Q_{EPCM, meas.}$. Knowing thermodynamic properties, the anticipated amount of energy stored in a given cycle $Q_{EPCM, exp.}$ can be calculated separately, using eqn. 2-12 and eqn. 2-13. Comparison of the experimental and expected values indicates whether or not the PCM performed as anticipated, with complete phase change. Table 6 shows the comparison of energy storage, measured versus expected, for the initial tests of the five EPCM samples.
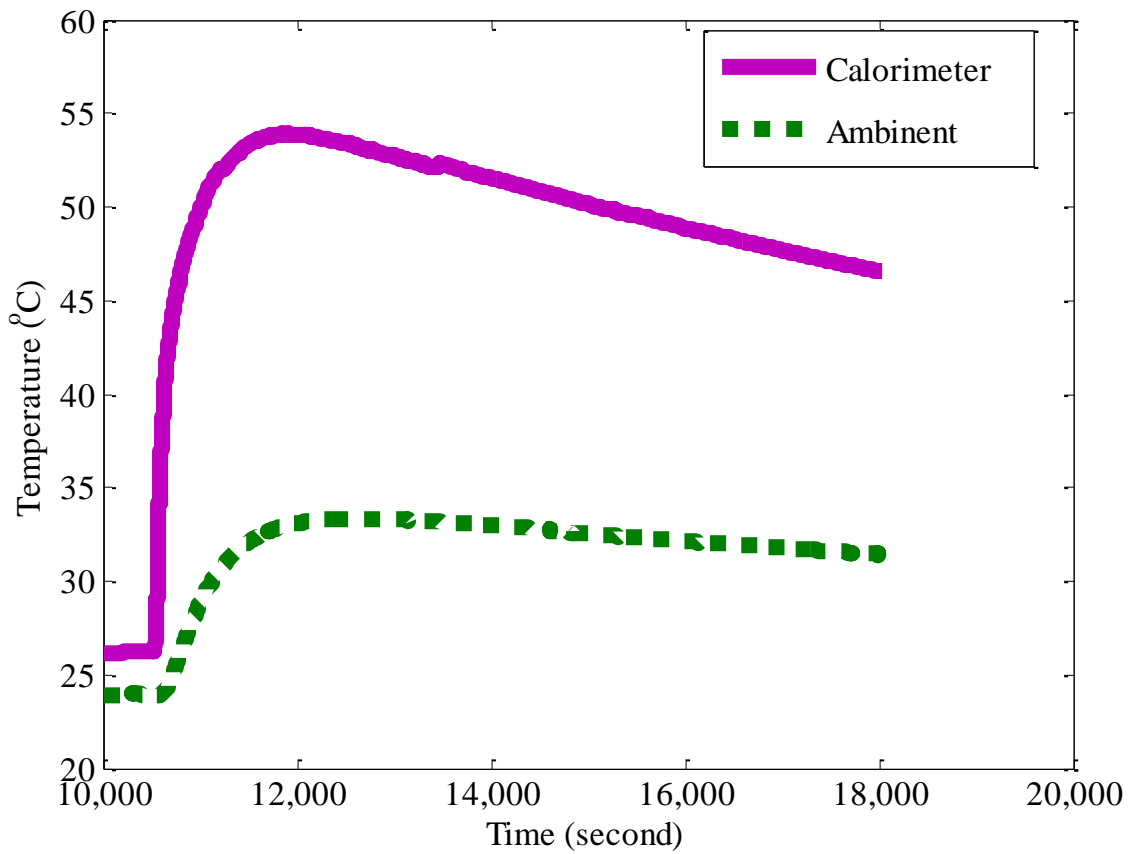
Figure 2-10. Expanded trace of temperature transients during discharge period in calorimeter experiment.

Table 2-6. Energy stored in EPCM in initial thermal-cycle.

Sample No.	Charged Temp. (°C)	Discharged Temp. (°C)	$Q_{EPCM, exp.}$ (kJ)	$Q_{EPCM, meas.}$ (kJ)	Discrepancy (%)
1	350	47	237.4	236.7	99.7
2	490	29	41.6	41.8	100.5
3	490	28	38.6	39.1	101.3
4	490	50	264.0	262.7	99.5
5	490	51	264.5	269.5	101.9

It is seen that both PCM salts, in 5 different samples, perform as designed, with agreement

of better than 2% between expected and measured values of energy storage. The fact that

ratio of experimental energy storage to anticipated energy storage is essentially 100% is an indication of complete phase change (melting/freezing) of the PCM.

A second question to address is whether or not the storage capacity will diminish with repeated thermal cycles. Such diminishment could imply undesirable changes in the salt medium, possibly due to chemical interaction with the capsule walls. To answer this question, all five samples of ECPM are subjected to multiple thermal cycles. The results for all samples (1-5), involving both $NaNO_3$ and $MgCl_2$-$NaCl$, are plotted in Figure 2-11, showing the level of agreement between expected storage and measured storage as the number of cycles accumulated. It is seen that the agreements remained within 2%, for all cycles and all samples with no discernible trend of diminishing storage capability. Thus, within the test ranges, storage deterioration is not observed.

A last issue to examine is storage performance of ECPM, after long exposure to high temperatures. This is of particular interest for the $MgCl_2$-$NaCl$ eutectic salt, since its operating temperature will exceed 400 $^{\circ}$C. Samples 2, 3 and 4, all with $MgCl_2$-$NaCl$ but in capsules of different dimensions and different steels, are subjected to long exposures at elevated temperatures. These capsules are preheated to 470 $^{\circ}$C (above the melting point of $MgCl_2$-$NaCl$ eutectic), held at that temperature for six hours, and then cooled down to 300 $^{\circ}$C (below the melting point) and held at 300 $^{\circ}$C for two hours – comprising one long-term thermal cycle. Repeating the cycle 50 times, accumulates 300 hours total exposure at 470 $^{\circ}$C. Table 2-7 presents test results of these samples, following the 300 hour high-

temperature exposure.
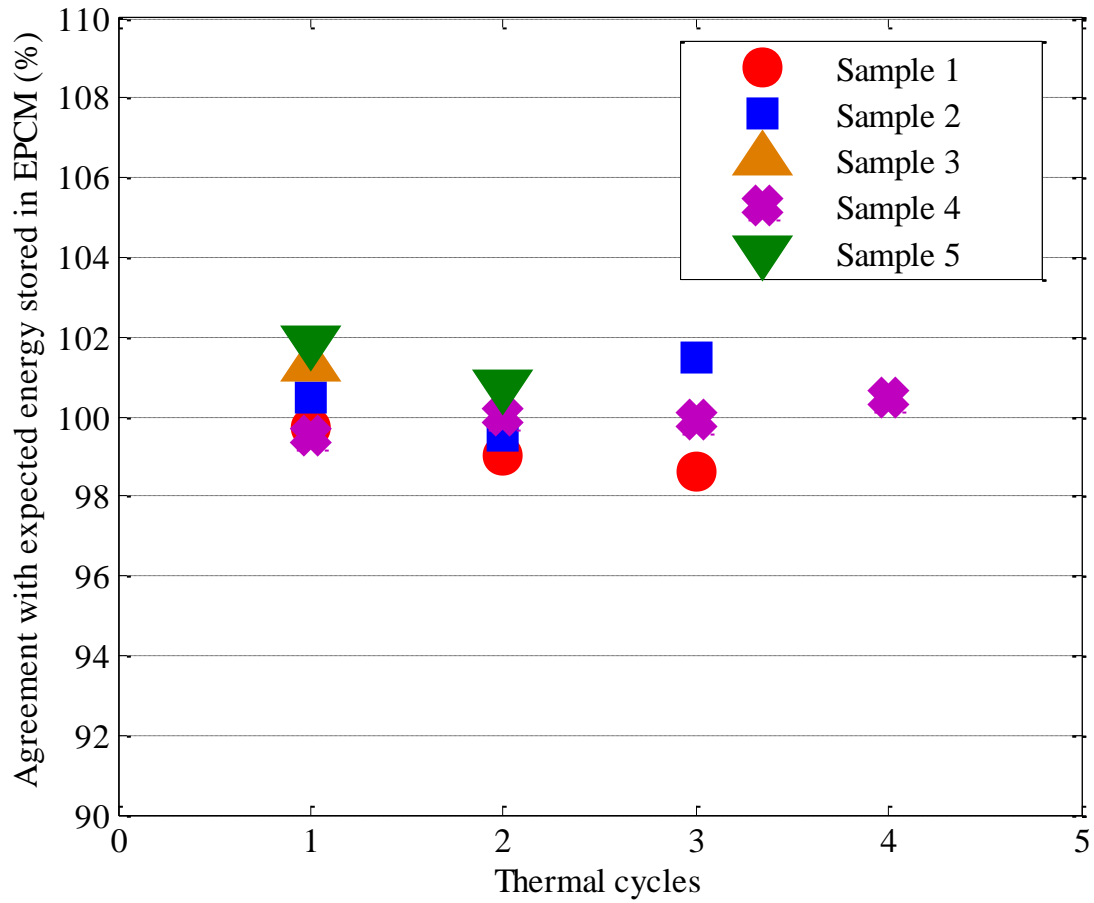
Figure 2-11. Storage performance of ECPM samples over multiple thermal cycles.

Table 2-7. Energy stored in MgCl2-NaCl EPCM in final thermal-cycle after high -

temperature exposure

Sample No.	Exposure	$Q_{EPCM, exp.}$ (kJ)	$Q_{EPCM, meas.}$ (kJ)	Discrepancy (%)
2	300 hours at 470 °C	41.9	41.5	99.0
3	300 hours at 470 °C	38.7	38.4	99.2
4	300 hours at 470 °C	265.5	265.5	100.0

It is seen that agreement between experimental and expected energy storage remains within 1%, similar to results from the first, short thermal cycle. Thus, within the test range, there is no sign of any significant deterioration in storage performance after 300 hours of exposure to high temperatures in 50 thermal cycles.

2.4   Summary of the Calorimetry Work

This experimental development and calorimetric investigation indicate that:

- The two salts, $NaNO_3$ and $MgCl_2$-NaCl eutectic, are promising phase-change materials which can be encapsulated for storage of thermal energy at temperatures up to range of 250-550 °C, suitable for concentrating solar power systems.

- For a 100 °C temperature swing (charged to discharged), bracketing the salts' melting points, the latent heat of phase change contributes 57% and 75% to the storage capacity of the PCM mass, for $NaNO_3$ and $MgCl_2$-NaCl respectively.

49

- It is possible to encapsulate these candidate PCMs in stainless steel or carbon steel containers, though possible corrosion of the shell should be further tested under longer exposures for the $MgCl_2$-NaCl salt.

- The encapsulated PCMs show no discernible deterioration in storage capacity over multiple thermal cycles.

- Long-term (multi-days) exposure of the EPCMs to elevated temperatures has not caused any discernible diminishment in storage performance.

3   A MATHEMATICAL MODEL OF THE EPCM-BASED TES SYSTEM

A simulation model for the EPCM based TES system is set up as sketched in Figure 3-1. For the numerical model, the overall height of the test section is denoted as Z, [m]. The total length of the test section is divided into N equal cells, where N equals the number of the EPCM capsules, and each cell contained one capsule. For each cell, energy balances are calculated for each component of the test section, i.e. HTF, EPCM capsules, T/S chamber, insulation and heat losses from the outside surface of the insulation, to investigate the transient heat transfer process during thermal charging and discharging cycles. Furthermore, the capsule and the PCM inside are radially divided into small meshes in order to calculate radial temperature variation as shown in Figure 3-2(b). When the PCM inside the capsule reaches melting temperature, it is allowed to melt or solidify by adding the latent heat. As a result at any given time the capsule has three different layers: the solid shell, liquid PCM and a solid PCM. For simplicity of calculations, it is assumed that the solid PCM stays at the center of the capsule and there is no natural convection in the liquid PCM layer.
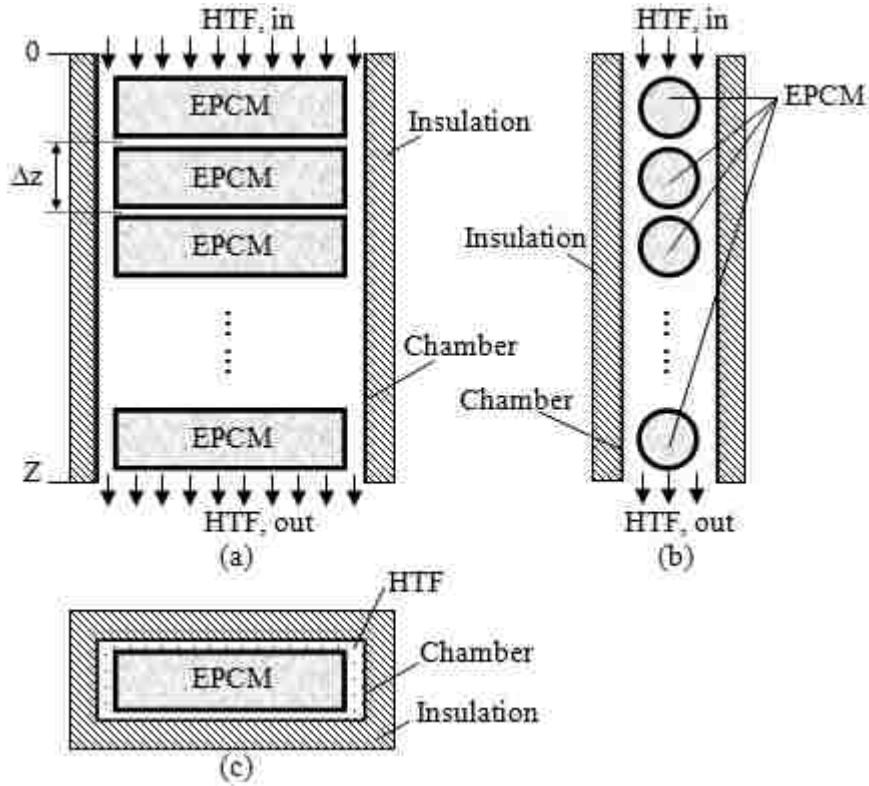
Figure 3-1. A simulation model of the EPCM based TES system. (a) front view; (b) side view; (c) top view.

The heat conduction is assumed to be in the radial direction only, that is the temperature of the PCM, and the temperature of the shell is the function of time and radial location only as described by

$$\rho_{PCM} C_{p,PCM} \frac{\partial T_{PCM}}{\partial t} = k_{PCM} \frac{1}{r_{PCM}} \frac{\partial}{\partial r_{PCM}} \left(r_{PCM} \frac{\partial T_{PCM}}{\partial r_{PCM}} \right)$$

eqn. 3-1

$$\rho_s C_{p,s} \frac{\partial T_s}{\partial t} = k_s \frac{1}{r_s} \frac{\partial}{\partial r_s} \left(r_s \frac{\partial T_s}{\partial r_s} \right)$$

eqn. 3-2

While eqn. 3 only accounts for the heat conduction inside the PCM in its single phase, the energy balance in the interface between two phases is analyzed when the temperature of the PCM reaches its melting point as described by

$$
\begin{aligned}
\rho_{PCM} \Delta H_{PCM} L_s \times \pi \frac{(S_{PCM}(t))^2 - (S_{PCM}(t - \Delta t))^2}{\Delta t} \\
= \left(k_{PCM} A_{PCM} \frac{\partial T_{PCM}}{\partial r_{PCM}} \right)_{r_{PCM} = S_{PCM} - \Delta r_{PCM}, solid} \\
- \left(k_{PCM} A_{PCM} \frac{\partial T_{PCM}}{\partial r_{PCM}} \right)_{r_{PCM} = S_{PCM} + \Delta r_{PCM}, liquid}
\end{aligned}
$$

eqn. 3-3

In this equation, S_{PCM} is the distance of the interface (moving front) from the inside surface of the shell, as sketched in Figure 3-2(c). It can be used as an indicator for the progress of the phase change – when its value is zero, it means that the PCM is 100% in single phase; when its value is equal to the radius of the PCM, it means that the PCM has completed the phase change. And the value of the displacement of the melting front can also be used to calculate the percentage of the molten fraction, and further decide the contribution of the phase change in the overall energy stored into and retrieved from the EPCM. As indicated in Figure 3-2, the capsule is considered to be filled with the PCM having uniform density. Since the real capsule has a specific void space in the capsule as an allowance for PCM's thermal expansion, the density is adjusted accordingly in this model to ensure a constant mass. The density is assumed to be independent of the temperature, therefore during the phase change the solid PCM would stay in the center when liquid phase forms on the outside as shown in the Figure 3-2 (c).

53
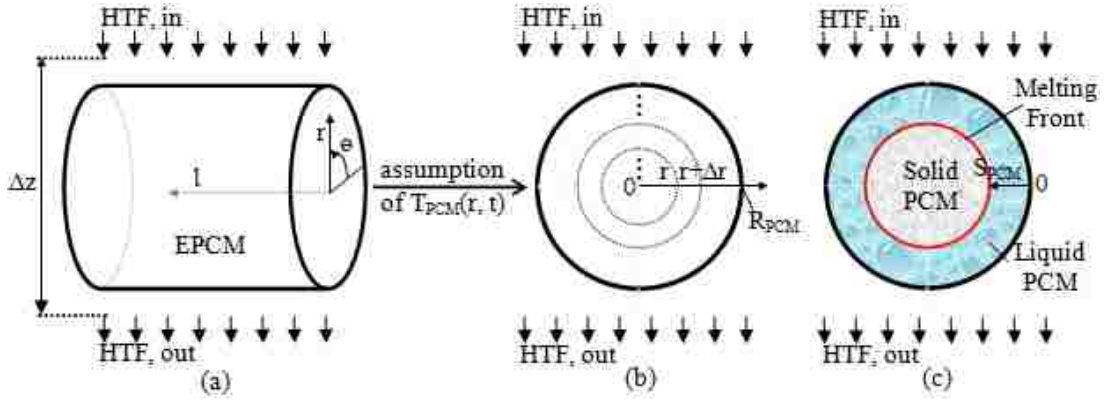
Figure 3-2. The details of the model for an EPCM capsule in a specific elevation. (a). temperature of PCM is a function of (r, ɵ, l, t) for a cylindrical EPCM capsule (front view); (b). temperature is dependent on the radial location r and time t in this model; (c). melting front inside the PCM during its phase change.

For the heat transfer fluid flowing across a specific zone of Δz, part of the total energy from the HTF is transferred to the capsule and T/S chamber by convection, while the other part is captured by the HTF itself in this section as described by

$$\rho_f C_{p,f} \frac{\partial T_f}{\partial t} = G_f C_{p,f} \frac{\partial T_f}{\partial z} - \left[h_s A_s (T_f - T_s)\right]_{r_s=R_s} - \left[h_c A_c (T_f - T_c)\right]_{x_c=0}$$

eqn. 3-4

The convective heat transfer coefficient from the HTF to the surface of the capsule is calculated using Zhukauskas correlation[47] for the circular cylinder in cross flow with the assumption that it is independent of the angular coordinate ɵ and length l. The average convective heat transfer coefficient from the HTF to the surface of the T/S chamber, is also calculated using Zhukauskas correlation considering that with the current design, the flow of HTF at the surface of the T/S chamber is similar to the flow of HTF at the surface of the EPCM capsule. It is found that the effects of radiation is negligible, amounting only less than 2% of the convective heat transfer power according to calculation for current facility.

One-dimensional model is applied for the inside heat conduction for the T/S chamber and insulation as shown in Figure 3-3(b). Including a varying surface area for heat conduction from the inside surface of the chamber to the outside surface of the insulation the energy equations are described by

$$\left(\rho_c C_{p,c} \frac{\partial T_c}{\partial t}\right)_{x_c} = \left(k_c A_c \frac{\partial T_c}{\partial x_c}\right)_{x_c - \Delta x_c} - \left(k_c A_c \frac{\partial T_c}{\partial x_c}\right)_{x_c + \Delta x_c}$$

eqn. 3-5

$$\left(\rho_i C_{p,i} \frac{\partial T_i}{\partial t}\right)_{x_i} = \left(k_i A_i \frac{\partial T_i}{\partial x_i}\right)_{x_i - \Delta x_i} - \left(k_i A_i \frac{\partial T_i}{\partial x_i}\right)_{x_i + \Delta x_i}$$

eqn. 3-6
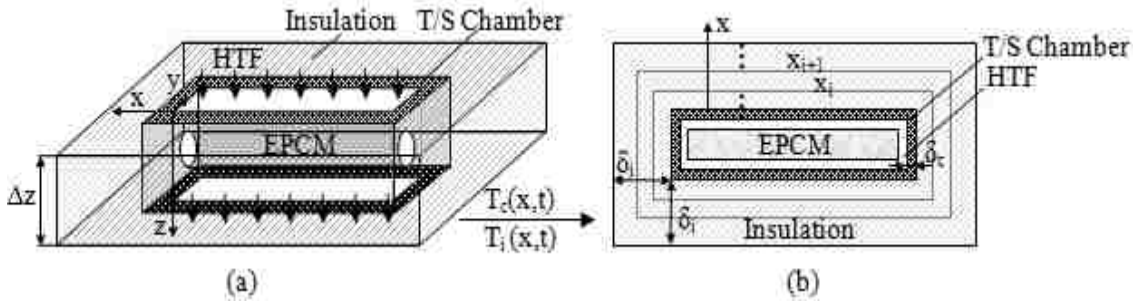
Figure 3-3. The details of the model for the insulation and T/S chamber in a given elevation. (a). the temperature is a function of (x,y,z,t) for the insulation and T/S chamber; (b). temperature of the insulation and T/S chamber are assumed as a function of (x,t).

At the outside surface of the insulation, natural convection with ambient air is considered with a heat transfer coefficient calculated using Churchill and Chu correlation[55].

$$\left(\rho_i C_{p,i} \frac{\partial T_i}{\partial t}\right)_{x_i = \delta_i} = \left(k_i A_i \frac{\partial T_i}{\partial x_i}\right)_{\delta_i - \Delta x_i} - [h_a A_i (T_i - T_a)]_{x_i = \delta_i}$$

eqn. 3-7

Finite difference method has been used to discretize eqn. 3-1 - eqn. 3-7. The temperature profiles for each of the component – EPCM, HTF, T/S chamber and insulation can be obtained to determine the dynamic nature of the TES system. Especially for the EPCM capsules, it is of great value to further calculate their energy storage and retrieval during the thermal charging and discharging cycles. The results of the simulations will be compared against the experimental data.

4 EXPERIMENTAL SETUP OF AN EPCM-BASED TES SYSTEM

In previous research for identification of qualified encapsulated phase change materials, cylindrical stainless steel capsule was found to be compatible with the $NaNO_3$ and $MgCl_2$ – $NaCl$ eutectic[30]. These investigators illustrated that the storage capacity has not been deteriorated under repeated thermal tests in a specially-made calorimeter. The present work aims to test and demonstrate the thermal energy storage and retrieval of multiple EPCM capsules in a realistic TES system. For TES systems with EPCM, most of the experimental research has been focused on low temperature applications[5,16,55,56], such as using encapsulated $CaCl_2 \cdot 6H_2O$ as a construction material for buildings' thermal management. There are very few process demonstrations being developed for high temperature applications, and most of the high temperature studies have been limited in the level of theoretical and computational studies[7,57-60]. Therefore, it is essential to develop and execute experiments for verification of technical feasibility of the EPCM in test facilities. On one hand, it can be a demonstration to evaluate viability of the technology before scale-up and commercialization. On the other hand, experimental test data, such as stored energy and temperature profiles of EPCM, can be obtained and compared with model predictions to verify and adjust the mathematical model.

In the design of the EPCM based TES system, several parameters need to be determined:

- Configuration of the EPCM based test section (T/S);

- Physical dimensions of the test section;

- Physical dimension, and number of the EPCM capsules

- Selection of heat transfer fluid;

- Operating conditions of the heat transfer fluid.

For determination of those parameters, a mathematical model is developed previously in Chapter 3 to analyze the effects of these parameters, and further optimize the test section design for desired performance.

4.1 Design and Operation of the EPCM-based TES System

For the current test facility, air has been chosen as the heat transport fluid to charge and discharge the overall test section, considering its chemical stability and its associated simple sub-heating system compared with liquid HTF. In the design of the test section for testing of EPCM capsules for process demonstration, there are six important design parameters that have been considered and computed in the simulation model for evaluation of their effects on the performance of the EPCM in the test section. These parameters are:

- Flow rate of the air.

- Temperature of the air at the inlet of the test section.

- Diameter of the EPCM capsules.

- Number of the EPCM capsules.

- Thickness of the insulation for the test section.

Each of the parameter has been investigated in this simulation model, for identification of its importance on the performance of the EPCM-based test section. There are four main criteria for quantification of these parameters:

- Majority of the energy should be stored into or extracted from the EPCM capsules. In other words, the thermal masses of the other components of the test section are desired to be minimized.

- The temperature drop of HTF should be large across the TES system, so that the errors for calculation of the total energy from the HTF will be small. In this research, experiments are conducted with air with temperature drops across the test section higher than 20 °C. Temperatures of air are measured using calibrated K-type thermocouples.

- All of the encapsulated PCM will be preferred to complete phase change in a time period that is applicable for solar power plants. Considering the scale of current facility, the desired experiment duration is expected to be about 2 − 6 hours for a charging/discharging process, and the experiment ends when the

temperature drop of the HTF decreases below 20 °C.

- Easy fabrications for the test facility.

With considerations of many configurations, one-column inline system is chosen with heat transport fluid flowing across horizontally-oriented EPCM capsules. Following these design criteria, the mathematical model has been run for a set of the above design parameters, including physical dimensions and operating conditions to identify desired test conditions of EPCM capsules. The optimization of each of the parameters is described below in details. In evaluating the different design parameters, the simulation results are shown for the case with encapsulated $NaNO_3$ as an example, which is at 200 °C at its initial state. The simulation results are shown below for each of the design parameter.

- Flow rate of the air.

In the current facility, the air flow rate is in the range of 0.01 kg/s – 0.05 kg/s, considering the requirement of the electric heater which will be detailed later. The simulation have been run for the air mass flow rates of 0.01 kg/s, 0.03 kg/s and 0.05 kg/s and the results are shown from Figure 4-1 to Figure 4-6.

Figure 4-1 shows the air temperature at the inlet of the test section in the simulation cases for different air mass flow rates. In this simulation, the air temperature is assumed to go through a transient process, that is, with a set point in the air heater, the air will go through

a short transient process because of the thermal mass of the piping and insulation between the test section and the air heater, and then reach to its steady state, just as described below in eqn. 4-1

$$m_f C_{p,f}\left(T_h - T_{f,in}\right) + \left(mC_p \frac{dT}{dt}\right)_{(piping+insulation)} = q_{heater}$$

<div align="right">eqn. 4-1</div>

Where m_f is the mass flow rate of the air, (kg/s). T_h is the set point of the heater, (°C). In this simulation case, the set point of the heater is 450 °C. q_{heater} is the power the heater at that set point, (W). Based on this equation, the temperature of the air can be predicted at the inlet of the test section for a given air flow rate. In the Figure 4-1, it is seen that with a lager mass flow rate, the air temperature at the inlet of the test section will reach to its set point more quickly. For the case of 0.03 kg/s air mass flow rate, the air is heated up quickly and reaches to 450 °C in ~ 1.5 hrs.
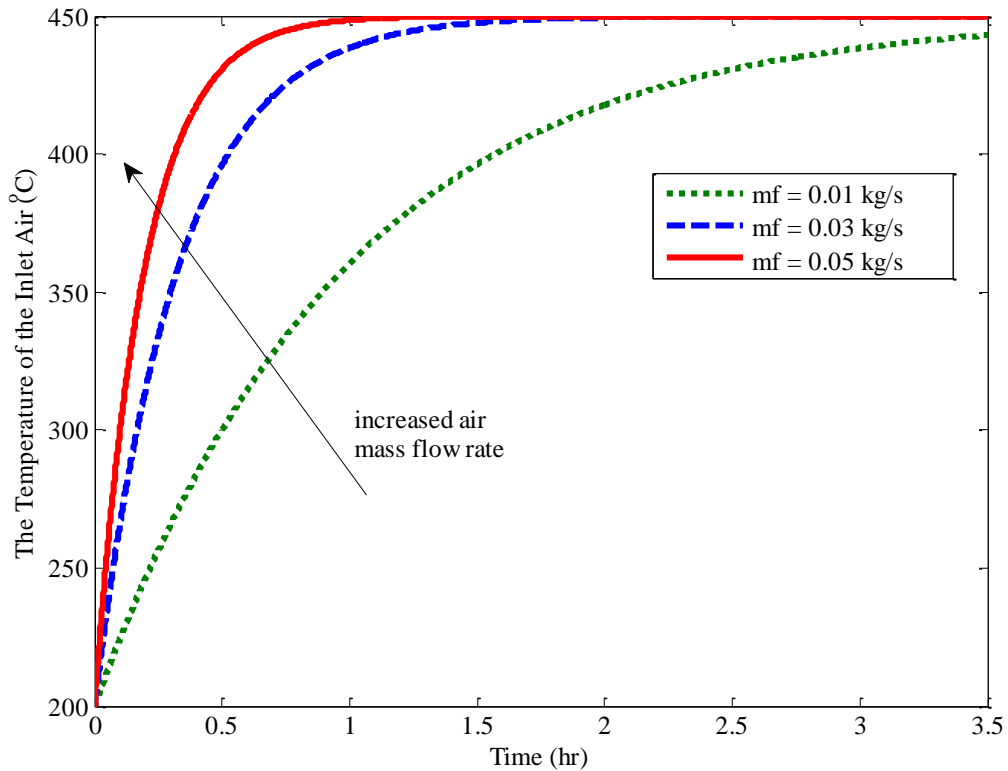
Figure 4-1. The air temperature at the inlet of the T/S with different air mass flow rates.

As discussed previously, the temperature drop of the air across the test section is preferred to be a large value (> 20 °C) in order to minimize the errors in calculating the total energy from the air. This temperature drop of the air, that is, the difference of the air temperature between the inlet and the outlet, is shown in Figure 4-2. It is seen that with a larger air mass flow rate, the overall temperature drop is higher at the very beginning of the charging process, and then decreases quickly with the progress of heating of the test section and stays smaller during the rest of the process compared with the case with smaller air mass flow rates. Therefore for a larger temperature drop of the air across the test section, it is preferable to operate the test section with a small air flow rate. However, with a small mass

flow rate, the total energy transferred to the EPCM capsules is small, as shown in Figure 4-3. For the case of the mass flow rate 0.01 kg/s, the total energy stored in the capsules is about 10 MJ, and ~ 65% of the total energy from the air is transferred to the EPCM capsules as shown Figure 4-4. With a larger air mass flow rate, the total energy stored in the capsule increases, and it has been found that with the maximum air flow rate, the EPCM capsules can capture up to ~ 80% of the total energy from the air. Therefore, for a larger ratio of the energy stored in the EPCM capsules to the total energy released from the air, it is preferable to have large mass flow rates.

Figure 4-2. The temperature drop of the air across the test section with different air mass flow rates.
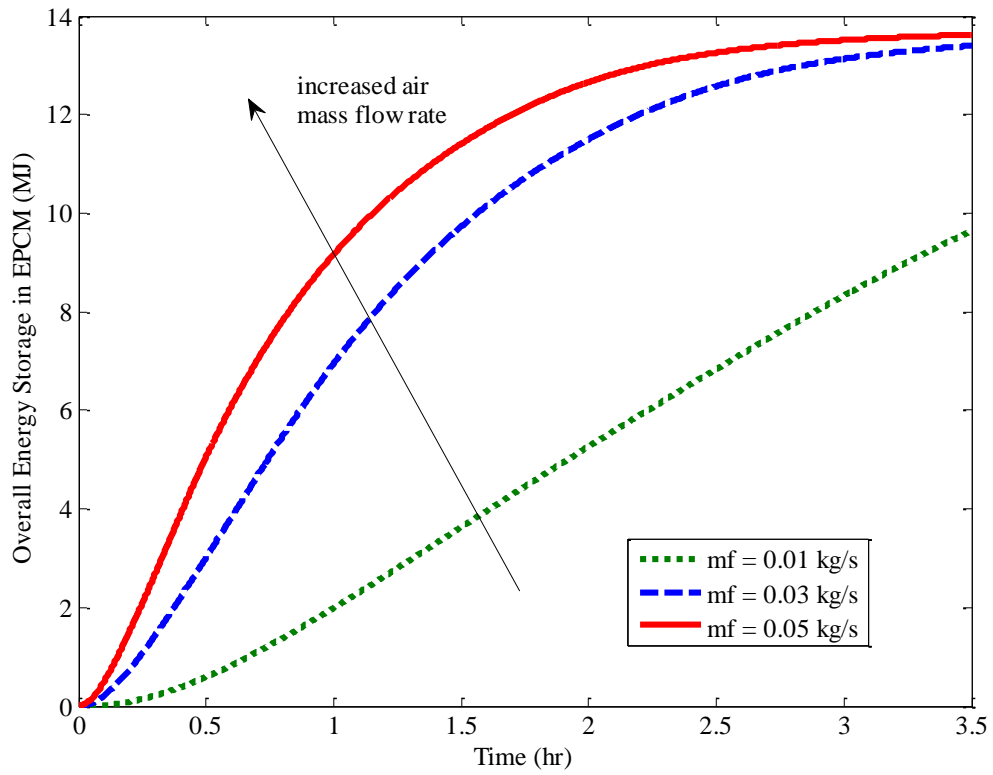
Figure 4-3. The total energy stored in the EPCM capsules with different air mass flow rates.
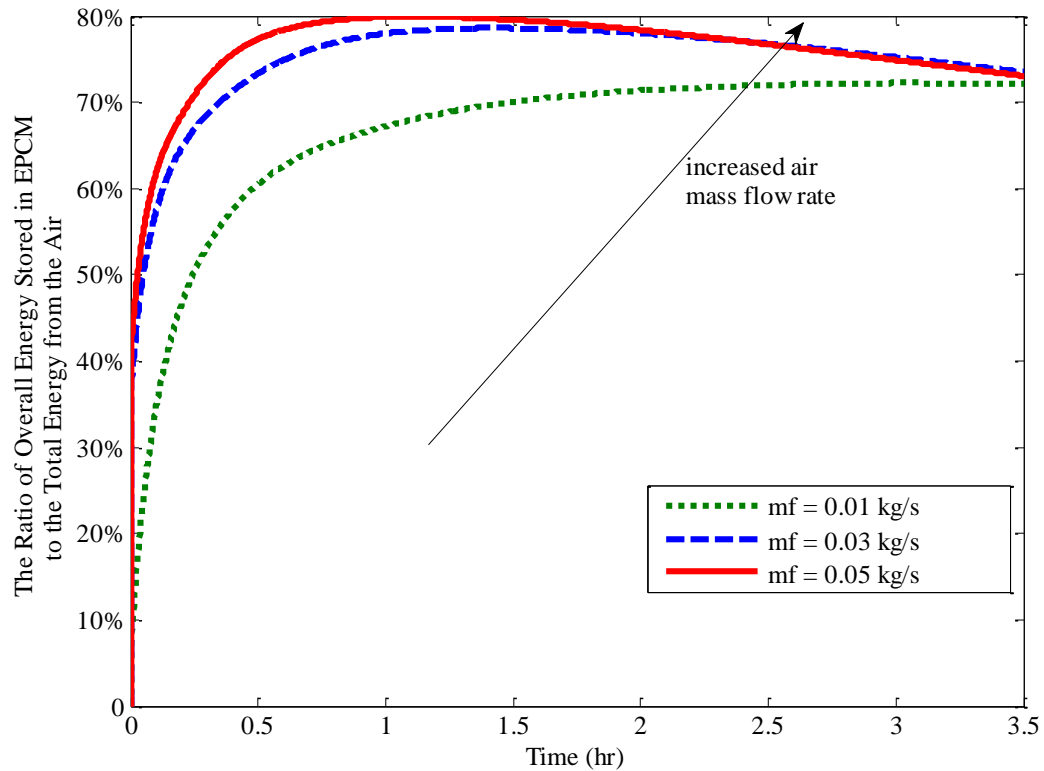
Figure 4-4. The percentage for the total energy stored in EPCM capsules of the total energy from the air in a charging process with different air mass flow rates.

Since the objective of this research is to utilize the latent heat of the PCM during its phase change, it is preferable that all the PCM go through the phase change that is, changing from one phase to another phase completely. In this simulation, the mass fraction of the phase change has been calculated, which indicates the progress of phase change for the overall EPCM capsules in the test section and the results are shown in Figure 4-5. It is seen that for the case of the 0.01 kg/s air mass flow rate, ~ 80% of the encapsulated PCM has completely melted and ~ 20% is still in its solid phase after a heating period of 3.5 hrs. For the cases of 0.03 kg/s, and 0.05 kg/s air mass flow rates, the PCM in the test section is

expected to complete the phase change in less than ~ 2 hrs. To summarize, a large air mass

flow rate causes the capsules heat up faster and a higher fraction of PCM to melt.

Besides considering the effects of the air flow rates on thermal performance of the EPCM

in the test section, the pressure drop of the air in the test section is also calculated for cross

flow geometry, based on Ergun equation for calculation of the pressure drop in a packed

column[61], and the results are shown in Figure 4-6 for the air flow rate range in the 0.01 kg/s

– 0.05 kg/s. It is seen that the pressure drop per unit length of the test section is pretty small,

about 0.9 kPa/m with the maximum air flow rate.

Considering all the factors with different mass flow rates, a large air flow rate is chosen for

the experimental testing and the value is ~ 0.038 kg/s.
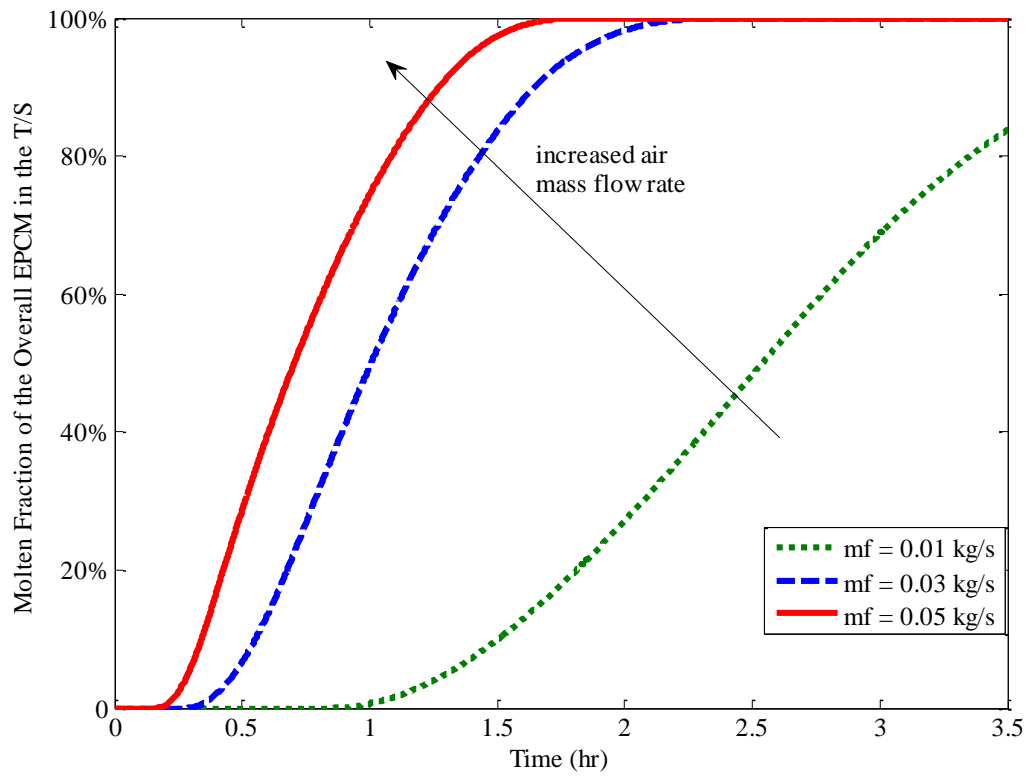
Figure 4-5. The molten fraction of the overall EPCM capsules in the test section with different air mass flow rates.
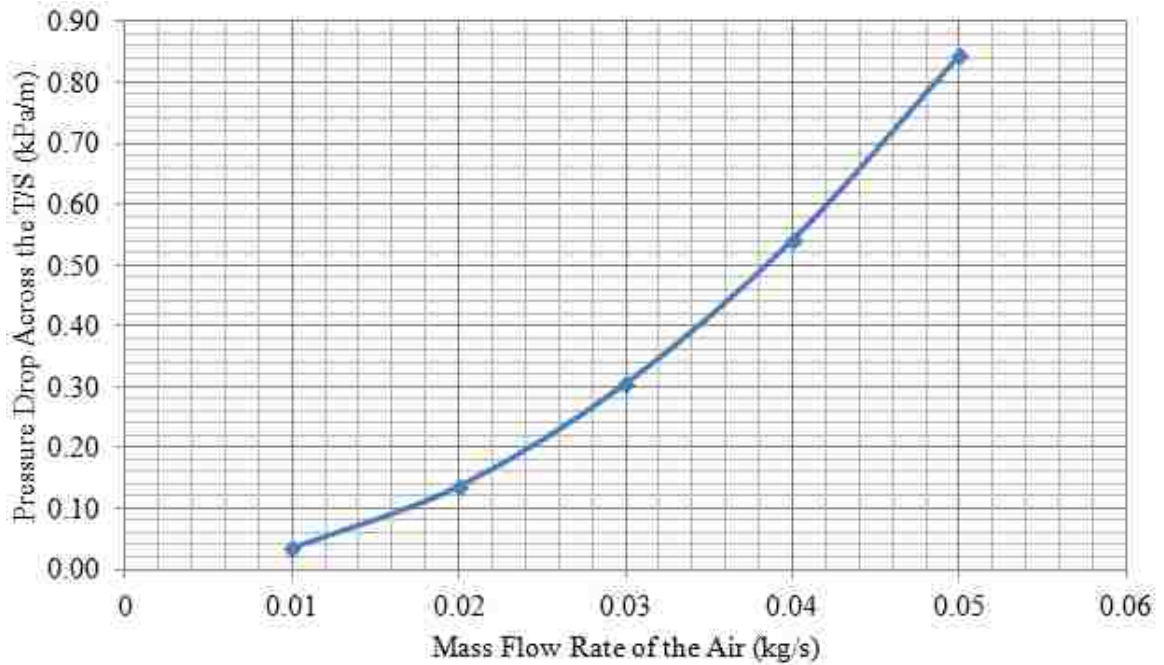
Figure 4-6. The air pressure drop over the test section with different mass flow rates.

- Air Temperature at the Inlet.

During the experiments the temperature of air at the inlet can be controlled by manually adjusting the set point for the temperature at the outlet of the air heater. An evaluation of the effects of the air inlet temperature to the test section is carried out to determine a range of inlet temperatures for the experiments. With a 36 kW air heater before the test section, the inlet air can be heated up to 650 °C in the current mass flow range. With consideration of a safe operation in the experimental testing, simulation cases have been run for the cases with 400 °C, 500 °C and 600 °C set points in the heater as shown in Figure 4-7 for the temperature of the air at the inlet of the test section. It has been seen that in all of these three cases with different set points in heater, the inlet air is capable to reach to its set point, the steady state in ~ 1.5 hrs.
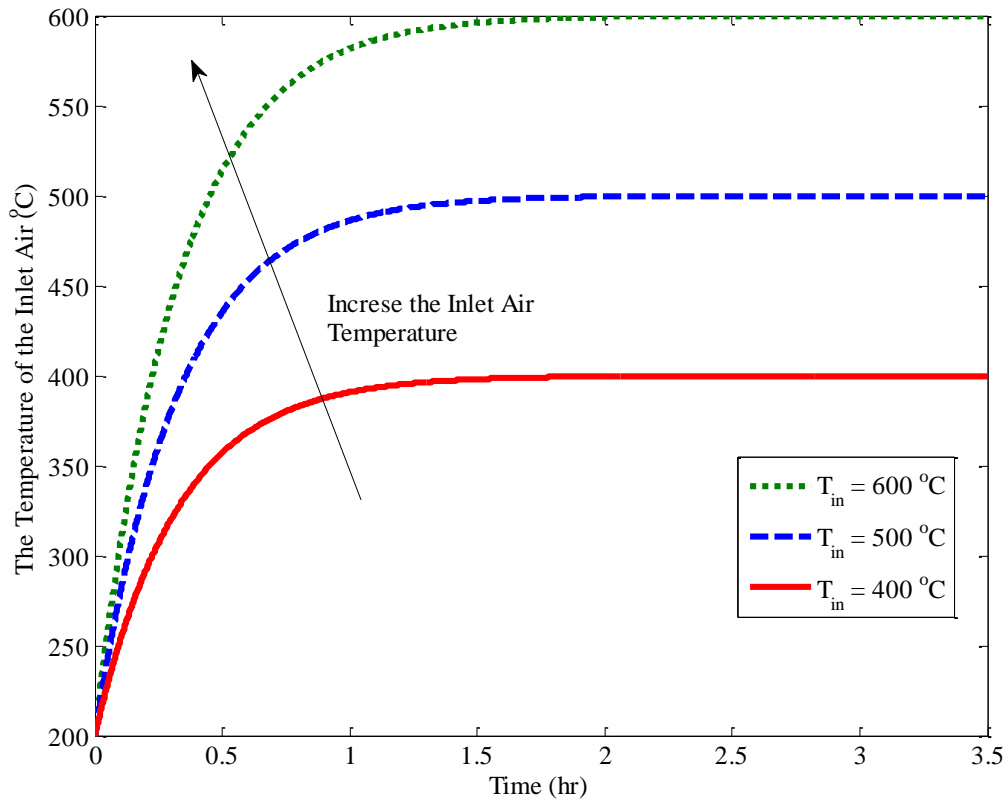
Figure 4-7. The temperature profiles of the air at the inlet of the test section with different set points in the air heater – 400 °C, 500 °C and 600 °C.

Figure 4-8 shows the temperature drop of the air across the test section with different inlet air temperatures. As shown in this figure, the temperature drop of the air is generally larger with a higher inlet air temperature, and at the end of the 3.5 hrs, the temperature drop is ~ 18 °C for all of the three cases. With a higher inlet air temperature, there is more energy stored in the overall EPCM capsules since the temperature of the EPCM is heated up to a higher temperature just as shown in Figure 4-9.

From the two figures Figure 4-8 and Figure 4-9, it seems like it is quite preferable to have

a high inlet air temperature considering a high temperature drop of the air and a large amount of energy storage in the EPCM capsules. However, if we look into the percentage of the total captured energy by the capsules, it has been shown that the contribution of the EPCM capsules for the energy storage are quite similar in these three cases, at ~ 80% from Figure 4-10. This tells that with a larger operating air temperature at the inlet of the test section, the overall energy stored in the EPCM capsules in the test section increase, so is the energy stored in insulation, in the T/S chamber. Therefore, there are not much advantages for operating the system with very high inlet temperature in the point view of high contributions from the EPCM capsule in the energy storage.
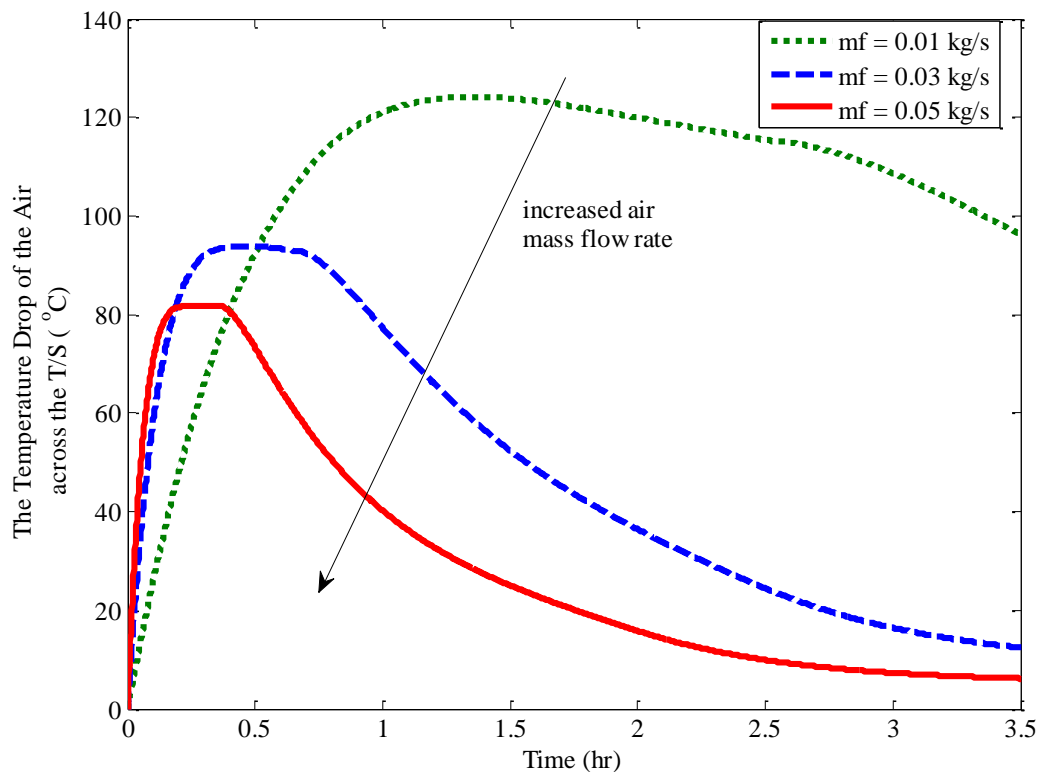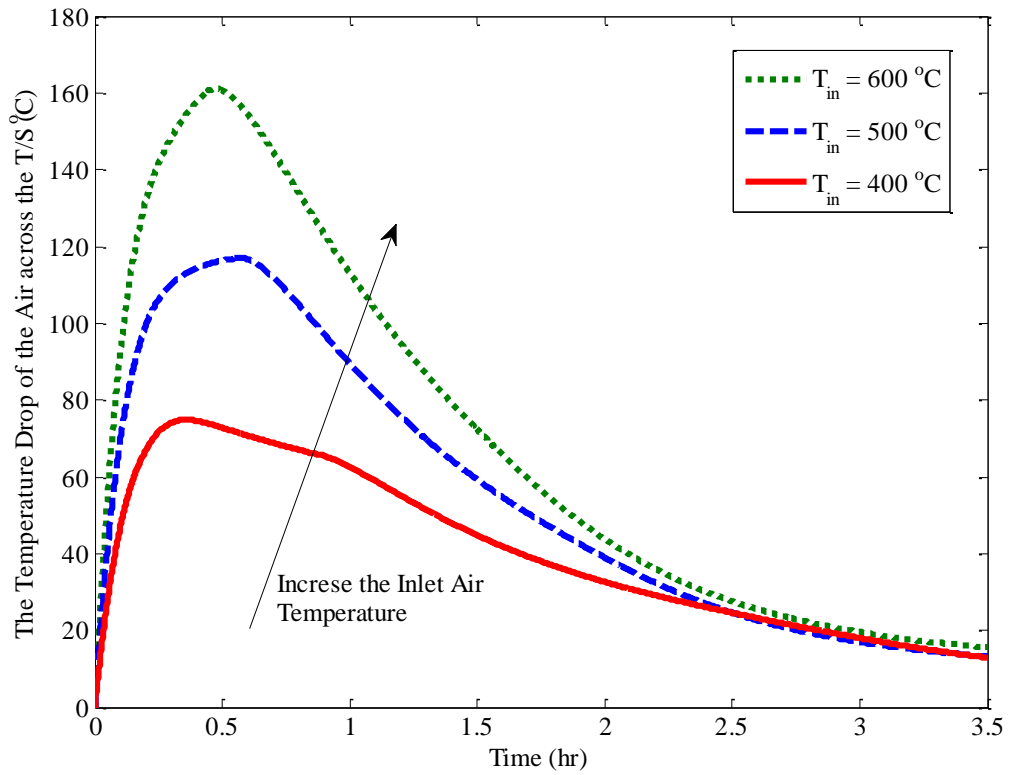
Figure 4-8. The air temperature drop across the test section with different air inlet temperatures.
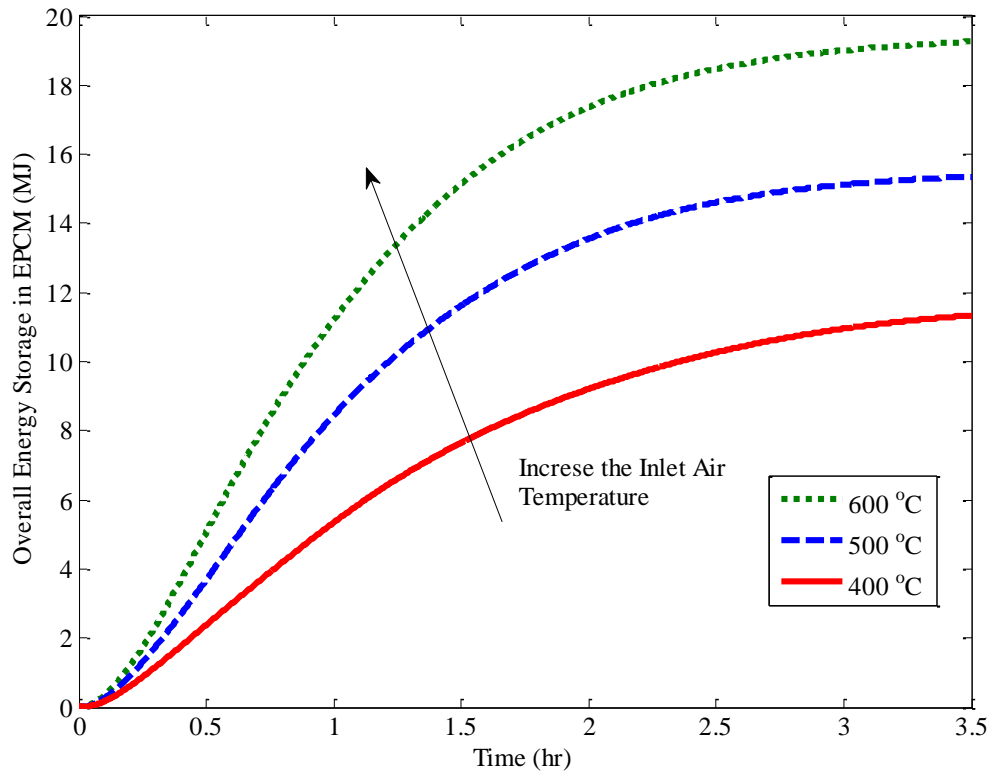
Figure 4-9. The total energy stored in the EPCM capsules with different air inlet temperatures.
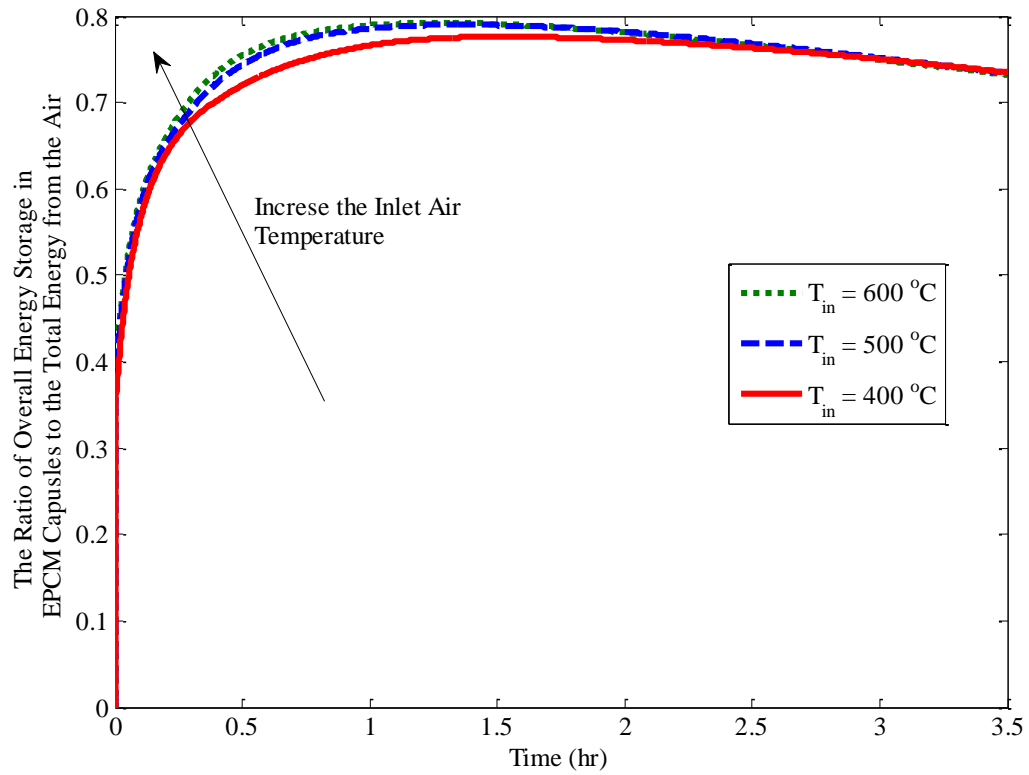
Figure 4-10. The percentage for the energy stored in the overall EPCM capsules to the total energy captured by the test section with different air inlet temperatures.
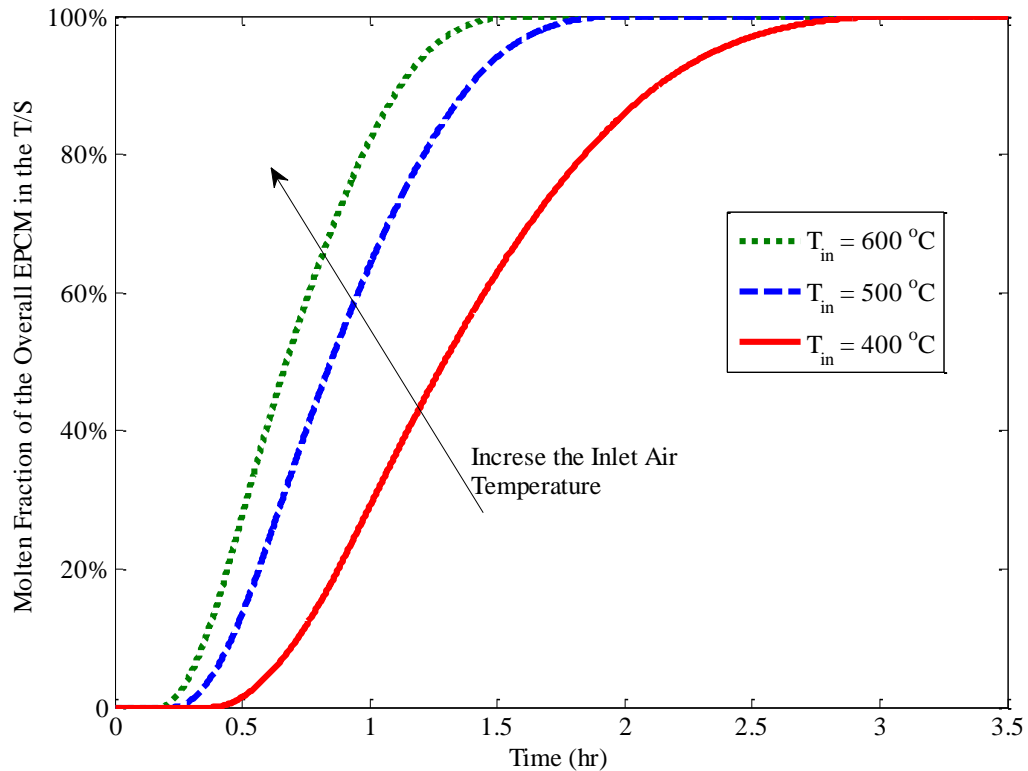
Figure 4-11. The molten fraction of the overall EPCM capsules in the test section with different air inlet temperatures.

Meanwhile, the progress of the phase change has been analyzed for the three cases with different inlet air temperatures, and the molten fraction of the EPCM is shown in Figure 4-11. It has been found that for all the three cases – with the temperature set above 400 °C, all the PCM can complete the phase change in ~ 3 hrs, and with a higher inlet air temperature, it takes a shorter time to complete the phase change in the all encapsulated PCM. However, for the cases with the set points at 600 °C and 500 °C, the phase change is already completed at ~ 1.5 hrs before the air reaches to this point as shown Figure 4-7. Since it is preferred to have the phase change happen with inlet air temperature at set point

instead of during transition period of the inlet air the temperature of inlet air is chosen to be 440 °C for testing $NaNO_3$ capsules. And for testing $MgCl_2$ - NaCl capsules, the inlet air temperature is chosen to be 540 °C following the same evaluation procedure.

▪ Diameter of the EPCM Capsule

One of the highlights of this research is placing limited amounts of the PCM in individual capsules to overcome the heat transfer issues associated with the tube-and-tank systems. By encapsulating the phase change in small-scale capsules, one minimizes the dimensional scale for conduction heat transfer paths within the PCM, and simultaneously increases the total contact area of the capsules for convective heat transfer with the HTF. The ideal dimensions for the capsules can be optimized to reduce conduction resistance within the PCM and to enhance external convective heat transfer between the capsules and the HTF. With the properties of the PCMs and HTF used in the current project, the simulation model has been run to analyze the effects of the capsule diameter and the results are shown from Figure 4-12 to Figure 4-16.

In this simulation model, the diameters of 5.1 cm, 7.6 cm and 10.1 cm have been discussed as the choices for the cylindrical EPCM capsules in the test section. All of the three cases (with different diameter sizes for capsules) are considered to be operated under same inlet air temperature just as shown in Figure 4-12. The temperature drop of the air is shown in Figure 4-13 for the three cases with different diameters for the capsules. It is seen that with a larger diameter for the EPCM capsules, the temperature drop of the air is higher

75

considering that the overall mass of the storage medium in the test section is larger in capturing the energy from the air. On the point of view of the convective heat transfer from the air to the EPCM capsules, the surface areas of the capsules are larger for larger size capsules; therefore the temperature drop of the air is larger when the diameter of the capsule is large. In other words, in design of the test section, it is preferred to have a large diameter for the EPCM capsules.
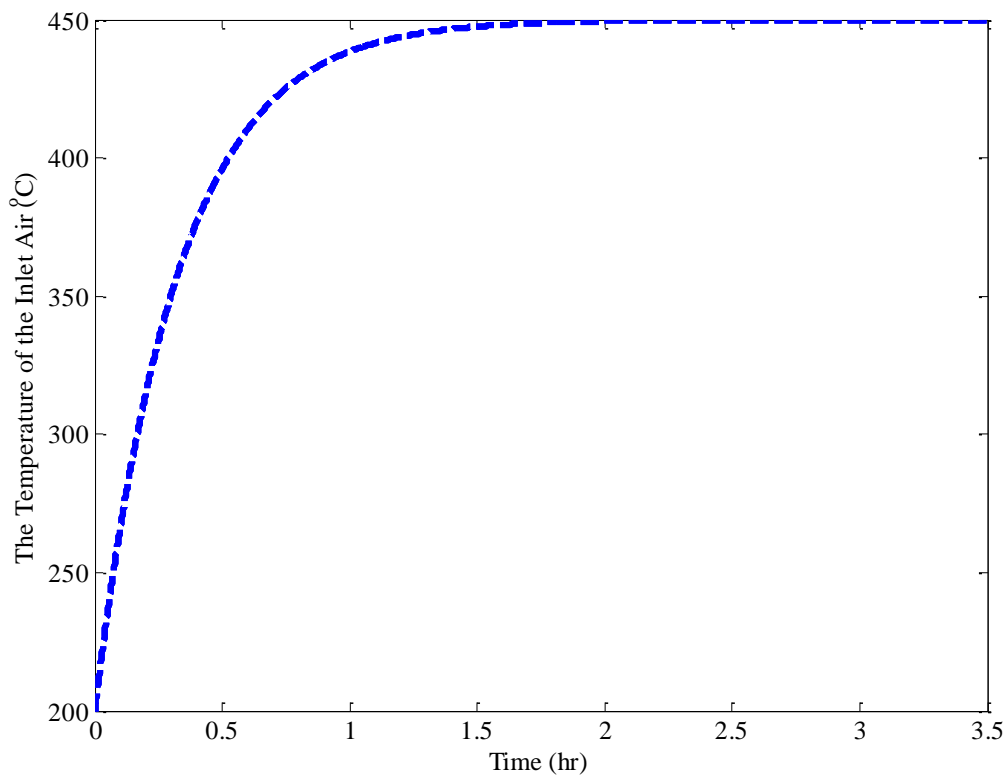
Figure 4-12. The temperature of the air at the inlet in analyzing the effects of capsules diameters on the performance of the test section.
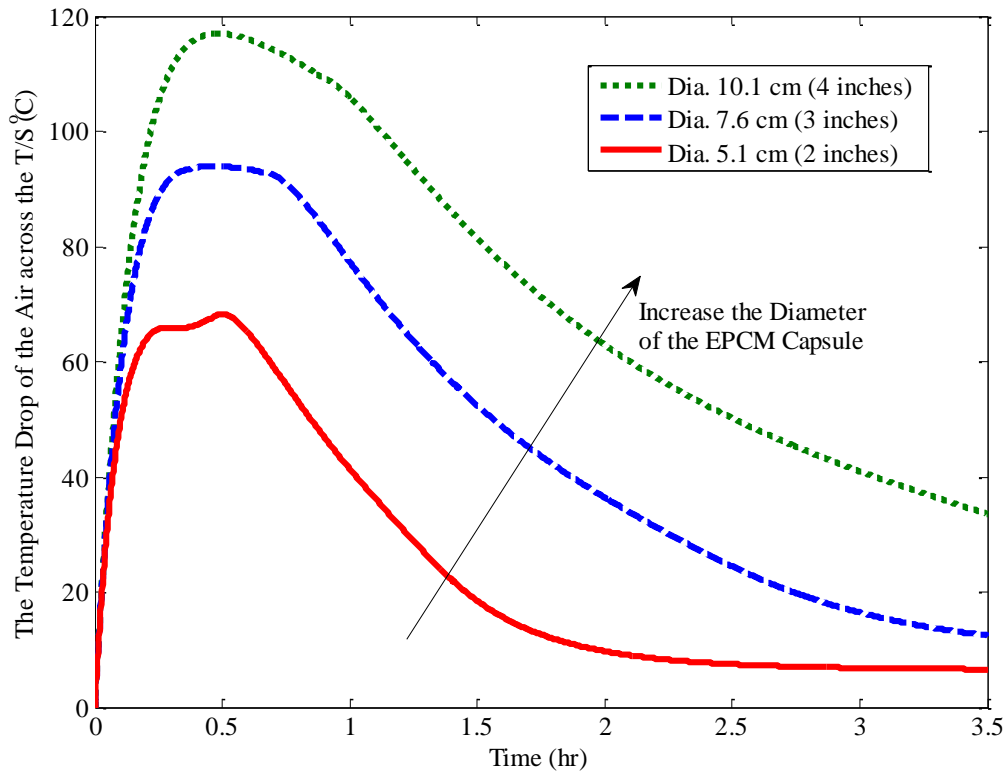
Figure 4-13. The air temperature drop of the air across the test section for different diameters of the EPCM capsules in the test section.

Since the number of the capsules in the test section is the same between the cases with different diameters for EPCM capsules, the test section will have more mass of the storage medium with a larger diameter. Therefore as shown in Figure 4-14, the total energy stored in the EPCM is higher with an increasing diameter for the capsules. Meanwhile, with a larger diameter for the EPCM capsules, the ratio of the overall thermal mass of the EPCM to the thermal mass of the other components in the test section (i.e. insulation and test section chamber) would be larger. Therefore the ratio of the total energy stored in the EPCM capsules increases with increasing diameter size for the capsules just as shown in

77

Figure 4-15. In other words, from the point of view of a large contribution of storage

medium in energy storage, it is preferred to have a large diameter for the EPCM capsules.
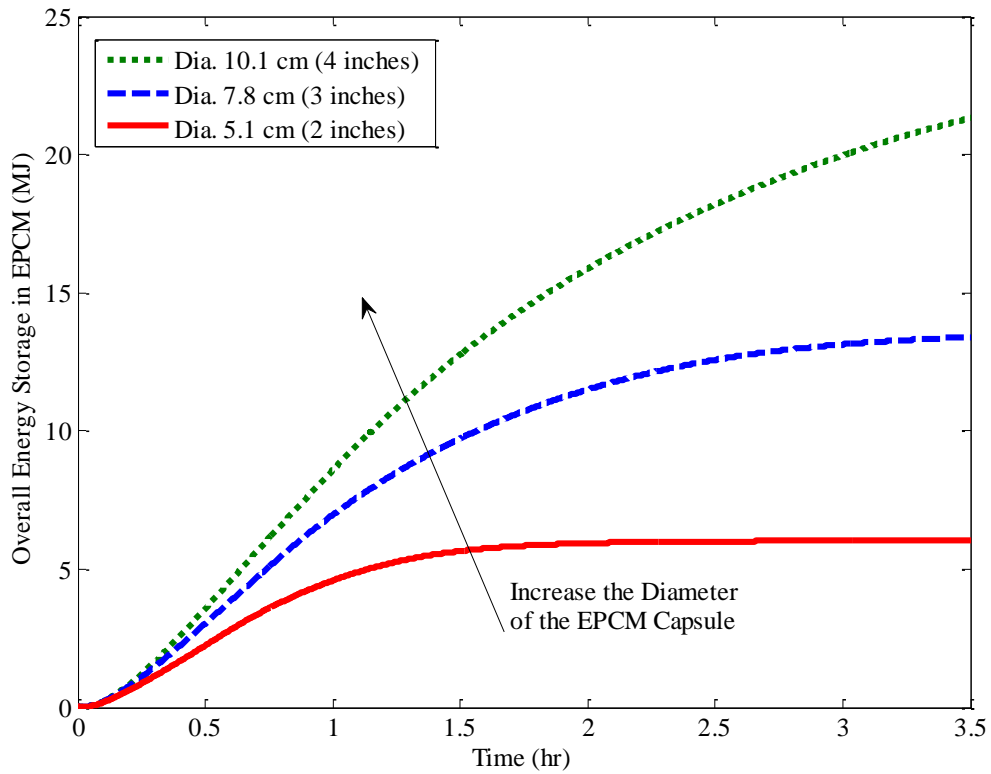
Figure 4-14. The total energy storage in the EPCM capsules with different diameters for the capsules.
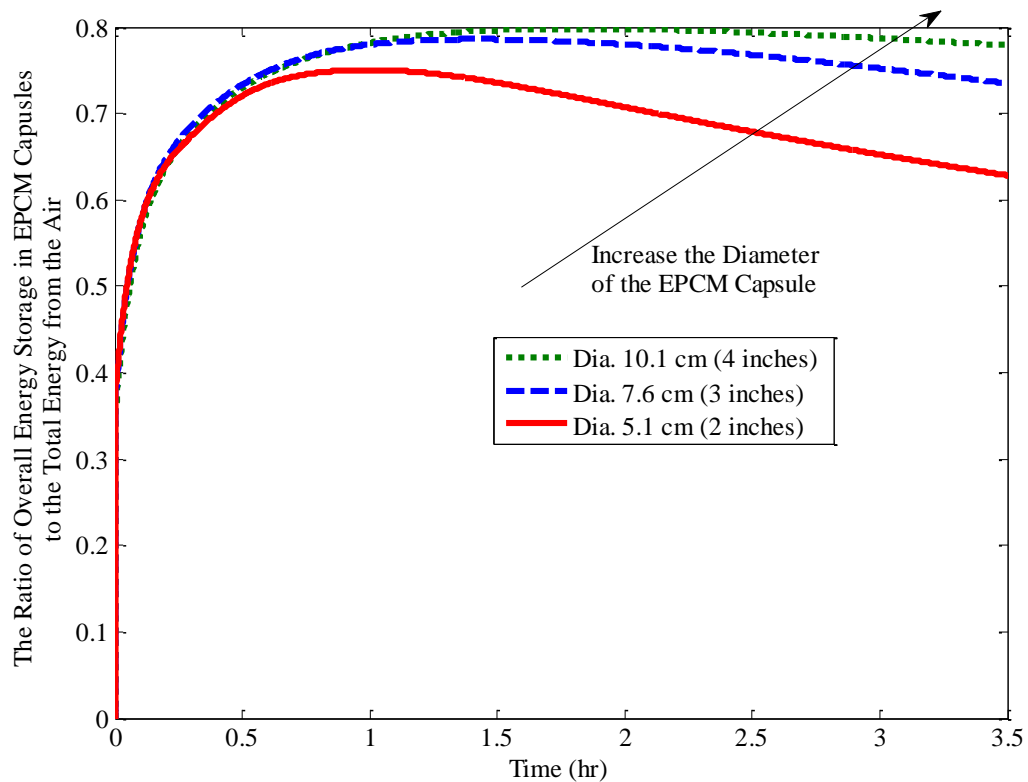
Figure 4-15. The ratio of the energy stored in the EPCM capsules to the total energy from the air for the test sections with different diameters of EPCM capsules.

However, with a larger diameter of capsule, it takes a longer time for the phase change considering that there is an increase in thermal mass for heat transfer and the PCM itself is a low-conductive material. As shown in Figure 4-16, for the case of 10.1 cm diameter, it takes about 3.5 hrs for the EPCM to complete the melting during a charging process, while for the case of 5.1 cm diameter, it takes about 1 hr for the EPCM to complete the phase change. Through carefully analyzing multiple diameter options and manufacturing costs, the size of the cylindrical stainless steel capsules are selected to be constructed with a diameter of 7.6 cm (3 inches), and a length of 25.4 cm (10 inches). Furthermore,

considering the significant thermal expansion [48,62], which is ~ 25% volume change for the NaNO$_3$ for temperature change from room temperature to 440 °C, approximately 30% void space is left in the NaNO$_3$ capsule as an allowance for its thermal expansion.
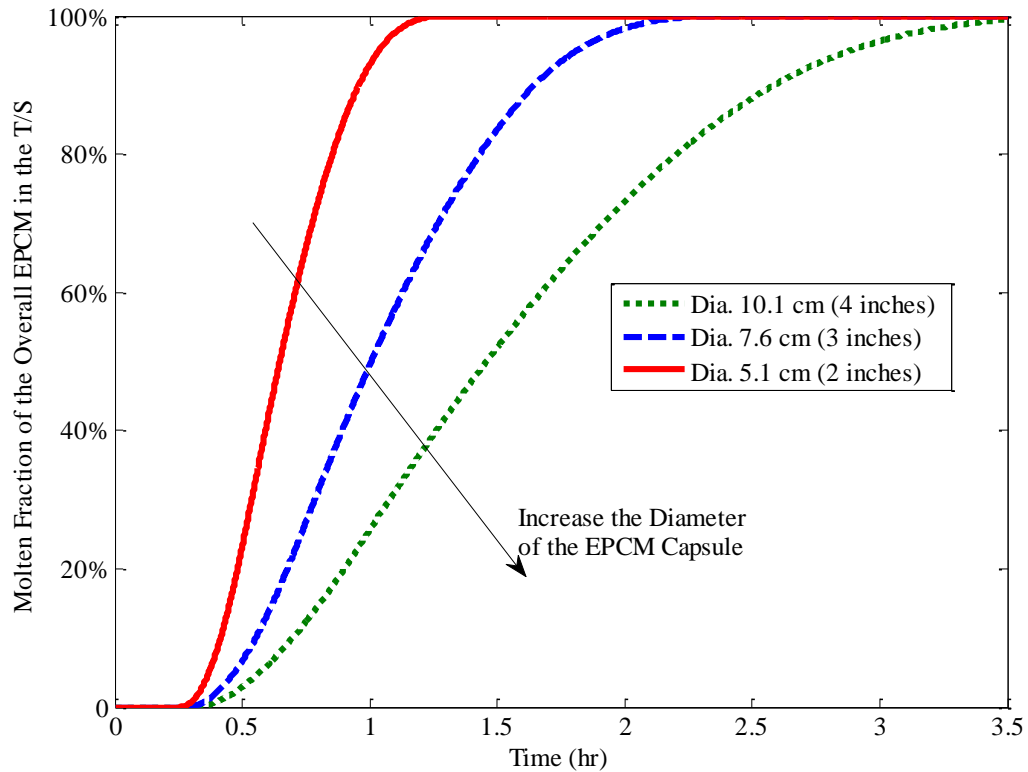
Figure 4-16. The molten fraction of the overall EPCM in the test section with different diameters of the capsules.

- Number of EPCM Capsules.

After we decided the diameter for the EPCM capsules, it is necessary to determine the number of the EPCM capsules to be loaded in the test section for the demonstration purpose. To be an effective pilot-scale demonstration, there will be multiple EPCM

capsules in the test section, in which the EPCMs are subjected to thermal charging and discharging by an air flow with varying conditions, such as temperature, along the test section. In that case, this project can be a good representative and ready for scale-up for further large application. In order to determine the appropriate number for the EPCM capsules in current test facility, the simulation model has been run with different numbers of the capsules in the test section.

Figure 4-17 shows the total energy stored in the EPCM capsules when there are different numbers of capsules in the test section, i.e. 5 capsules, 10 capsules and 15 capsules. As shown in the figure, the total energy captured by the capsules increases with an increasing number for the capsules, and obviously it is because of the larger mass of the storage medium with more capsules in the test section. At the end of 3.5 hrs, it is seen that the total energy stored in the capsules are about proportional to the number of the capsules in the test section. For a less number of capsules, like the case with 5 capsules, the energy storage of capsules is quickly approaching to its "saturated" point, or steady state within ~ 2.5 hrs, then the rate of energy storage slows down because of a decreasing temperature drive from the air to the overall capsules. While for the test section with more capsules, it will take a longer time for the energy storage of the EPCM capsules to reach to its steady state as shown by the cases of 10 capsules and 15 capsules in Figure 4-17.

Figure 4-18 shows the ratio of the energy stored in the EPCM capsules to the total energy from the air with different numbers of the capsules in the test section. It is seen that the

effect of the numbers of the capsules is quite small to this ratio. With current design of the

test section, the energy stored in the EPCM capsules can be ~ 80% for all the three cases.
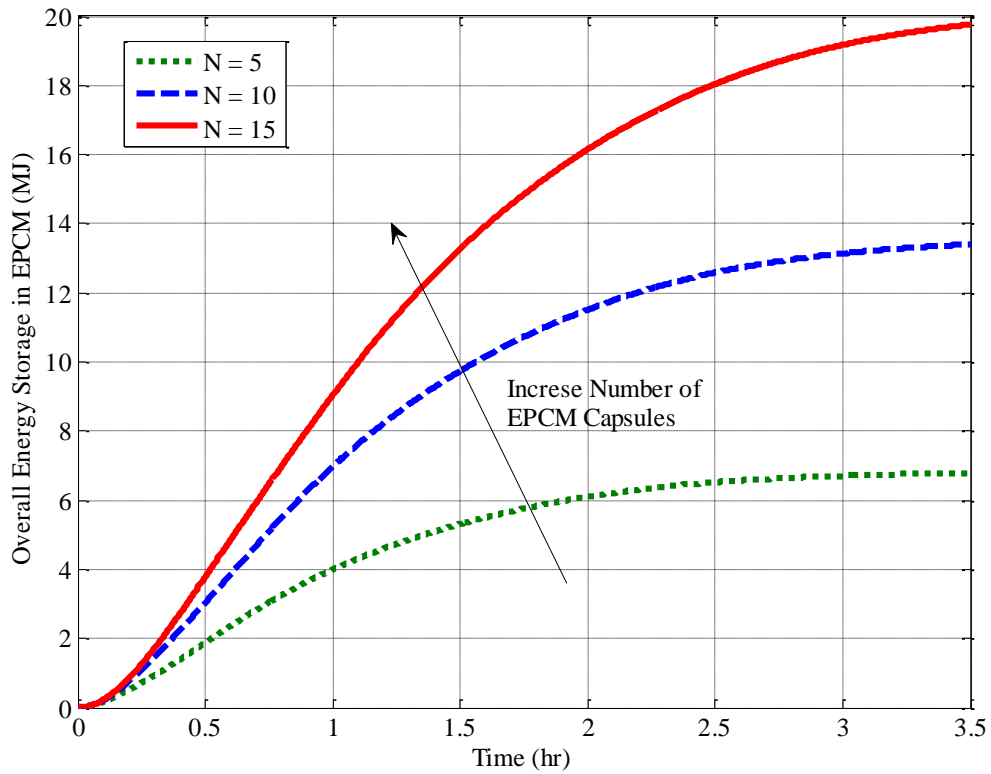
Figure 4-17. The total energy stored in the EPCM capsules with different numbers of the capsules in the test section.
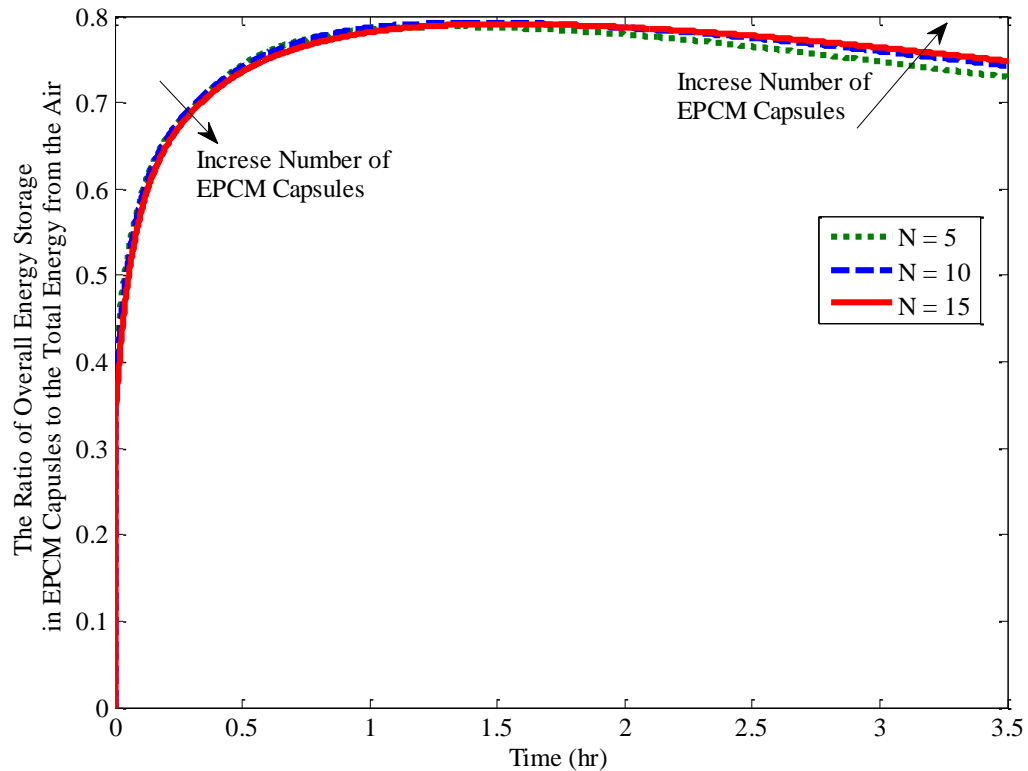
Figure 4-18. The ratio of the total energy stored in the EPCM capsules to the total energy from the air with different numbers of capsules in the test section.

Figure 4-19 shows molten fraction of the encapsulated PCM in the test section with different numbers of the capsules in the test section. It is seen that with more capsules in the test section, it will take a longer time for all the EPCM to complete the phase change. For the test section with 15 capsules, it will take ~ 2.5 hrs for the PCM to melt completely, while for the test section with less capsule, 5 capsules, it will reduced to ~ 1.8 hrs for the PCM to melt completely. This difference about the time for phase change is not very significant compared with the effects of diameters as shown previously in Figure 4-16.

During a charging process of the test section, the hot air flows into the test section at the inlet, and the air temperature will drop along the test section since its energy is transferred to the EPCM capsules and T/S chamber. Therefore, with more capsules in the test section, the air temperature at the outlet will be cooler. As shown in Figure 4-20, the air temperature drop across the test section is higher with more capsules in the test section. Therefore, to minimize the errors in determining the total energy from the air with these temperature difference measurements, it is preferred to have more capsules loaded in the test section. Considering the fabrication cost associated with the EPCM capsules, the test section is chosen to be loaded with 10 capsules.
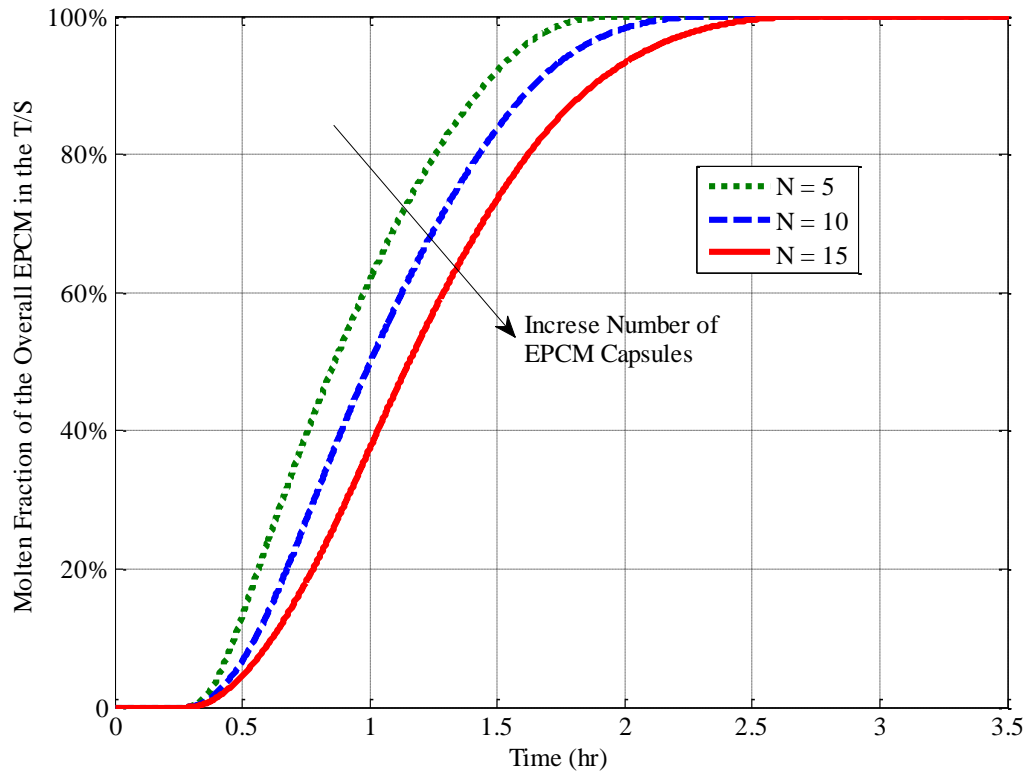
Figure 4-19. The molten fraction of the overall EPCM capsules in the test section with different numbers of capsules.
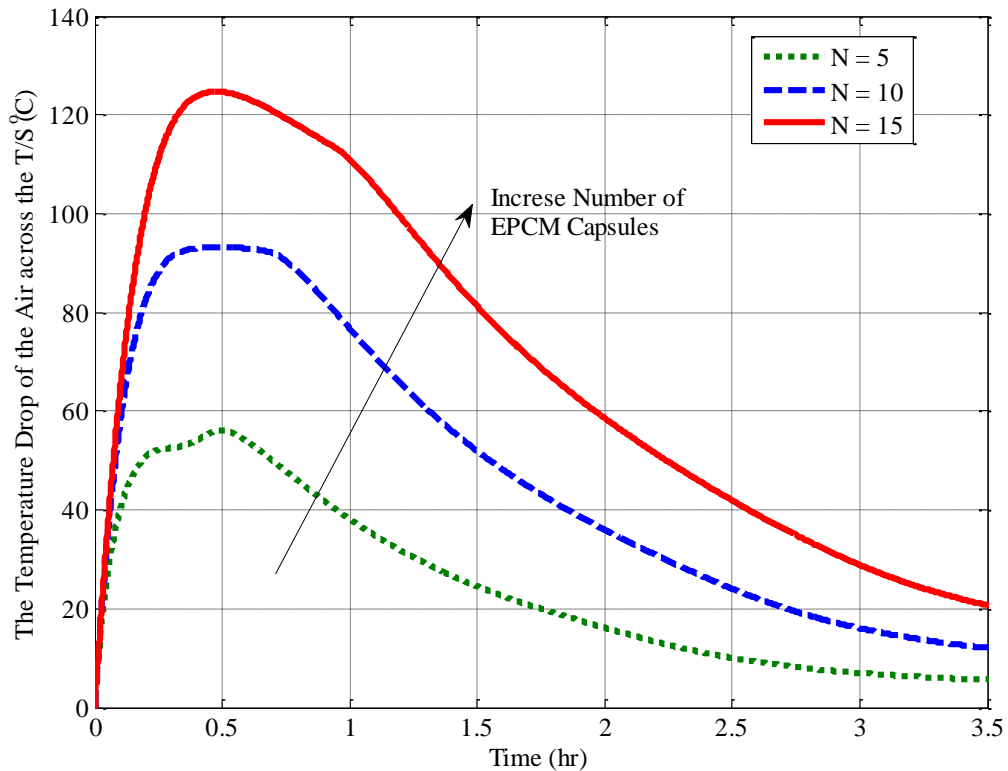
Figure 4-20. The air temperature drop across the test section with different numbers of EPCM capsules.

- ▪ Thickness of the Insulation in the Test Section.

Since the surface of the test section will be at high temperatures up to 550 °C, the test section is insulated externally by layers of insulation to reduce the heat losses to the ambient, but meanwhile some of the energy will be captured by the insulation itself. With thicker insulation, the temperature at the outside surface of the insulation will be smaller and the heat losses to the environment will be smaller, however, the energy stored into the insulation will be larger with the more mass for the insulation and vice versa. Therefore it is necessary to evaluate the effects of the thickness of the insulation and determine an

appropriate thickness for the insulation for desired performance.

Figure 4-21 shows the predicted temperature and heat flux at the outside surface of the insulation in the mid-height of the test section with different thicknesses of the insulation. It is seen that with a thicker insulation, the temperature at the outside surface of the insulation is lower because of the thermal energy captured by the insulation itself and thermal resistant for heat transfer, and the heat flux to the environment is smaller because of the smaller temperature difference between the ambient and outside surface of the insulation. As seen in the figure, when the thickness of the insulation is 5.1 cm (2 inches), the outside surface temperature can reach up to ~ 110 °C and the heat losses is ~ 420 W/m^2. If the insulation thickness increases to 20.3 cm (8 inches), the outside surface temperature is barely change compared with its initial state, and the heat flux is about 70 W /m^2. It is also found that the outside surface temperature and the heat flux decreases slightly at the very beginning of the simulation. As described previously, this simulation has been run with the initial conditions that the inside surface of the insulation, that is the surface of T/S chamber, is at 200 °C, and with the assumption of a linear temperature profile in the insulation with the heat losses to the ambient (25°C). This condition dictates an outside surface temperature of ~ 40 °C at the start of the test. Then with a hot air charging the test section, there is a continuous heat conducted through the insulation from the inside surface to the outside surface. Due to the relatively quicker convection loss on the outside surface compared to low thermal conduction from the inners of the insulation at this outside surface location at the very beginning, the temperature of the surface, and the heat flux at this

87

location drop down slightly at the very beginning, and with more heat conducted from the inside insulation, they start to increase as shown in the figure.
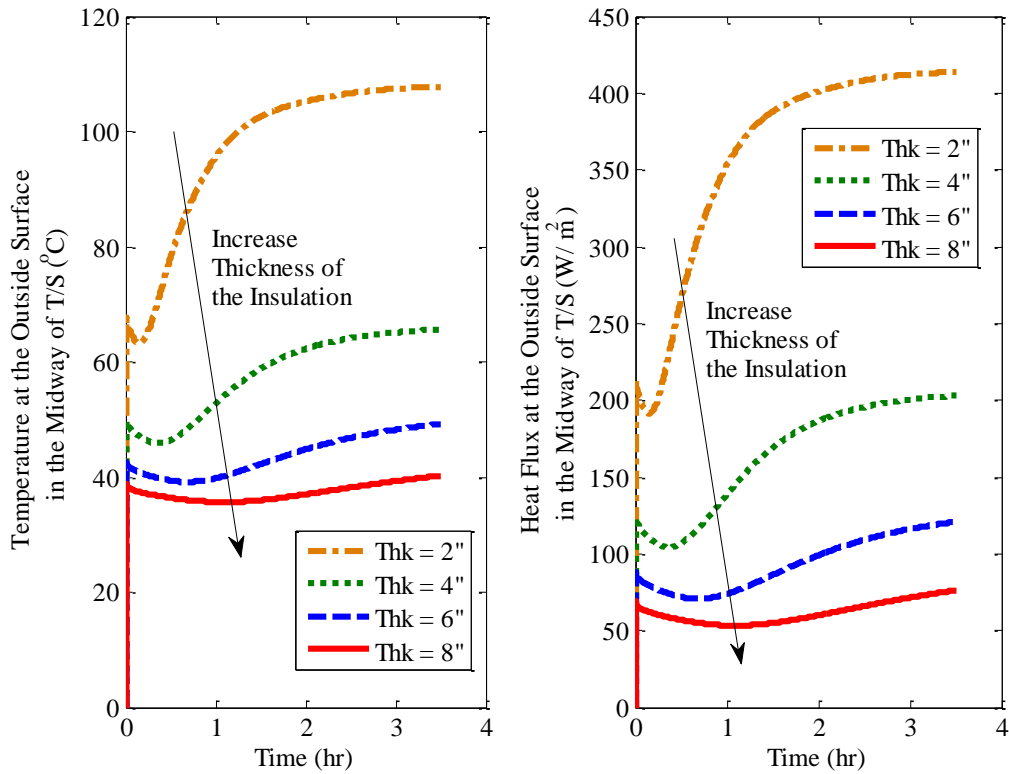
Figure 4-21. The temperature and heat flux at the outside surface of the insulation in the midway of the test section with different thicknesses of insulation.

With the information of insulation temperature as shown in Figure 4-21, the total energy stored in insulation is calculated with such temperature information in all other locations in the insulations. With the information of the heat flux per unit area of outside surface, the total heat losses is calculated by integrating the heat flux over the simulation time. And the results are shown in Figure 4-22. It is seen that the total energy stored in the insulation

increases with increasing thickness of the insulation because of its higher mass and higher temperatures, while the total heat losses decrease with increasing insulation thicknesses because of smaller temperature differences from the outside surface to the ambient.
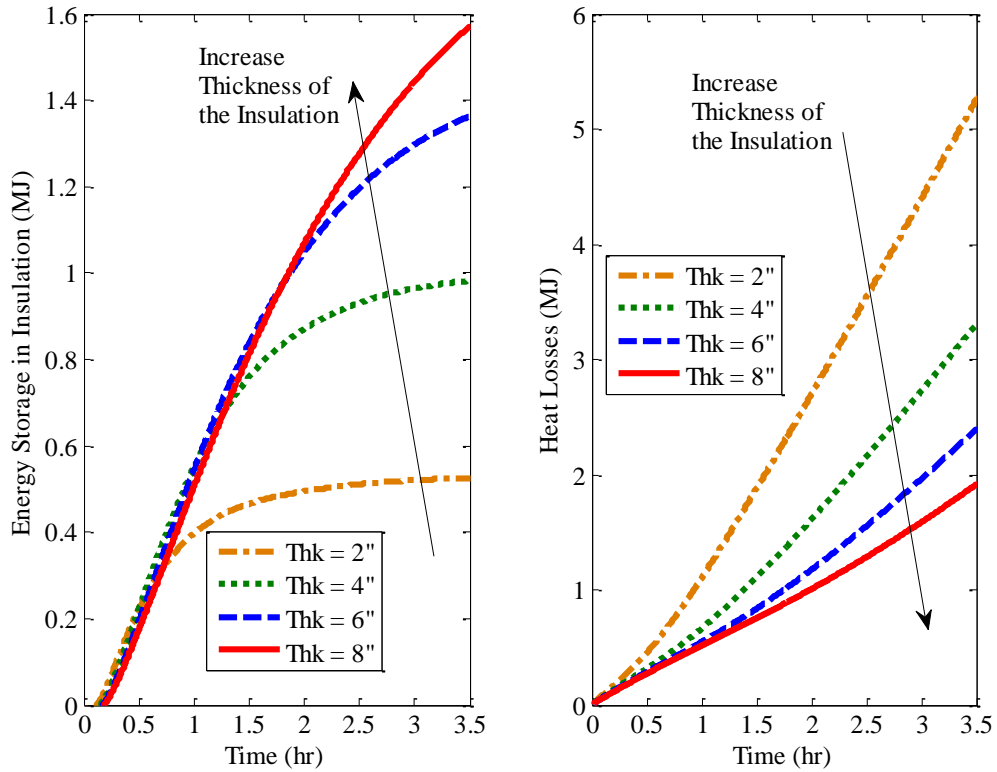
Figure 4-22. Energy stored in the insulation and the heat losses at the outside surface of the insulation for the test section with different thicknesses of insulation.

In order to find the thickness of the insulation on the energy storage of EPCM capsules, the total energy stored in the EPCM capsules is calculated by energy balance and shown in Figure 4-23. As seen in the figure, the energy stored in EPCM capsules are very close between the cases with different thicknesses changing from 5.1 cm (2 inches) to 20.3 cm

(8 inches). As a result the molten fraction of the EPCM is barely affected by the different thicknesses of the insulation in the T/S neither. In other words, the effects of the insulation thickness can be negligible on the total energy stored in the EPCM capsules, and the progress of the phase change of the EPCM in the T/S.
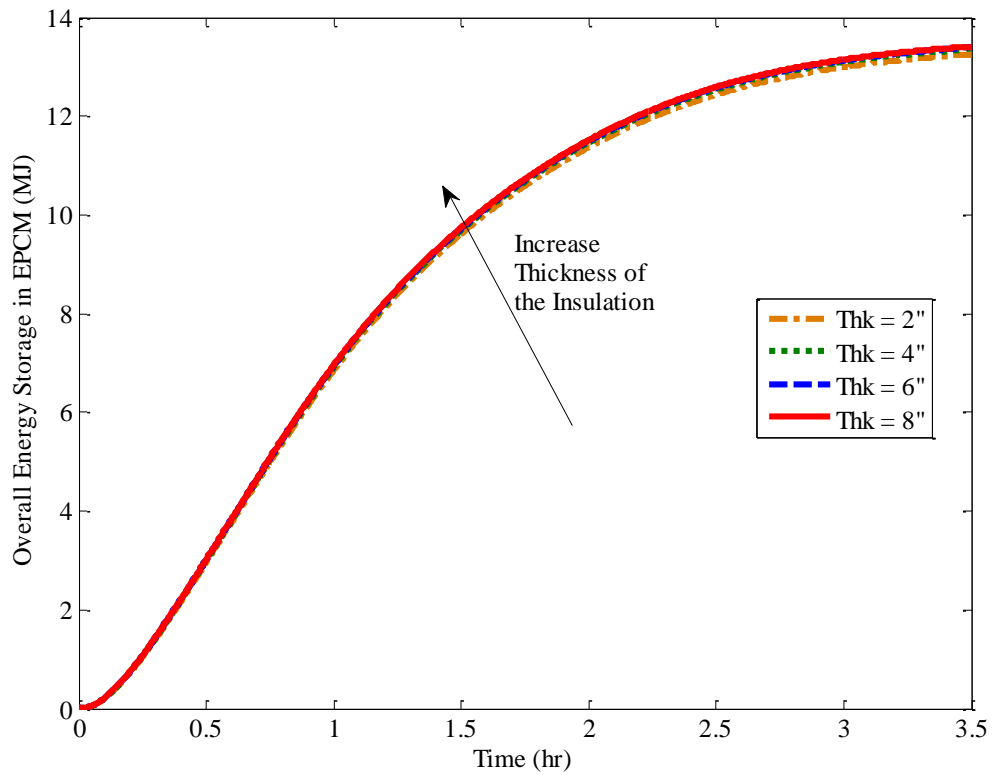
Figure 4-23. The total energy stored in the EPCM capsules in the test section with different thicknesses of insulation.
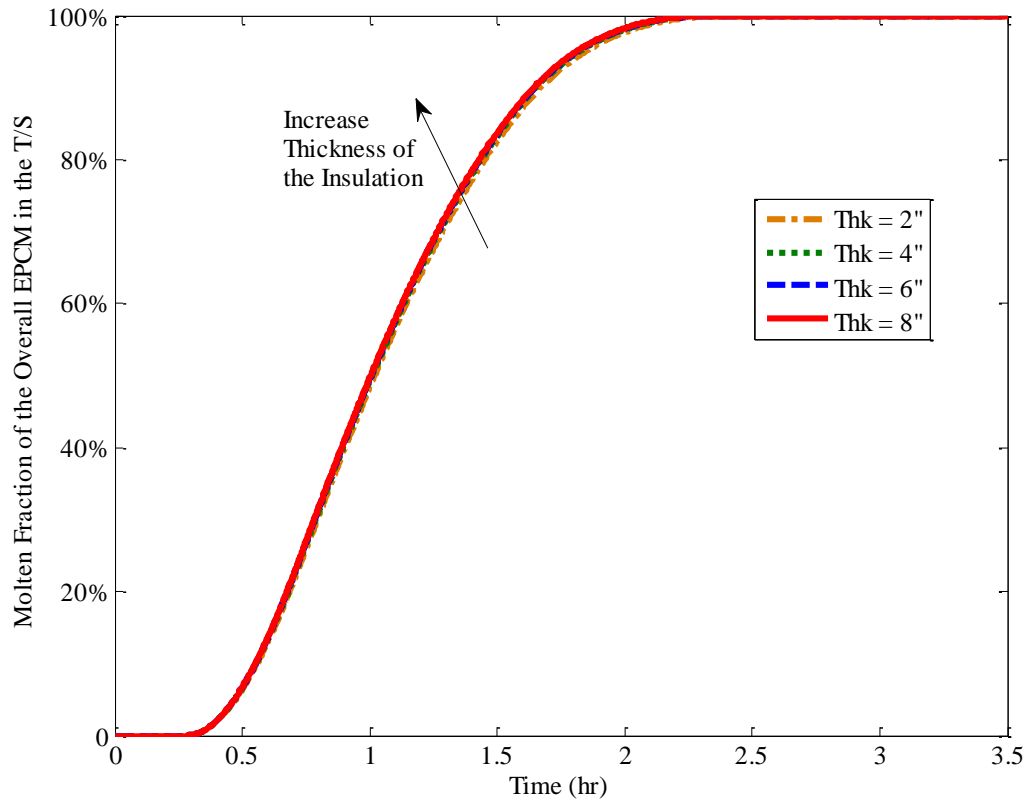
Figure 4-24. The molten fraction of the EPCM in the test section with different thicknesses of insulation.

Figure 4-25 shows the ratio of the total energy stored in the EPCM capsules to the total energy from the air. This information is to combine the effects of the insulation on the heat losses and the energy storage of the insulation, since the total energy from the air is equal to the energy captured by the test section, which includes the energy stored in the EPCM capsules, in the T/S chamber, in the insulation and heat losses to the ambient. As seen in the figure, this ration would increase by 10% when the insulation thickness increase from 2 inches to 8 inches. The reason for this trend is because the total energy captured by the test section increase with the increasing thickness of insulation while the total energy stored

in the EPCM is barely changed as shown previously in Figure 4-22 and Figure 4-23. Therefore, it is preferred to have a thicker insulation considering a higher percentage of the energy will be captured by the EPCM capsules.
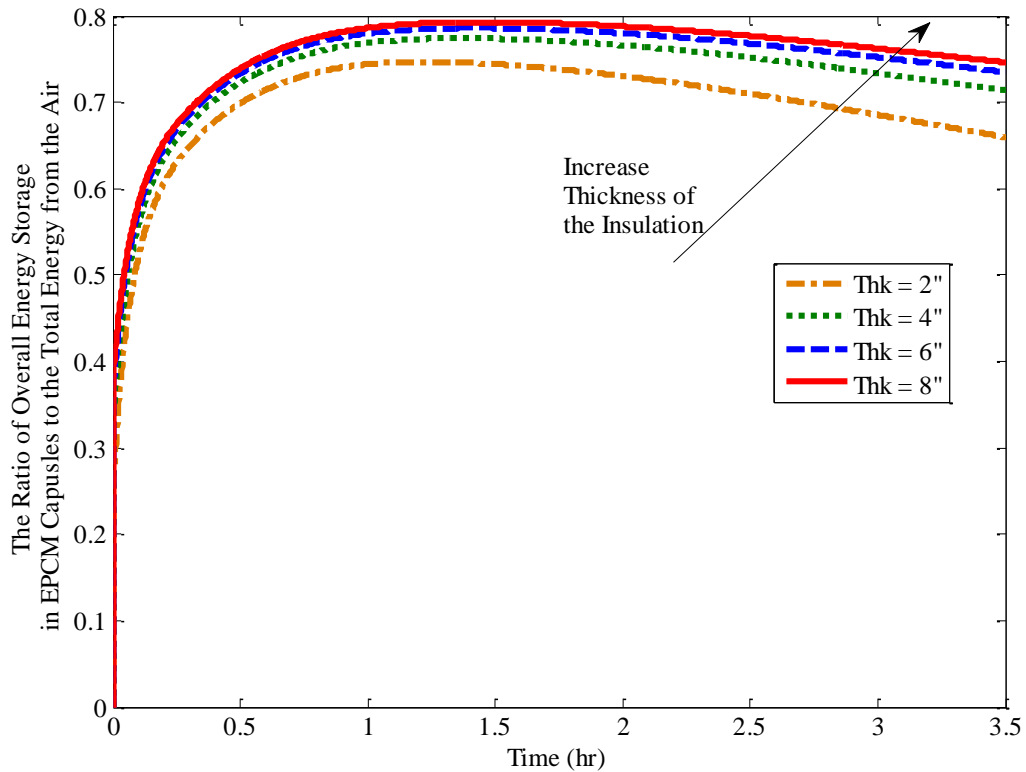
Figure 4-25. The ratio of the energy stored in the overall EPCM capsules to the total energy from the air in the test section with different thicknesses of insulation.

However, with a thicker thickness of the insulation in the test section, the air temperature drop across the test section is smaller as shown in Figure 4-26, because of the more energy captured by the test section. Therefore, after carefully consideration of the all the effects, it has been decided to have a 15 cm (6 inches) thick insulation for the test section.
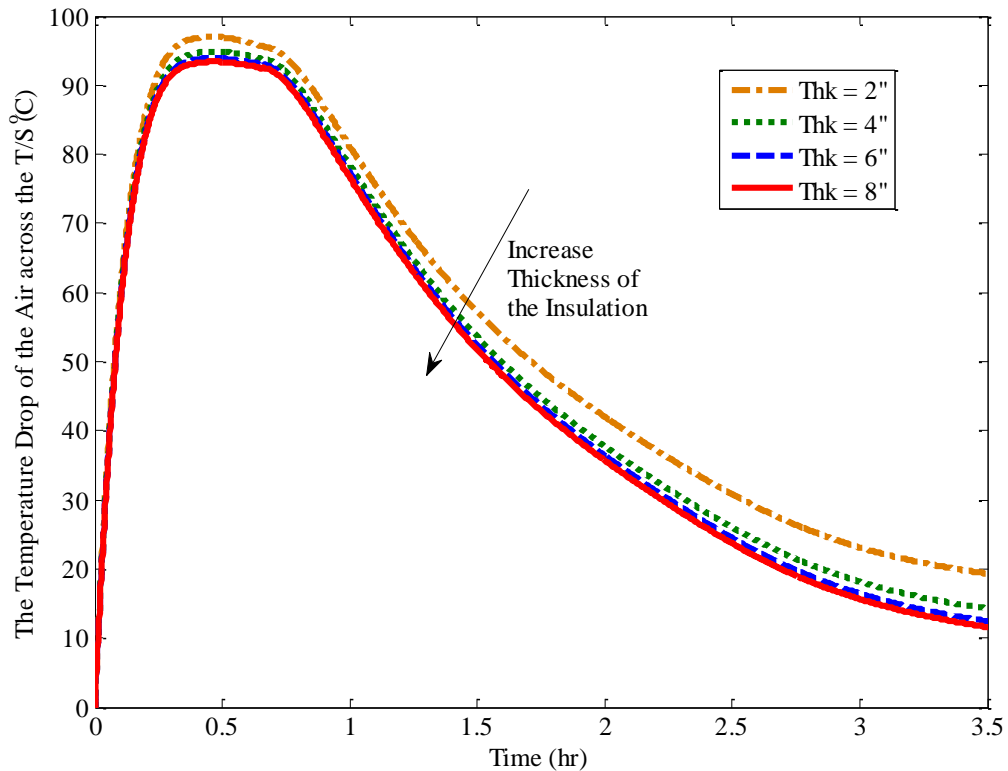
Figure 4-26. The air temperature drop across the test section with different thicknesses of insulation.

4.2   Methodology for Energy Measurements in the EPCM based TES System

The general layout of the test facility is shown in Figure 4-27. The key component of the

test loop is the vertical test section with ten EPCM capsules. The chamber of the test section

is fabricated in rectangular, with a height of 111.8 cm, a width of 9.3 cm and a length of

26 cm. It is made of stainless steel 304 with a thickness of 3.175 mm which is chosen so

that the relatively narrow T/S is strong enough to stand up without an external support. It

is thin enough so that the thermal residue stored in it is minimized in the thermal charging

and discharging process. The gap between the T/S surface and capsules is 8.3 mm, which has been minimized within the fabrication capabilities to provide a good contact area for the heat transfer between the HTF and the capsules. In the test section, the ten EPCM capsules are separated into two stacks, with five capsules in the top section and the other five capsules in the bottom section as numbered #1 to #10. In each stack, the capsule is horizontally orientated and sits on the lower one with their special-made square end plates as shown in Figure 4-28. To avoid dead zones of the HTF flow, a flow distributor, made of a porous metal plate, is installed at the inlet and at the outlet of the test section respectively, and locates before the capsule #1 and after capsule #10. Meanwhile as sketched in Figure 4-28, four thin deflectors are assembled on each capsule, to guide the HTF to flow closer to the outside surfaces of the capsules. In other words, the deflectors and flow distributors ensure a uniform HTF flow across the test section and a good surface contact for heat transfer. The overall test section is externally insulated with 15 cm thick mineral wool insulation to reduce limit energy residue captured by the insulation itself and its heat losses to the ambient.
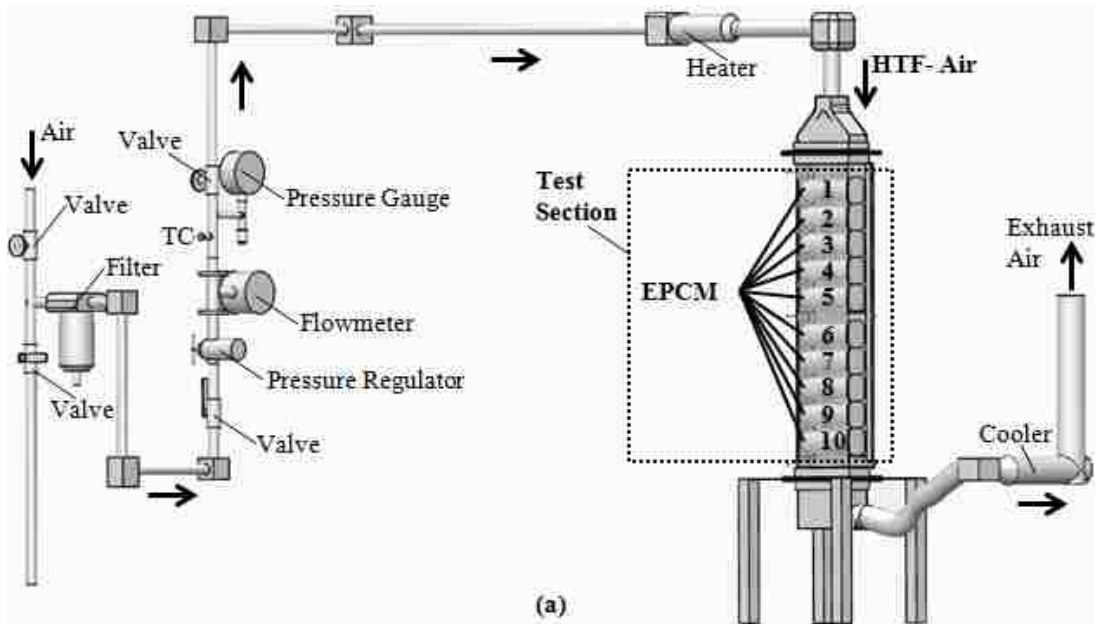
Figure 4-27. The test facility with EPCM based TES system for process demonstration. (a). schematic of the general test loop (without insulation); (b). a photo of the test section with insulation (the front insulation is removed); (c).a photo of the encapsulated NaNO3 capsules in the test section.
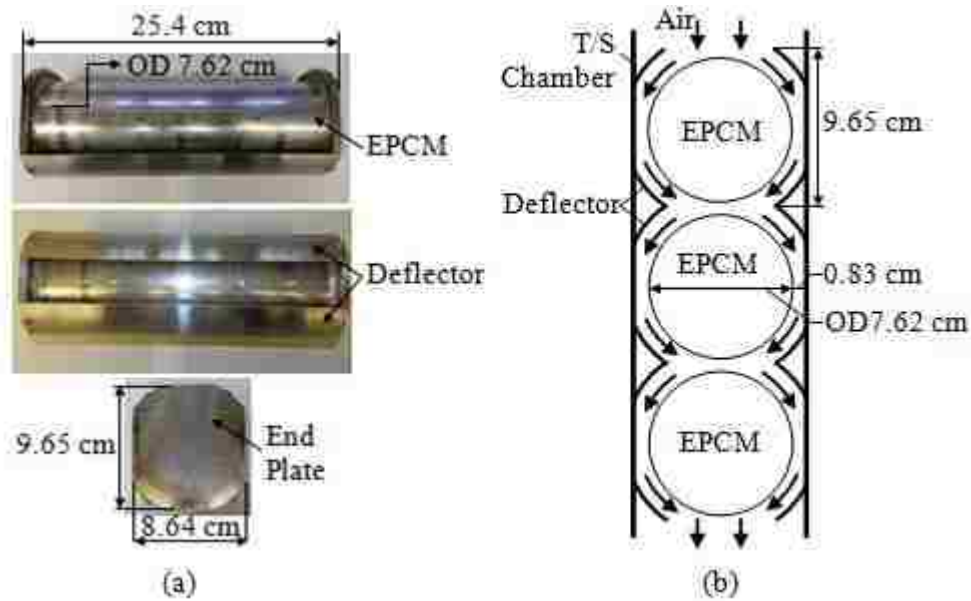
Figure 4-28. The design details about the EPCM capsule for performance test in the test section. (a). photo of a single EPCM capsule; (b). schematic of the air flow across the EPCM capsules with current designs (not at scales).

In order to charge and discharge the EPCM based test section, the air is selected as the HTF considering its chemical stability and simple sub-heating systems compared with liquid HTFs (such as synthetic oil and molten salts). In a typical charging or discharging process, the air is preheated to a selected temperature by an external electric heater which is shown in Figure 4-27(a), and flows from the top of the test section to transfer the heat to or extract the energy from the EPCM capsules. With the considerations of the expensive valves and the potential difficulties in their operations at high temperatures, the air is chosen to always be sent into the test section downwards, i.e., flow from the top of the T/S to the bottom in current demonstrations, so that a simulation model for the EPCM based test section can be verified first and capable of working further on the cases using different air flow directions. In this test facility, the air can be operated in the range of 0.01 kg/s − 0.05 kg/s for its mass

flow rate, and up to 600 °C for its temperature. To accommodate an 1- 5 psi pressure drop across the flow distributors at the inlet and at the outlet of the test section, the air is slightly pressurized with ~ 20 psig pressure before the first EPCM capsule. At the outlet of the test section, the air still possess considerable heat and is hot, therefore, a cooler is assembled with spraying water inside to cool the air to 40 – 60 °C for safety before exhausting the air to the outside.

In order to demonstrate the energy storage within and retrieval from the EPCM caspules, it is necessary to measure the total energy stored in the capsules in the charging process and the total energy extracted from the capsules in the discharging process. For the PCM salts – $NaNO_3$, and $MgCl_2$ – $NaCl$ eutectic, it is very difficult to determine its total energy change directly with temperature sensors, since it is hard to measure and identify the molten fraction or solidification fraction inside the capsules. However, the energy storage and retrieval of the EPCM capsules can be measured indirectly by subtracting the energy stored into the other components – chamber, insulation and heat losses, from the total energy from the HTF, as described below in eqn. 4-2.

$$Q_{Capsules}(t) = Q_{HTF}(t) - [Q_{Chamber}(t) + Q_{Insulation}(t) + Q_{Losses}(t)]$$
<div align="right">eqn. 4-2</div>

where t indicates the time; Q_{HTF} is the total energy exchanged between the TES system and the HTF; $Q_{Chamber}$ is the energy stored in the chamber of the TES system; $Q_{Insulation}$ is the energy stored in the insulation; and Q_{Losses} is the heat losses to the ambient at the outside surface of the insulation. And each of the energy term in the right-hand side of the eqn. 4-2

can be explored further as below for measurements,

$$Q_{HTF}(t) = \int_{t_0}^{t} \dot{m}_f(t) C_{p,f} \big(T_{f,in}(t) - T_{f,out}(t) \big) dt$$

<div align="right">eqn. 4-3</div>

$$Q_{Chamber}(t) = \sum_{j} m_{c,j} C_{p,c} \big(T_{c,t} - T_{c,t_0} \big)$$

<div align="right">eqn. 4-4</div>

$$Q_{Insulation}(t) = \sum_{j} m_{i,j} C_{p,i} \big(T_{i,t} - T_{i,t_0} \big)$$

<div align="right">eqn. 4-5</div>

$$Q_{Losses}(t) = \sum_{j} \int_{t_0}^{t} \dot{Q}_{loss,j}(t) \cdot A_{loss,j} dt$$

<div align="right">eqn. 4-6</div>

With known thermal properties of the air, T/S chamber and insulation as tabulated in Table 4-1 the amount of energy captured by the components – HTF, T/S chamber, insulation and heat losses can be determined through measuring the other parameters in the eqn. 4-3 - eqn. 4-6, and further determine the total energy storage and retrieval of the EPCM capsules by using equation eqn. 4-2.

Table 4-1. Density and heat capacity of the air, T/S chamber and insulation [52].

	Density (kg/m^3)	Heat Capacity (J/kg·°C)	Conductivity (W/m·°C)
Air	0.5	$3\times10^{-4}T(°C)^2 + 3\times10^{-2}T(°C) + 1005.1$	
Stainless Steel 304L	7900	$-0.0002T(°C)^2 + 0.3009\,T(°C) + 473.49$	15
Insulation	93*	$2\times10^{-6}T(°C)^3 - 2\times10^{-3}T(°C)^2 +1.4T(°C) +735.7^*$	0.08*

*: the density, heat capacity and thermal conductivity of the insulation were from the G.I.S, Inc.

For the total energy exchanged between the HTF and the TES system, the mass flow rates of the HTF are calculated with the measurements of its volumetric flow rate (m^3/s) before the heater with temperature and pressure compensations, as shown in Figure 4-27. Thermocouples with aspirating subsystem are specially designed to measure the high temperature air flow at the inlet and at the outlet of the TES system. This aspirating subsystem consists of a stainless steel tube to cover the air thermocouple, and a pump to aspirate a specific amount of air out of the TES system. With delicate calculations and designs, the aspirating subsystem is effective to minimize the errors in measuring the high temperature air due to the radiation loss of thermocouples tips to the chamber surface, and it is expected to have the total energy of the HTF measured within +/- 2% errors with error analysis. Though about 20% of the energy from the air is lost through the insulation in the experiment, T/Cs are located in 9 groups at selected locations and 7 depths of the insulation to establish heat transfer through the insulation, and 12 heat flux meters are located in 3 groups at selected locations to determine the heat losses at the surface of the insulation, which are generally sketched and shown in Figure 4-29. It has been found that the energy storage and retrieval of the EPCM capsules can be measured within 5% errors with the

99

measurement facilities, of which the details are discussed in the validation tests.
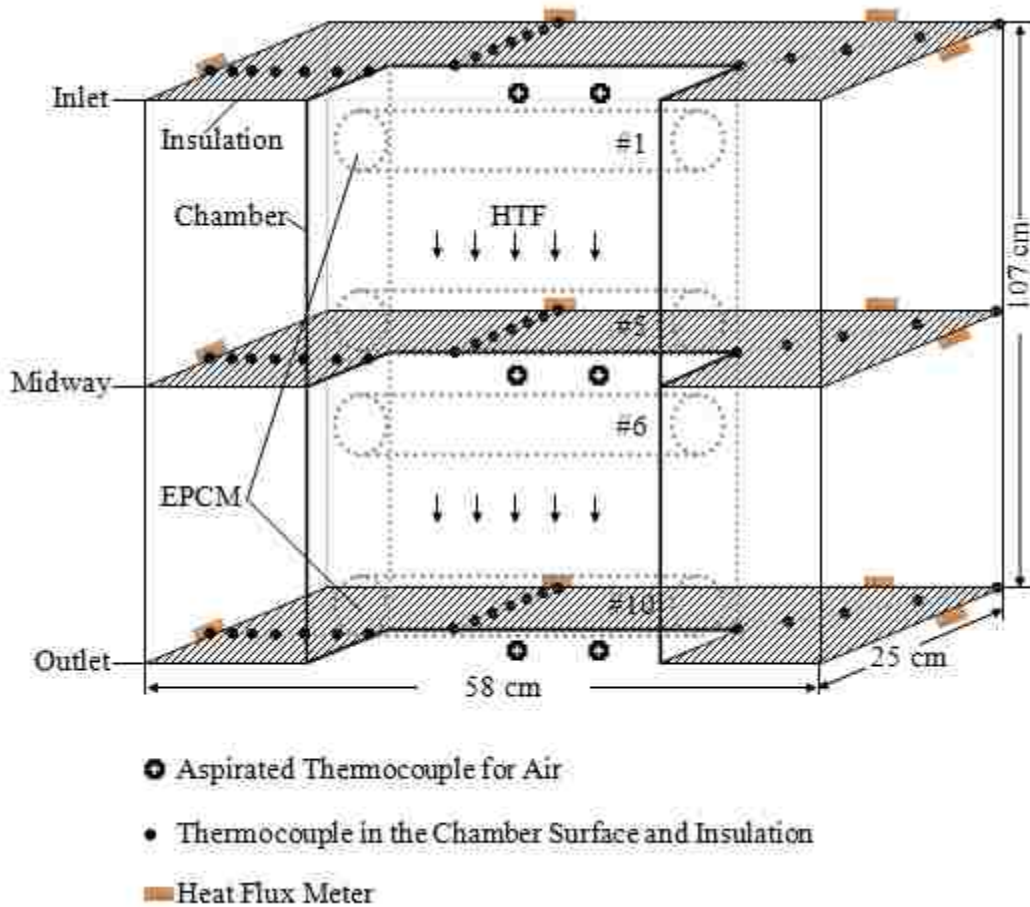
Figure 4-29. Measurement facilities in the TES system for determination of energy storage and retrieval of the EPCM capsules.

4.3 Verifications of the Experimental Methodology

As described previously, the energy storage and retrieval of the $NaNO_3$ capsules can be determined from measured data. The question followed is how reliable are those facilities for measuring the energy change of the EPCM capsules using this methodology. To address this question, measurements have been conducted using solid copper capsules. The copper

100

capsules are fabricated with the same dimensions and designs as EPCM capsules. There is a thermocouple well in the center of the capsule with a depth of the capsule radius for each of the copper capsule as shown in Figure 4-30. During the thermal tests, a thermocouple is inserted into the end of the well to measure the center temperature of the copper capsule. Through simulations, it has been found that the temperature variation is smaller than 0.1 °C in every capsule with current operating conditions and capsule sizes. Therefore, the center temperature is well representative of the average temperature of the copper for each capsule.

With known thermal properties of copper as tabulated in Table 4-2, the energy stored in the copper capsules $Q_{Copper}(t)$ can be determined by using measured temperature as

$$Q_{Copper}(t) = \sum m_c C_{p,c}(T_{c,t} - T_{c,t_0})$$

eqn. 4-7
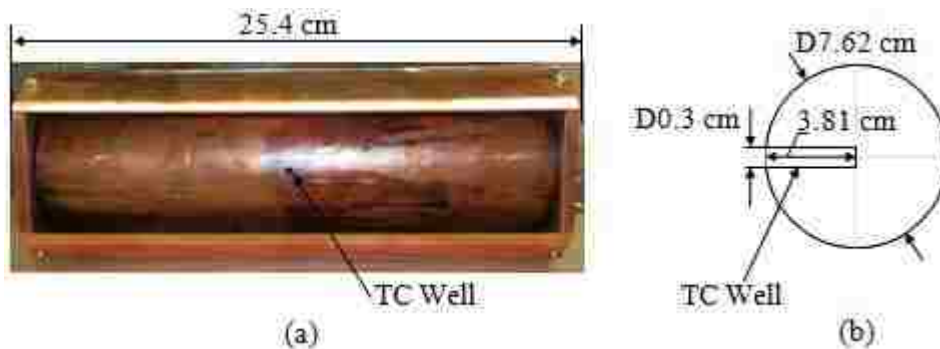
Figure 4-30. The design of copper capsule for verification tests. (a). photo of copper capsule with TC well (front view); (b). sketch of the TC well (side view, not at scale).

Table 4-2. Heat capacity and thermal conductivity of the copper [52].

	Heat Capacity (J/kg-°C)	Conductivity (W/m-°C)
Copper	$0.0963T(°C) + 384.45$	400

The energy stored in the copper capsules can also be determined from the energy balance described in eqn. 4-2 - eqn. 4-6. Examining the difference, as defined in eqn. 4-8 in the energy storage determined by these two approaches can help validating the experimental techniques utilized here.

The thermal responses for each of the components in the test section have been recorded, as shown in Figure 4-31 for the key information in a typical charging process. It is seen that the inlet air, with a mass flow rate of 0.038 kg/s, have been well maintained at high temperature 440 °C after a short transient process due to the preheating of the piping and insulation between the furnace and TES system. The temperature drop of the air across the system, that is, the temperature difference between the inlet air and outlet air, decreases with the time when the test section is being thermally charged. The #1 copper capsule near the inlet has been heated up quickly and its temperature is close to the inlet air temperature within one hour. Compared with the #1 copper capsule, the #10 copper capsule located near the outlet, is heated up slower since the air flow is cooler on the outside surface of the capsule in the lower section. At the end of the testing, the temperatures of the ten copper capsules are in the range of ~ 360 °C - 425 °C, and with about 65 °C temperature difference between the capsules near the inlet and near the outlet. Besides the temperature history of

the copper capsules and air flow, Figure 4-31(c) also shows an example for a group of insulation temperature from the outside surface of the T/S chamber to the outside surface of the insulation at the midway of the test section. It is seen that the temperatures of the insulation increase following the similar trend as the copper capsule's, with the surface of the chamber at ~ 380 °C and the outside surface of the insulation slightly higher than room temperature at the end of this charging process. For the heat flux at the outside surface of the insulation, it is seen that it increases from ~ + 2 W/m^2 to ~ + 12 W/m^2 in Figure 4-31 (d). The positive sign means that the heat losses are from the insulation surface to the ambient.

$$\text{Discrepancy} = \frac{Q_{copper,energybalance}(t) - Q_{copper,temp.measurement}(t)}{Q_{copper,temp.measurement}(t)}$$

eqn. 4-8
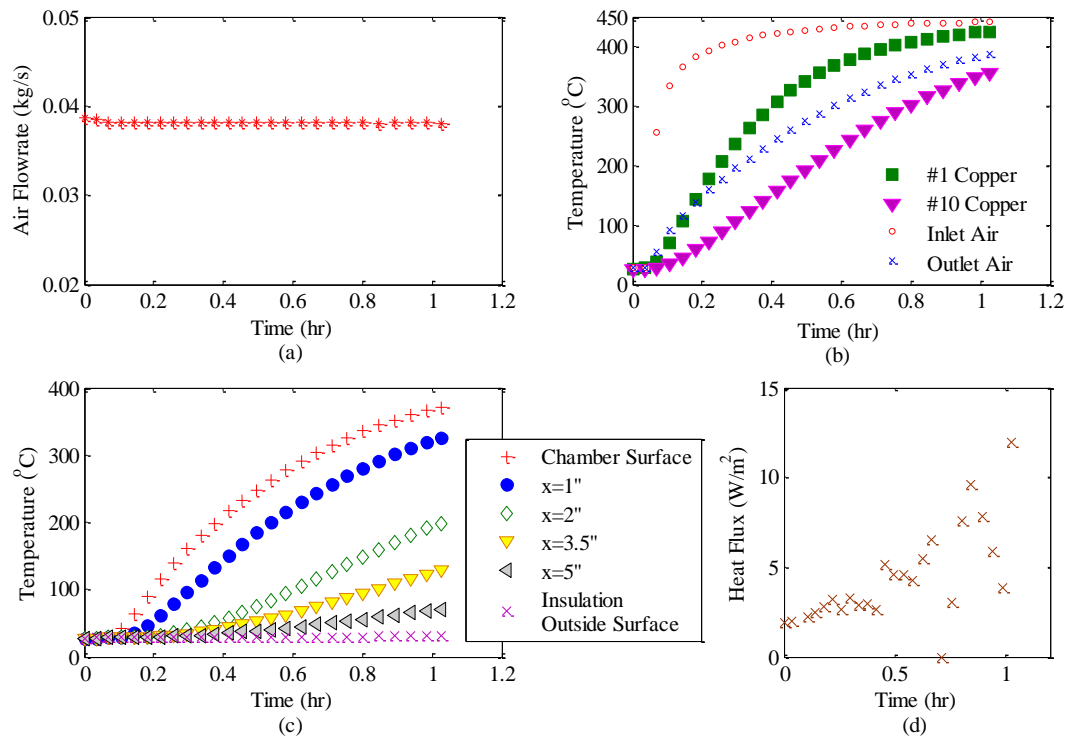
Figure 4-31. Key information for a verification test with copper capsules in a typical charging process. (a). mass flow rate of HTF – air; (b). temperature history of the copper capsules and air; (c). insulation temperatures from chamber surface to outside surface at midway of the test section; (d). heat flux on the outside surface of the insulation at the midway of the storage system.

The air mass flow rates, and its temperature drops across the test section are integrated over the time to calculate the total energy from the air as indicated in eqn. 4-3. The temperatures at the outside surface of chamber are used to calculate the energy captured by the test section itself, with the assumption of a linear temperature change along the elevation direction. The energy residue in each layer of the insulation has been calculated with the assumptions of linear temperature change between the measurements of the two layers and along the elevations directions. The heat losses at the outside surface are calculated by integrating the heat flux over the experimental time for a certain surface area with the

104

assumption that a uniform heat flux (W/m^2) in this area. The total energy from the air, the energy stored in the chamber and insulation, and the heat losses are shown in Figure 4-32(a) in the charging test with copper capsules. From this figure, it is seen that at the end of the experiment, there is ~ 22 MJ energy transferred from the air to the overall test section, of which ~ 20% is stored into the chamber and insulation, and a negligible part is the heat losses to the ambient.

The total energy stored in the copper capsules that is calculated with the measurements of the copper temperatures is shown by purple squares in Figure 4-32(a) and (b). The stored energy that is calculated by the energy balance is denoted by the blue crosses in Figure 4-32(b). It is seen that the energy measurements of the copper capsules from these two methods are in a very good agreement, with a ~ 1% discrepancy at the end of this charging test. The verification tests have been carefully conducted by testing the copper capsules in multiple thermal cycles. The total energy stored in the charging process, and the total energy extracted in the discharging process have been analyzed for the tested copper capsules in different temperature ranges as tabulated in Table 4-3. The energy change of the copper capsules that is calculated by two methods is listed in Table 4-3. It is seen that the difference are within +/-5% in current test ranges, which is leading confidence to the experimental method and measurements in determination of the energy storage of the capsules in the test section.
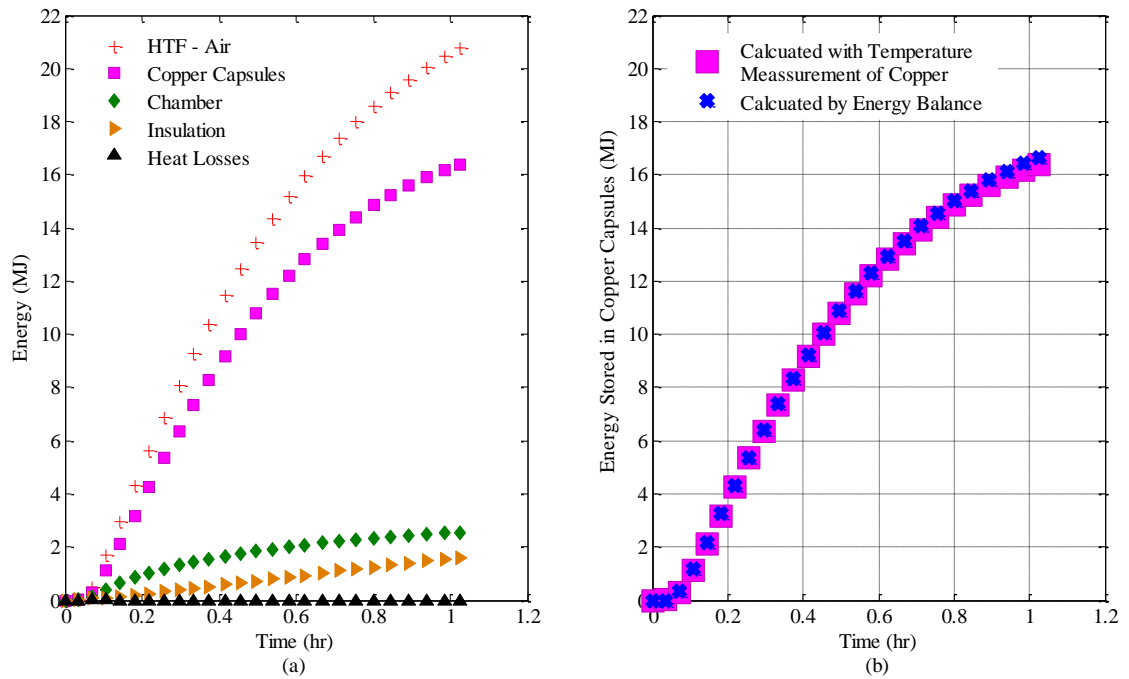
Figure 4-32. Energy storage of the TES system in a typical thermal charging test. (a). energy storage by every component from measurements. (b). energy stored in copper capsules calculated in two ways.

Table 4-3. Measurements of energy storage and retrieval in the verification tests with

multiple thermal charging and discharging processes.

Verification Test	Temperature Range of Copper Capsules (°C)	Energy Stored into/Retrieved from the Copper Capsules (MJ)		Difference Percentage
		Calc. by Energy Balance	Calc. by Copper Temperature Change	
Heating #1	27 - 425	16.54	16.38	1.0%
Cooling #2	425 - 65	13.37	13.26	0.8%
Heating #3	65 - 421	13.05	12.82	1.8%
Cooling #4	421 -148	8.34	8.16	2.2%
Heating #5	148 - 421	9.04	8.62	4.9%
Cooling #6	421 - 53	14.25	14.05	1.4%
Heating #7	281 - 431	9.67	9.83	-1.6%
Cooling #8	431 - 47	15.82	15.79	0.2%
Heating #9	47 - 426	15.19	15.24	-0.3%

5 TESTS RESULTS WITH EPCM-BASED TES SYSTEM

5.1 Test Section with NaNO$_3$ Capsules

5.1.1 Performance Tests with NaNO$_3$ Capsules

The thermal energy storage and retrieval of the NaNO$_3$ capsules are analyzed to demonstrate the viability of the storage technology for thermal energy using encapsulated phase change materials. As described previously, the energy stored in the NaNO$_3$ capsules is calculated by the energy balance with all the verified measurement facilities. Meanwhile it is also essential to monitor the thermal behavior of the NaNO$_3$ in the charging and discharging process, therefore a thermocouple is placed in the last capsule to track the temperature of the NaNO$_3$ near the outlet of the test section. As indicated in Figure 5-1, this thermocouple measures the temperature of the NaNO$_3$ at the very bottom of the capsule, where the temperature indicates the possible lowest temperature of the NaNO$_3$ in a charging process, and the higher temperature in a cooling process in the current test section. Choosing this measurement point and this length of the TC well is also based on the consideration to avoid the break-down of the TC well from the hanging of the solid NaNO$_3$ when liquid phase NaNO$_3$ is formed from outside shell of the capsule.
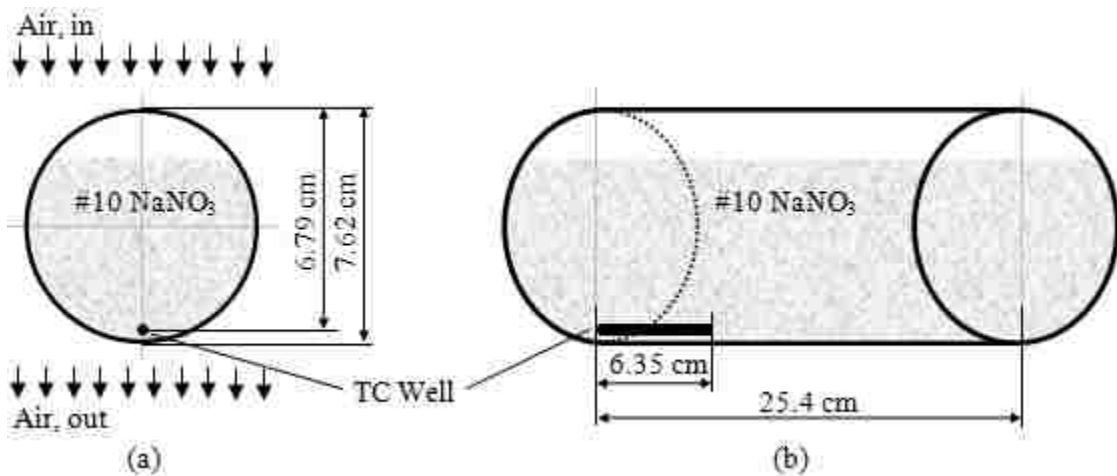
Figure 5-1. The thermocouple location in the #10 NaNO₃ near the outlet of the T/S (not at scale). (a). side view; (b). front view.

Figure 5-2 shows the temperature history of the air and the NaNO₃ near the outlet of the T/S in a typical thermal cycle. It is seen that in the charging process, the air is heated by the external heater to 440 °C to charge the NaNO₃ capsules, while in the discharging process, the heater is turned off and the cool air is sent to the test section to extract the energy from the capsules. After a short transition, the inlet air temperature approaches 440 °C in the charging process and about 28 °C in the discharging process. The temperature of the air at the outlet shows a similar trend. During the charging test run, the temperature increase of the NaNO₃ significantly slows down when it is approaching to the melting point, 308 °C. After the NaNO₃ completely melts, the NaNO₃ is superheated quickly in the liquid phase with ~ 380 °C at the end of this charging process. In the discharging process, the NaNO₃ cools down quickly with a sharp turn as its temperature decreases below the freezing point. One of the reasons for the appearance of the longer melting process is because the cold solid sodium nitrate sinks and touches the thermocouple.
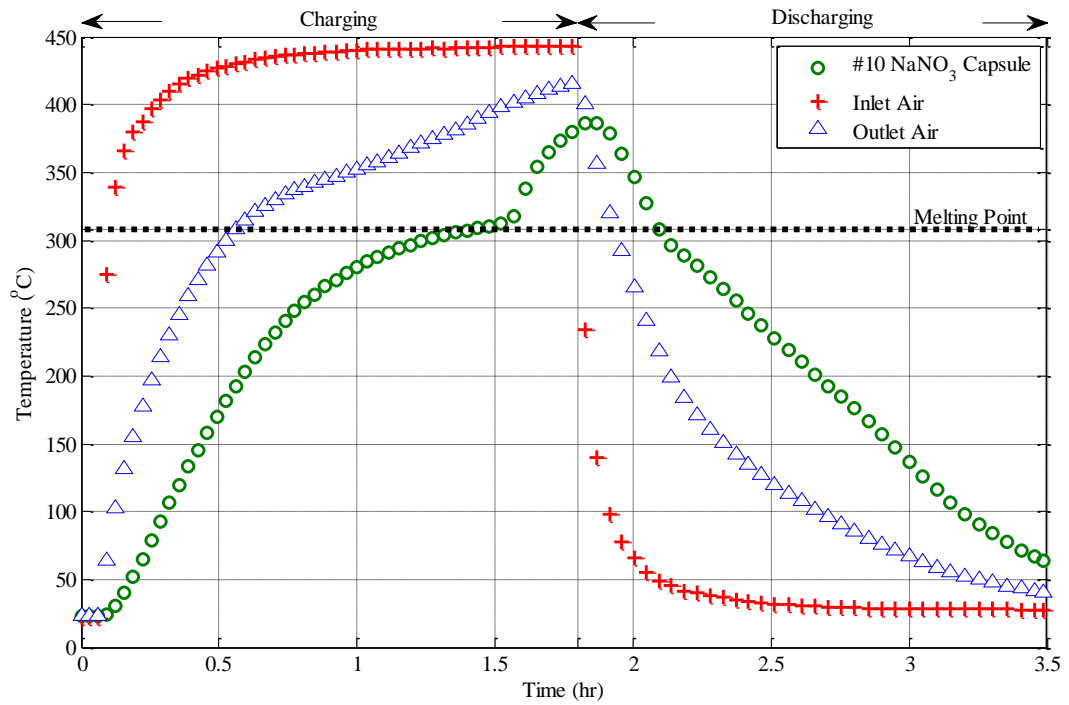
Figure 5-2. The temperature history of the NaNO₃ near the outlet, and the air at the inlet and at the outlet of the TES system in a thermal cycling

Figure 5-3 sketches this behavior of the solid NaNO₃ with the liquid formed from outside shell during a charging process. With the current design for the location of TC in the EPCM capsule, the TC senses a temperature near the melting point of NaNO₃ for a long period, until the NaNO₃ in its surrounding area is completely melted and becomes liquid.
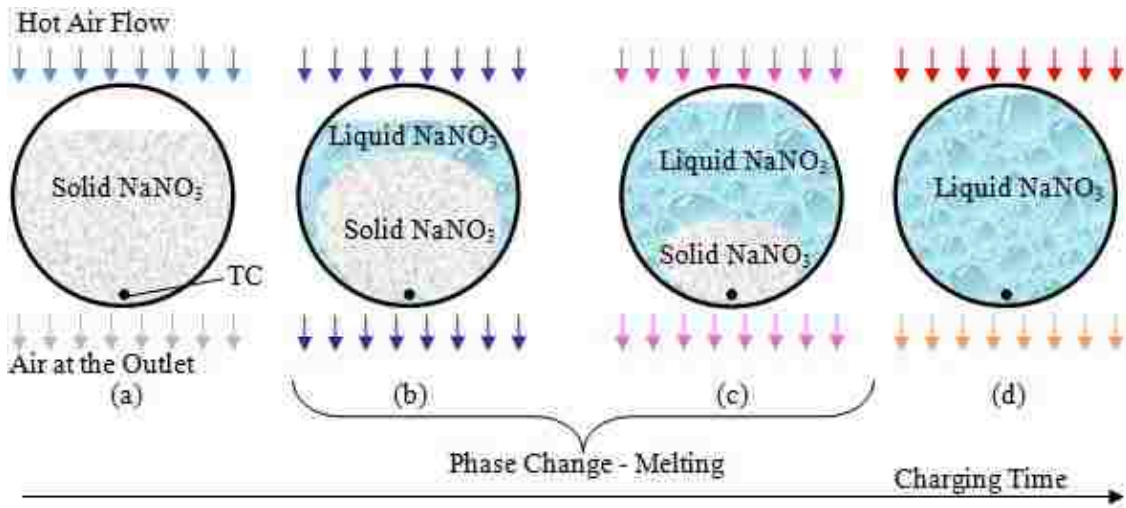
Figure 5-3. The sketch of the behavior of the #10 $NaNO_3$ undergoing the melting process in a charging process. (a). solid phase $NaNO_3$ before melting; (b) and (c). two phase $NaNO_3$ during the phase change; (d) liquid phase $NaNO_3$ in superheating.
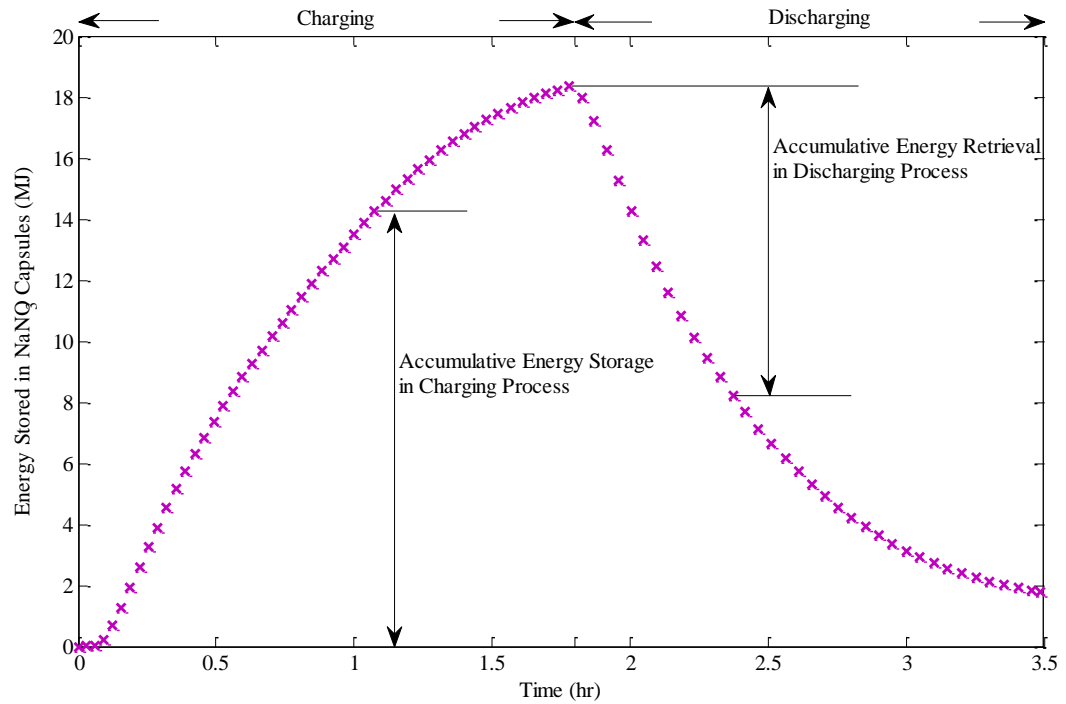
Figure 5-4. The energy stored in the ten $NaNO_3$ capsules in a thermal cycling

Figure 5-4 shows the total energy stored in the 10 $NaNO_3$ capsules in this thermal cycle.

111

All the energy values are referred to initial state of the $NaNO_3$ capsules at t = 0. It is seen that the 10 $NaNO_3$ capsules successfully capture the energy from the air during the charging process with an accumulated 18.4 MJ stored by the capsules at the end of the experiment. Then during the continued discharging process, the total energy stored in the capsules decreases since air is extracting the energy from the capsules. At the end of the discharging process, there is still approximately 1.8 MJ energy left in the $NaNO_3$ capsules since they are slightly warmer than their own initial state, as indicated by the temperature of $NaNO_3$ in Figure 5-5. In other words, at the end of the discharging process, the total energy retrieved from the capsules is about 16.6 MJ with the $NaNO_3$ capsules changing from ~ 400 °C to ~50 °C. Since we do not know temperature distribution within the capsules it is hard to what fraction of this energy is coming from the $NaNO_3$ inside the capsules. However we can estimate this energy released by the $NaNO_3$ by estimating temperatures of the capsule shells. If we assume the temperature of the shell of the #1 and #10 capsules are the same as the air at the inlet and at the outlet, respectively, and a linear temperature variation from the #1 to #10 capsules shell, the total energy stored into the shells of capsules can be estimated. This value is close to the actual value but would be slightly overestimated since the shell temperature should be lower than its surrounding air. Subtracting this estimated energy stored by the capsule shells, there is about 12.5 MJ energy stored in the 16.0 kg sodium nitrate at the end of the charging process, which accounts for ~ 75% of the energy stored by the EPCM capsule. The latent heat of the phase change contributes about 23% of the total energy stored by the EPCM. The storage capacity (kJ/kg) of encapsulated $NaNO_3$ is expected to be even higher with a larger capsule or larger

112

scale test section without the penalties from current limited test facility.

Besides the storage capacity of the EPCM capsules, the rate of energy storage and removal is another key parameter for evaluation of the storage performance of EPCM capsules. The rate of storage is related to: the thermal properties of the storage materials, the heat transfer rates from the HTF to the capsules, the properties of the heat transfer fluid, and EPCM capsules and capsules' geometry. In the current experiment, rate of the energy storage and removal is obtained by calculating the derivative of the energy stored in the $NaNO_3$ capsules over the time of thermal testing, which are shown in Figure 5-6.
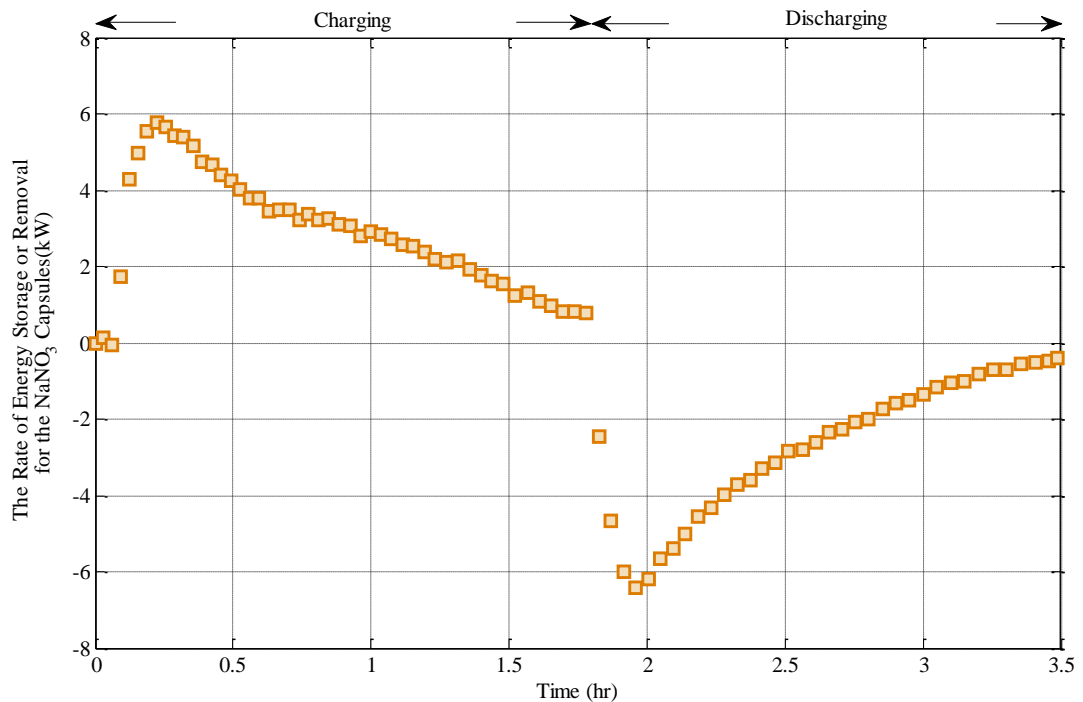
Figure 5-6. The rates of energy storage and retrieval of the 10 $NaNO_3$ capsules in current test facilities in a typical thermal charging and discharging cycle

113

As shown in Figure 5-6, the rate of energy storage increases quickly first and reaches a maximum of 6 kW, and then slows down and decreases to ~ 1 kW at the end of the charging process. During the discharging process, since the energy is leaving the capsules, the rate of the energy storage is shown with a negative sign, as depicted in Figure 5-6. It is seen that the absolute value of the rate of the energy storage in the cooling process has a similar trend with the charging period. It increases quickly to its maximum of ~ 6.2 kW and then decreases to ~ 0.5 kW at the end of the discharging process as the temperature of $NaNO_3$ drops. It is shown that the maximum rate of the energy storage or removal does not occur at the very beginning of the process. It happens when the temperature difference between the air and the capsules is at maximum, which occurs after the initial transient as the air temperature settles. With the current test facility, the average of the energy storage and removal rate is about 3 kW, which corresponding to a ~ 50 °C temperature difference between the air and capsules and an estimated 60 $W/m^2 \cdot °C$ for the convective heat transfer coefficient-- surface area of the capsules is ~ 1 m^2. It is expected that the rate of the energy storage and removal would be greater by using liquid HTF with which the convective heat transfer coefficient to the EPCM capsules would be significantly larger.

From the first thermal cycle test, it has been well demonstrated that the $NaNO_3$ capsules based test section can successfully store and retrieve thermal energy at temperatures up to 440 °C, with phase change at its melting point 308 °C. The next question to address is to determine the behavior of encapsulated $NaNO_3$ during multiple thermal cycles. With regards to the overall test section, it is necessary to examine the energy storage performance

114

of the NaNO$_3$ capsules over several thermal cycles. It is of great importance to investigate the thermal behavior the PCM in thermal cycling, and ensure its compatibility with the encapsulation materials in current scale and design. Therefore, in this experiment, the test section is tested with continuous charging and discharging processes. Figure 5-7(a) shows the temperature history of the encapsulated NaNO$_3$ in three thermal cycles. The test section is charged by the hot air at ~ 440 °C, and discharged by the cool air at ~ 25 °C consecutively three times. In order to ensure the thermal behavior of the encapsulated NaNO$_3$, the charging process is always ended after the measured temperature for the bottom capsule is above the melting point of NaNO$_3$. The discharging processes are ended at different point with the NaNO$_3$ cooled down to different temperatures and re-charged up with various initial states. As shown in Figure 5-7(a), the NaNO$_3$ at the #10 capsule is heated up from room temperature to ~ 400 °C in the first charging process, and then cooled down to ~ 50 °C at the end of the first cycle. In the second and third cycles, it is recharged to ~ 400 °C high temperature, and cooled down to ~ 100 °C at the end of both second and third cycles. It is seen that the measured temperature trace of the NaNO$_3$ follows the same trend in the melting and solidification respectively during these three thermal cycles, which indicates a sustained thermal behavior of the encapsulated NaNO$_3$ in the current test runs. Meanwhile, it is seen that the air temperature at the outlet also follows similar traces between the three heating process and three cooling process, which demonstrate the stable behavior of the energy storage and retrieval of the overall test section under multiple thermal tests in different temperature ranges. With the measurement facilities, the amount of the energy stored into and retrieved from the 10 NaNO$_3$ capsules is quantified and

115

plotted in Figure 5-7(b) for each of the thermal tests. It is seen that the encapsulated $NaNO_3$ capsules can continuously store and release the thermal energy during the thermal cycling. Take heating #2 and cooling #2 as an example, the $NaNO_3$ capsules capture about 17.5 MJ thermal energy from the air with their temperature raised from ~ 50 °C to ~ 440 °C, and reliese about 16 MJ thermal energy when the capsules are cooled from ~ 440 °C to ~ 100 °C. The differences between the amounts of the energy stored and retrieved are due to the ranges of operating temperatures and progress of the phase change in the 10 $NaNO_3$ capsules. Another comparison can be made between cooling #2 and heating #3, where beginning and end points of tests have similar ranges for $NaNO_3$ temperature. The energy stored into the capsules is again slightly higher than the energy extracted from the capsules, which might potentially be due to different temperature distributions in each capsule with the progress of the continuous thermal cycles. In that case, the average temperature in each capsule at the end of the heating #3 would be higher than the one at the end of the heating #2 (the beginning of the cooling #3).
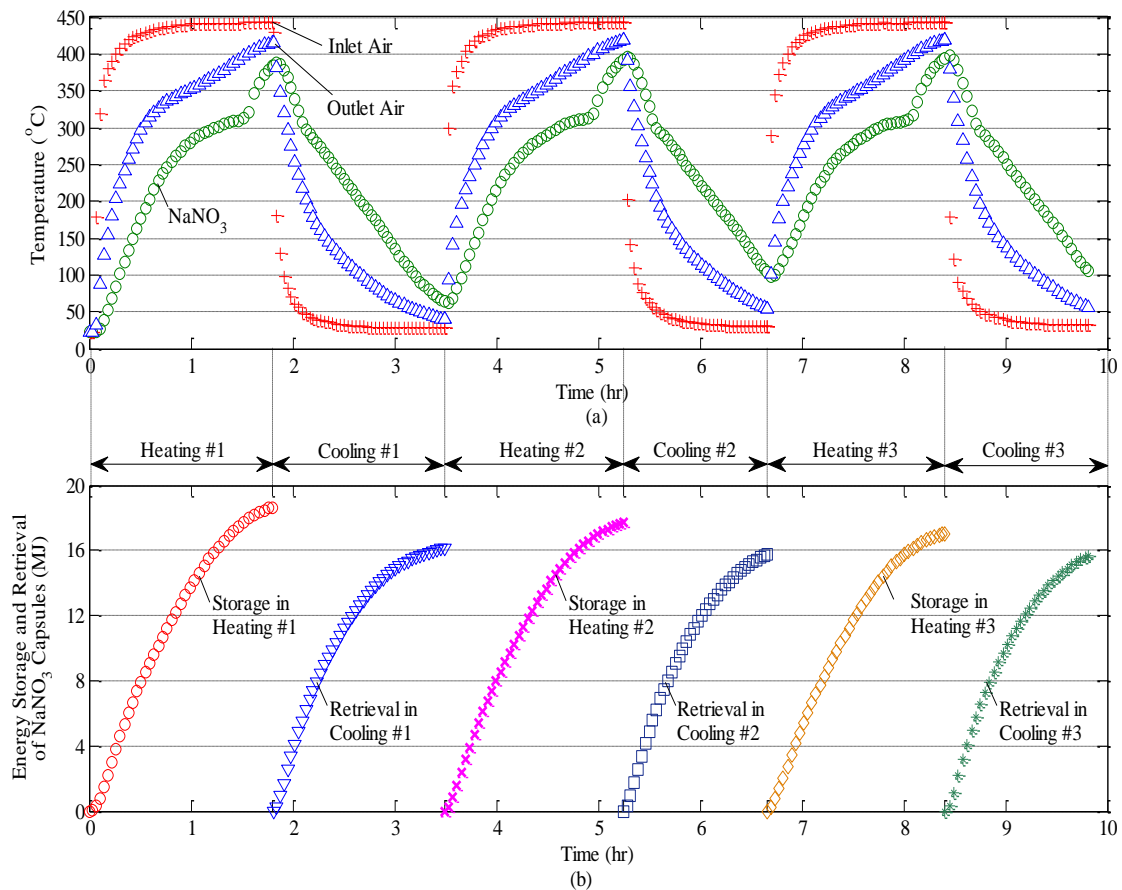
Figure 5-7. Test of the NaNO$_3$ capsules in three continuous thermal charging and discharging processes. (a). temperature history of the #10 NaNO$_3$ and air; (b) energy storage and retrieval of the encapsulated nitrate capsules.

The test section with 10 encapsulated NaNO$_3$ has been tested four times in 45 days with ~ 10 hours thermal cycles every time just as shown in Figure 5-7 . After the 45 days, a charging test is conducted with the same operating conditions (inlet air temperature and mass flow of the air) as its first charging process for the NaNO$_3$ capsules as shown in Figure 5-8(a), to repeat the experiment and investigate whether or not the energy storage is sustained after the NaNO$_3$ is encapsulated in the stainless steel capsule for 45 days and subject to occasional thermal test with ~ 40 hours in thermal charging and discharging. In

Figure 5-8, it has been found that the temperature trace and the energy storage performance of the NaNO$_3$ capsules are consistent with the ones in first charging test. And for the energy stored in the 10 NaNO$_3$ capsules, the discrepancy between the two tests is ~ 2.5% within the accuracy of the measurements in current test facility. It can be concluded that the encapsulated NaNO$_3$ capsules have sustained storage performance without the deterioration in their storage performance in current test range.
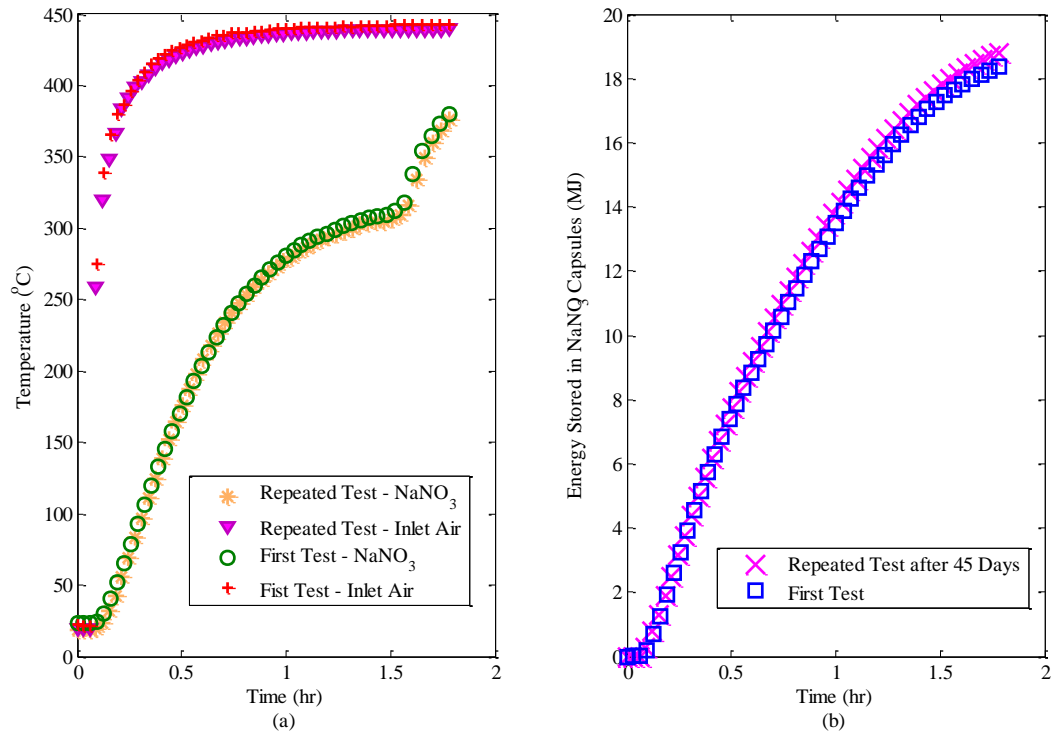
Figure 5-8. Storage performance of the NaNO$_3$ capsules with the same operating conditions as the first charging process after 45 days. (a) temperature profiles of the NaNO3 and inlet air; (b) energy stored in the 10 NaNO$_3$ capsules.

5.1.2   Comparison with Predicted Results for NaNO$_3$ Tests

Simulations have been conducted for charging and discharging processes with NaNO$_3$ capsules. This is aimed to compare the experimental data with the simulation results, to investigate the capability of the model, and to improve performance of the model if necessary for more accurate predictions. The mathematical model is also used to investigate the dynamics of the encapsulated NaNO$_3$ in the T/S during thermal cycles.

The model uses the measured mass flow rates of the air, and the temperature of the air at the inlet as inputs. The thermal properties of every component of the test section are listed in Table 5-1. The temperature profiles of the NaNO$_3$ and insulation at various locations and the air temperature at the outlet are predicted.

Table 5-1. Thermal properties of each component of the test section in the simulation model [30,52,64,65].

	Density (kg/m^3)	Heat Capacity (J/kg·°C)	Conductivity (W/m·°C)
Air		$3\times10^{-4}T(°C)^2 + 3\times10^{-2}T(°C) + 1005.1$	
Chamber		$-0.0002T(°C)^2 + 0.3009\ T(°C) + 473.49$	15
Insulation	93[*1]	$2\times10^{-6}T(°C)^3 - 2\times10^{-3}T(°C)^2 + 1.4T(°C) + 735.7$[*1]	0.08[*1]
NaNO$_3$	1706.3[*2]	1601(solid), 1650(liquid)	0.55(solid), 0.68 (liquid)

[*1]: the density, heat capacity and thermal conductivity were from the provider G.I.S Inc..

[*2]: density of the NaNO$_3$ is adjusted accordingly to ensure its mass in each of the capsule in the model is equal to the mass in real capsule.

Figure 5-9 shows the predicted and measured air temperatures and the temperatures of NaNO$_3$ in a typical thermal cycle. For the temperature of NaNO$_3$ at the specific measurement point (the bottom capsule), there is a very good agreement between the

119

experimental data and simulation results before the melting point of the $NaNO_3$ in the charging process, but a considerable difference is shown as the temperature is approaching the melting point. This difference is reasonable considering that in the experiment, thermocouple contacts with the colder solid $NaNO_3$ which is sinking to the TC location as PCM melts. The model makes the unrealistic but computationally efficient and practical assumption that the solid $NaNO_3$ stays in the center without sinking. Therefore, the simulation shows higher values than the experimental measurements when the melting process starts.
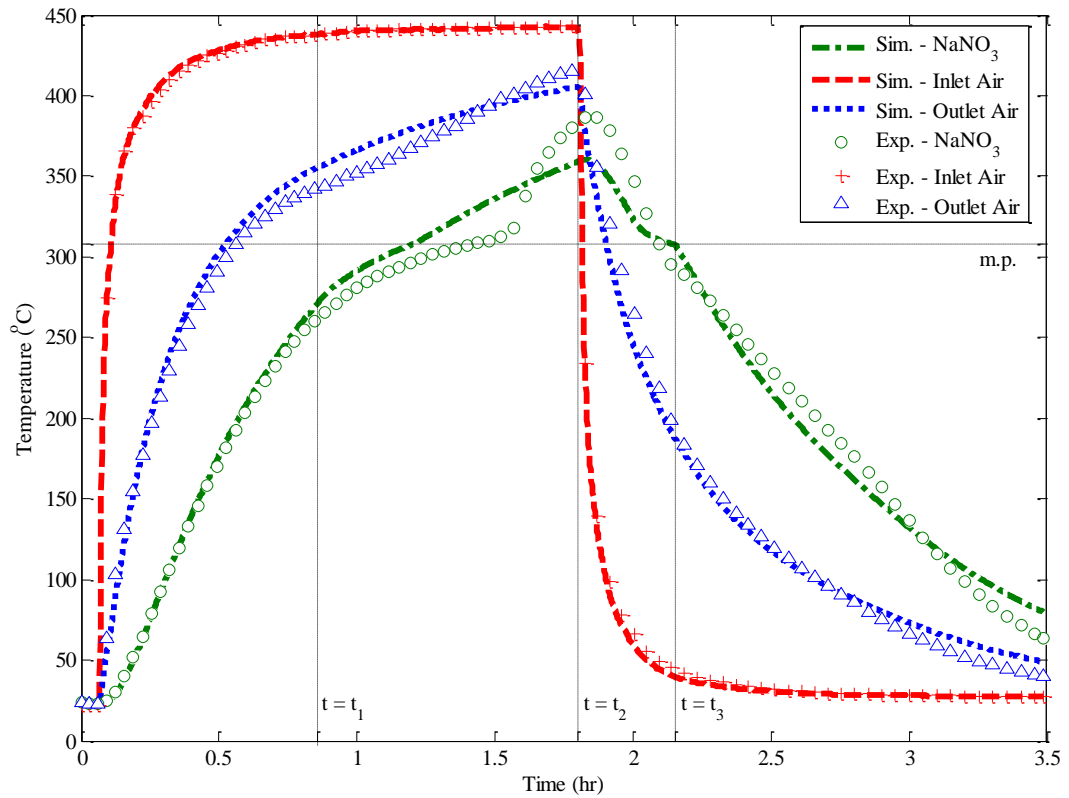
Figure 5-9. Comparison of the simulation results with the experimental data for the measured NaNO₃ temperature and air temperature in a typical charging and discharging process.

This is confirmed with the temperature profiles at other radial locations in the #10 NaNO₃ capsule predicted by the model, as shown in Figure 5-10. The red dash line shows the temperature history of the NaNO₃ at the inside surface of the capsule $r = R_{PCM}$. It is seen that the deviation between the experimental measurements and simulation results for the measurement points appears at the time of $t = t_1$ when the NaNO₃ at the $r = R_{PCM}$ starts melting; while with the liquid NaNO₃ formed at this time from the outside shell, the solid NaNO₃ sink to the bottom in the realistic operating system, therefore a lower temperature

121

is sensed in the experiment. At the end of the charging process $t = t_2$, the measured temperature for the $NaNO_3$ agrees with the predicted temperature at the inside surface of the capsule. This implies that a well-mixed $NaNO_3$ bulk is present during the melting process due to the natural convection.
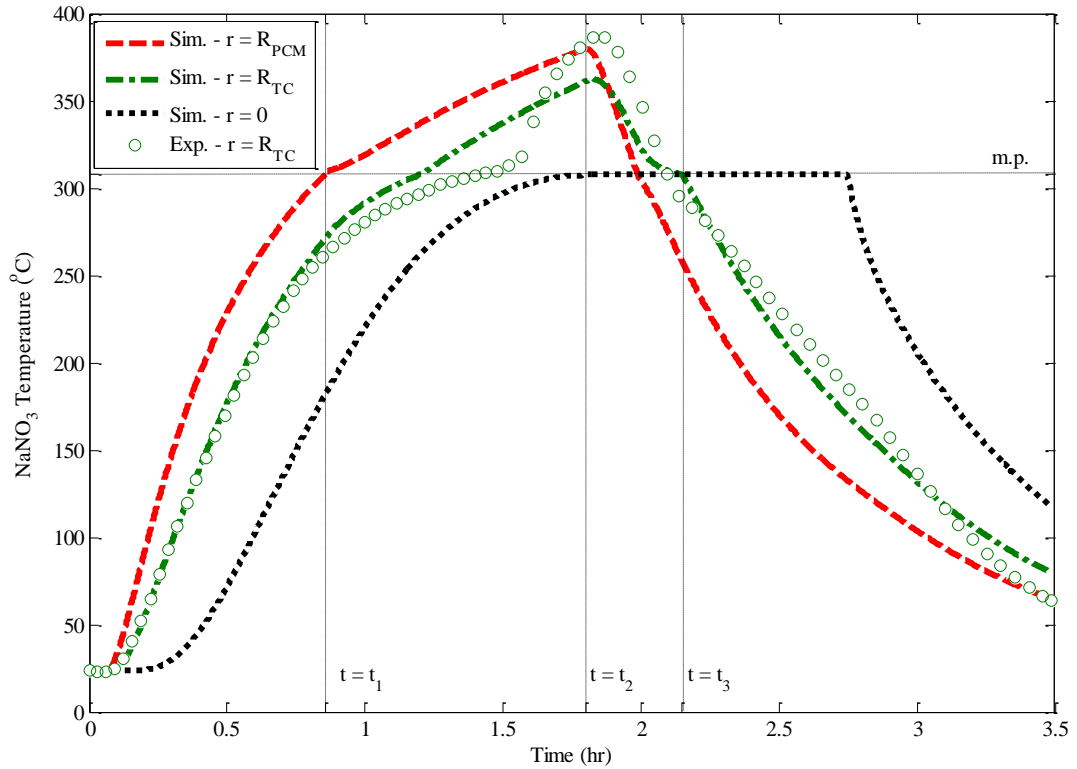
Figure 5-10. The temperature profiles of $NaNO_3$ in various radial locations in # 10 capsule in the T/S.

The temperature of the air at the outlet has been well predicted at the beginning of the charging process when the $NaNO_3$ is in its solid phase, as shown in Figure 5-9. The model overestimates the outlet temperature as $NaNO_3$ approaches the melting point. In other

words, the temperature drop of the air across the T/S is slightly underestimated during this time. This may be due to the assumption of no natural convection in the liquid phase of the $NaNO_3$. For the discharging process with the solid $NaNO_3$ solidified from the surface of the capsule, it is seen that the outlet air temperature and the measured $NaNO_3$ temperature have been both well predicted by the model.

In order to investigate the heat conduction in the encapsulated $NaNO_3$, the temperature distribution of the $NaNO_3$ in the capsule is plotted along the radial direction and shown in Figure 5-11 for the #1 $NaNO_3$ capsule near the T/S inlet, and #10 $NaNO_3$ capsule near the T/S outlet with the progress of time during the thermal cycle. Figure 5-11 (a) and (c) are shown for this temperature information of the $NaNO_3$ during the charging process, while Figure 5-11 (b) and (d) are for the ones during discharging process. In the two figures Figure 5-11 (a) and (c), it is seen that the $NaNO_3$ in the test section has been charged from room temperature to high temperature up to 430 °C with thermal resistances from the conduction and the "heat sink" due to phase change at the melting point of the $NaNO_3$. Here we take the cases at time $t1 = 0.4$ hr for example to explain the low thermal conduction in the $NaNO_3$. As it is seen in Figure 5-11, the $NaNO_3$ at the inside surface of #1 capsule has already reached to the melting point 308 °C at this time, while the $NaNO_3$ at its center is still cold with an about 100 °C temperature. At this time, the inside surface of the #10 $NaNO_3$ capsule is about 200 °C with further cooler center which just warmed up to ~ 50 °C. Following the progress of radial temperature distribution with time for both of the capsules, it is clear that the melting process is the major resistance for heat transfer to the

central solid core. In other words, the solid core at the center of the capsule warms uo to temperatures close to the melting point and almost all of the heat penetrating from the outside surface is used to mely the $NaNO_3$ at the interface. At the end of the charging process, there are ~ 30 °C temperature variations in the #1 $NaNO_3$ capsule, and ~ 80 °C temperature variations in the #10 $NaNO_3$ capsule along the radial direction. For the temperature distribution during the discharging process, an interesting phenomena has been observed from the simulation from time tc to time t3 in both of the capsules, the temperature of $NaNO_3$ close to the outside surface of the capsule decreases because of the heat has been extracted by the outside cool air. But at inner locations toward to the centerline of the capsule, temperature keeps rising even there is cooling at the surface. This is because at initial stages of the discharge process the maximum temperature is still not at the centerline but at a radius which keeps getting smaller as the heat extraction from the capsule continues.
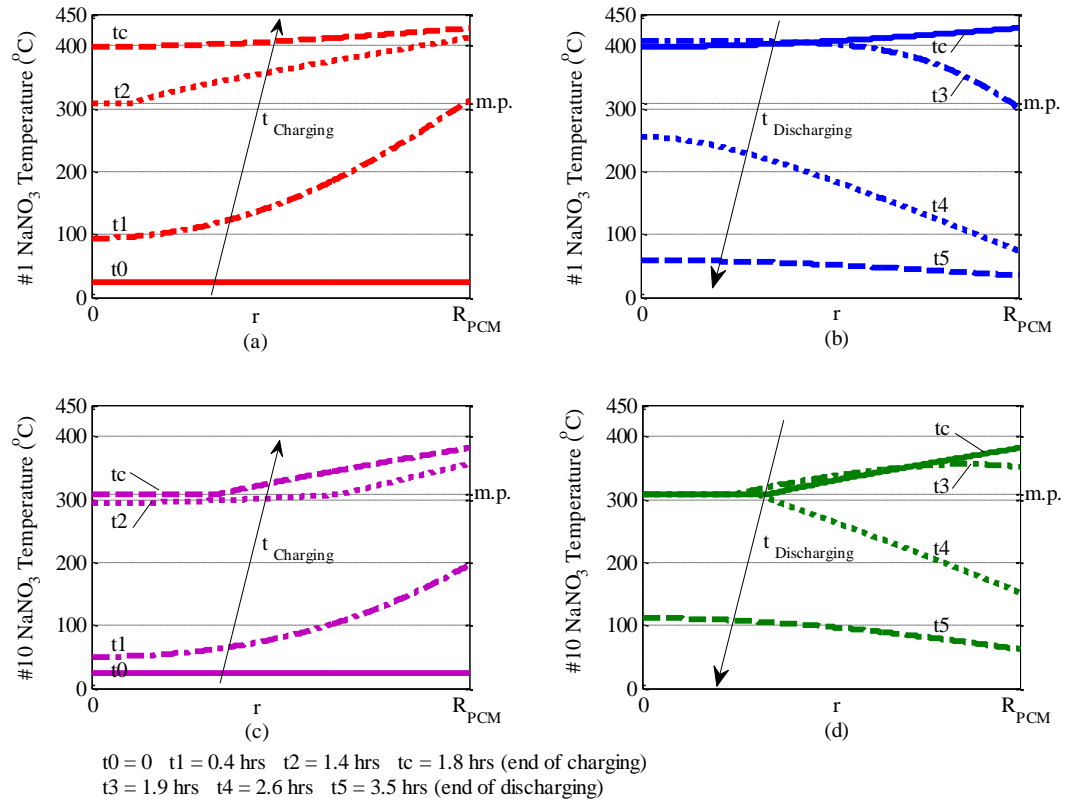
Figure 5-11. The temperature distribution in the NaNO$_3$ in the radial direction at various times in a thermal cycle. (a). charging #1 NaNO$_3$ capsule; (b). discharging #1 NaNO$_3$ capsule; (c). charging #10 NaNO$_3$ capsule. (d). discharging #10 NaNO$_3$ capsule.

Numerical simulation allows us to track the radial location of phase change as a function of time. Such information for the displacement of the melting front is shown in Figure 5-12 for the NaNO$_3$ capsule of #1 and #10. During either charging or discharging process, when the radius of the interface (the melting front) is equal to the inside radius of the capsule, it means that the PCM (NaNO$_3$) is in its single phase (either solid or liquid). When this value drops down to zero, it means that the NaNO$_3$ in the capsule has completely melted or solidified. In this figure it is seen that the NaNO$_3$ in the #1 capsule starts to melt at ~ 0.4 hrs and it takes another ~ 1.1 hours to complete the phase change. For the #10 NaNO$_3$

125

capsule, it starts to melt about ~ 0.5 hours later than the #1 capsule, and at the end of the charging process t = 1.8 hrs, it is partially melted with the melting front at r = 0.4 R_{PCM}, with a solid core at the center and liquid on the outside. Once the discharging process starts at t=1.8 hrs, solidification starts at the inner surface of the capsule. For the top capsule the solidification continues to grow from the inner surface toward the centerline and solidification is completed at t=2.6 hrs. For the bottom capsule however, since solidification starts from the inner surface of the capsule there are two meting fronts one developing from the inner surface of the radius and one at inners of the capsule, which still continues to shrink (melt) during initial stages of the cooling process. The green dash line shows the second melting front in this bottom capsule which is actually continuation of the melting front formed during the previous charging process. As seen in this figure, there is still some energy conducted towards to the center to melt down more $NaNO_3$ with the melting front moving towards to the center, which has been discussed in Figure 5-11 (d). At the time ~ 2.7 hours, these two melting front meet each other, and the liquid phase is completely solidified in this capsule at that time. With current operating conditions, i.e., ~ 440 °C hot air for charging process and ~ 25 °C cool air for discharging process, the overall solidification process is quicker in the discharging process as shown in this Figure 5-12 because of an overall higher temperature difference between the $NaNO_3$'s melting point and the air temperature.
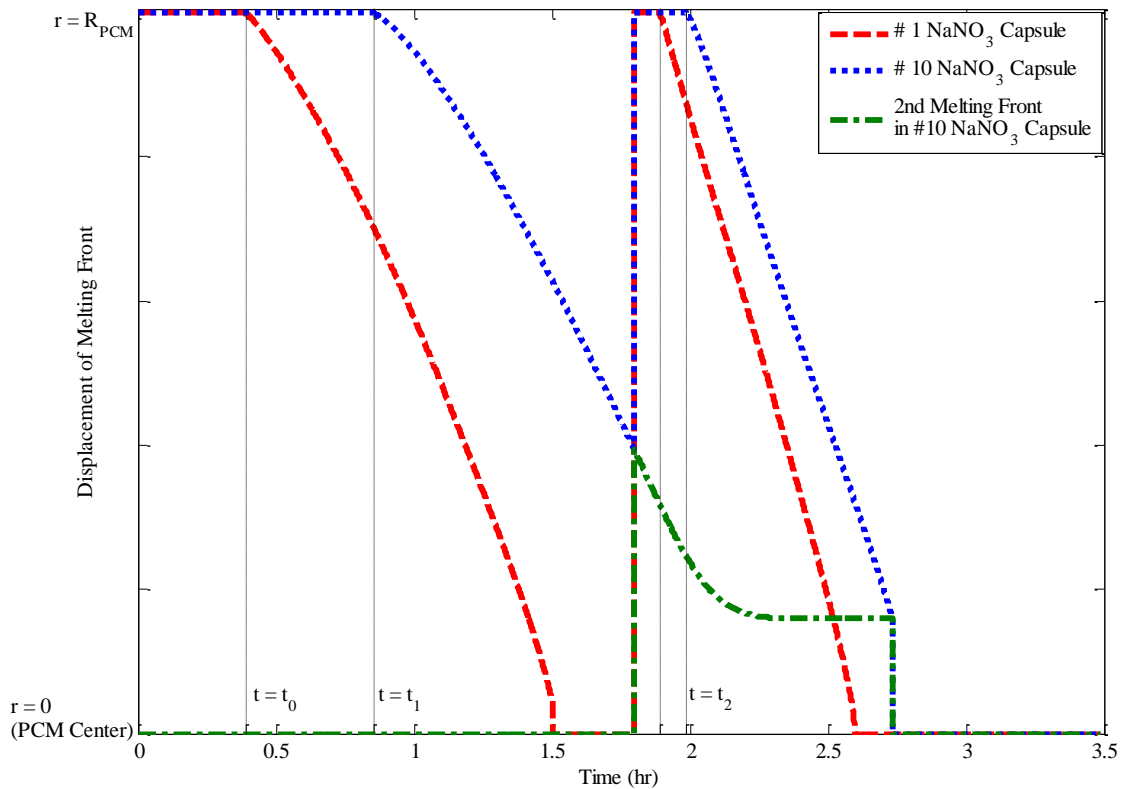
Figure 5-12. Displacement of the melting front in the #1 NaNO₃ capsule and # 10 NaNO₃ capsule.

The simulation model provides detailed information both in regard to radial variation and in time. The information of the temperature of NaNO₃ as shown in Figure 5-11, and the location of the melting front as shown in Figure 5-12, can be used to calculate the energy stored in each of the NaNO₃ capsule at any time during the thermal cycle with its phase change. Figure 5-13 shows the energy stored in each of the capsule along the test section at various times. Figure 5-13 (a) shows the case during the charging process and Figure 5-13 (b) for discharging process. In this thermal cycle, the energy stored in the single capsule would change from zero, which is referred to its own initial state at time t = 0, to

it's theoretical value, Q_s^*, with the temperature of the capsule equal to the inlet air temperature of 440 °C, which could happen if the experiment is run for an infinitely long time. It is obvious that the capsule close to the top section stores and releases the energy more quickly compared with the capsule at the bottom section—this is true for both charging and discharging periods because in the current test facility both the hot and cool air are both sent in from the top of the T/S. During the charging process, the variation of the stored energy between capsules is large at the beginning along the test section since the top section has larger temperature driving force. However as the time progresses, the capsules at the upper levels heat up and the driving force becomes smaller, when the lower capsules gain higher rates of energy compared to the ones at the top. During the discharge period, at the beginning the energy stored in #1 capsule drops significantly by 0.4 MJ in ~ 0.1 hrs from time t = 1.8 hrs to time t = 1.9 hrs, while the energy stored in #10 capsule barely changes because its surrounding air is warmer after extracting the heat from the capsules in its upper section. At the end of the discharging process t = 3.5 hrs, there are still some energy residue in each of the $NaNO_3$ capsule.
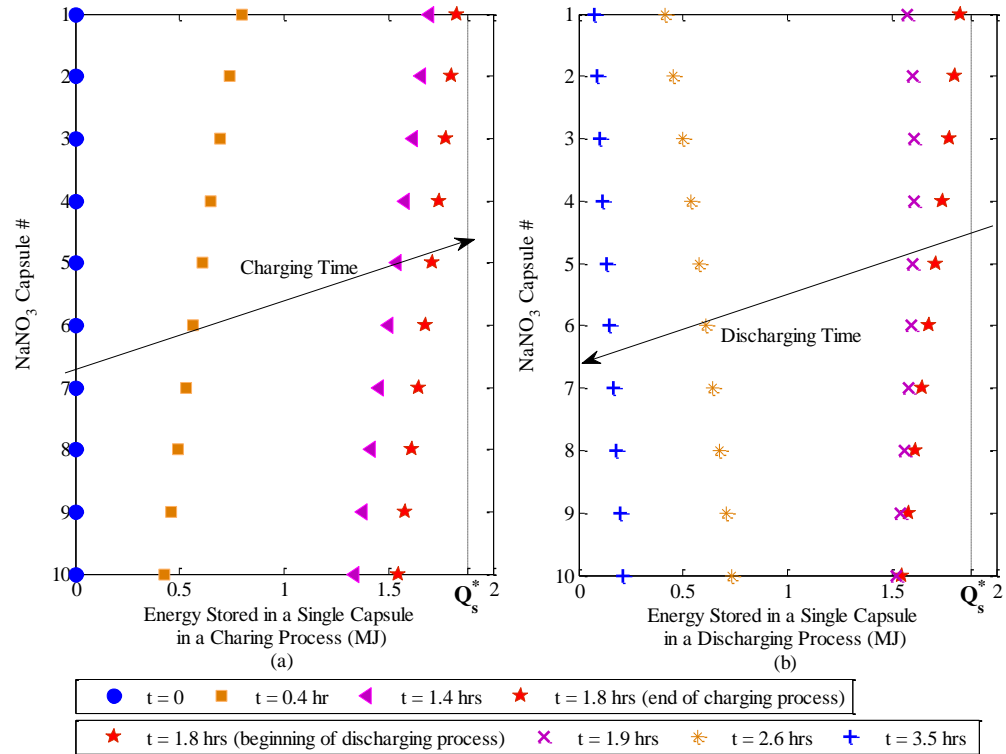
Figure 5-13. Energy stored in the single NaNO$_3$ capsule at various elevations of the T/S. (a) charging process;(b) discharging process.

By summing up the energy stored in the each single capsule, the total energy stored in the 10 NaNO$_3$ capsules can be obtained, as shown in Figure 5-14. It is seen that the experimental measurements for the energy stored in NaNO$_3$ capsules have been well predicted at the beginning of the charging, when the NaNO$_3$ is mostly in solid phase. The difference appears especially after time = ~ 0.8 hr when the encapsulated NaNO$_3$ are undergoing melting process. At the end of the charging process, the difference between the prediction and experimental measurement is approximately 7% for the energy stored in the 10 NaNO$_3$ capsules. As discussed previously, one of the reasons for the discrepancy is that the model neglects the natural convection and the sinking of the solid inside the capsule. It

has been reported that for a single encapsulated $NaNO_3$ capsule heating up by the 400 °C air, the time for the phase change would be shortened by ~ 10 % if the gravity and natural convection is considered [66]. But our case is more complicated with multiple EPCM capsules with the air flowing at different temperatures along the T/S. A potential extension of the simulation model to include the effects of gravity and the natural convection on the performance of the EPCMs is strongly suggested.
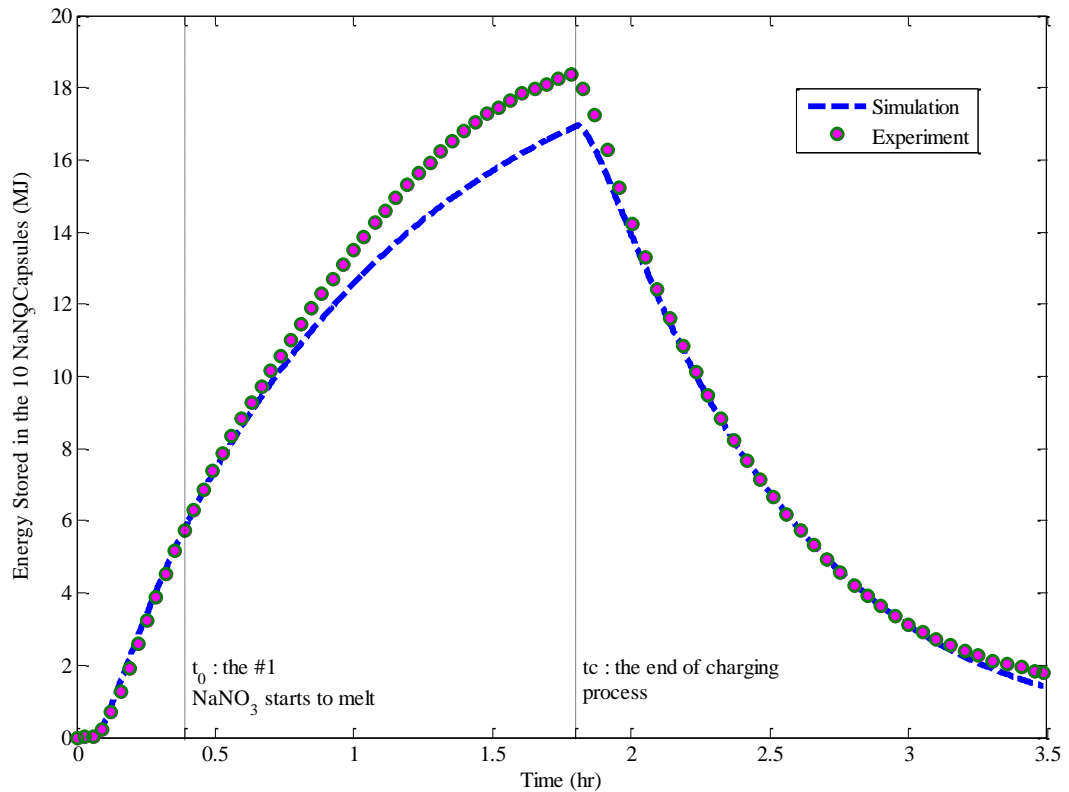
Figure 5-14. The comparison of the energy stored in the overall $10NaNO_3$ capsules in a thermal cycle between the simulation model and experimental measurements.

From the analysis of the comparison of the experimental data with the predicted results for

NaNO$_3$ tests, it is found that the energy storage can be predicted with ~ 7% discrepancy as shown in Figure 5-14. One of the reason for the difference is due to the natural convection in the liquid NaNO$_3$ and movement (sinking) of the solid NaNO$_3$ during the melting process. In order to be better predict the stored energy in the EPCM capsules, one of the parameters in the simulation model - the thermal conductivity of the NaNO$_3$ is adjusted absolutely when the NaNO$_3$ is in liquid phase. And the thermal conductivity of the NaNO$_3$ PCM is chosen to be a larger value considering that the effects of the natural convection and movements of the solid PCM would enhance the heat transfer during its melting process in the liquid phase. Figure 5-15 shows the comparison of the experimental data with the predicted results with the adjusted model for the total energy stored in the NaNO$_3$ capsules in a thermal cycle. The thermal conductivity of the liquid NaNO3 has been increased to 3 W/m.K during the melting process, while in the original simulation model, the thermal conductivity of the liquid NaNO$_3$ is 0.68 W/m.K as shown in Table 5-1. It has been found that with the adjusted thermal conductivity of the liquid NaNO$_3$, the total energy stored in the encapsulated PCM has been better predicted, with a less than 2% difference compared with the experimental data.
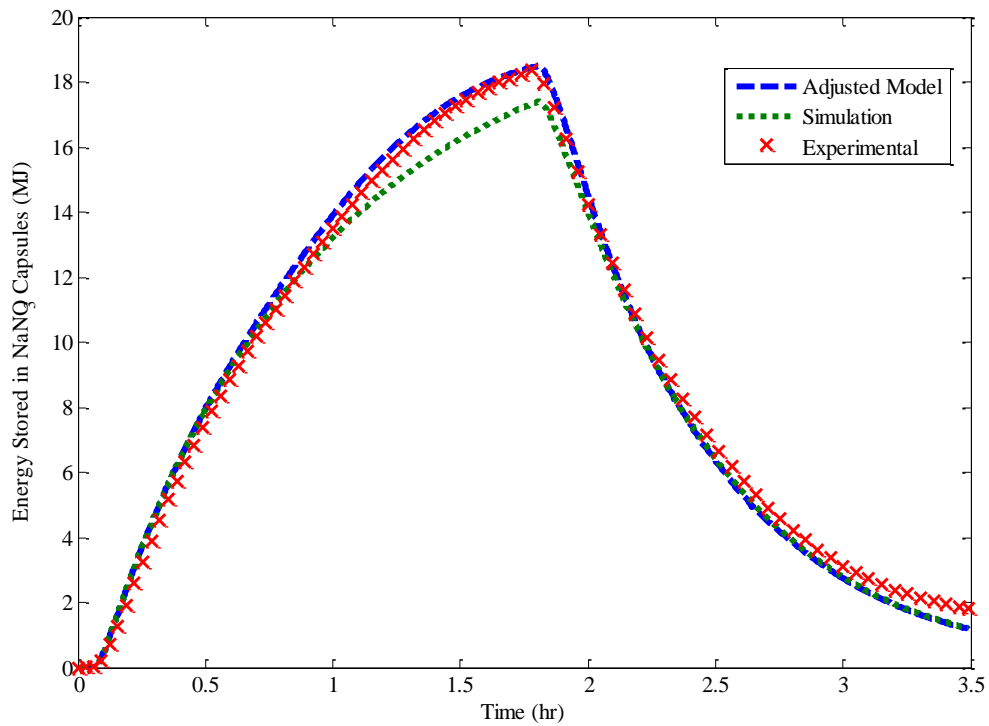
Figure 5-15. Adjustment of the simulation model based on the experimental data of $NaNO_3$ tests.

5.2 Test Section with $MgCl_2$-NaCl Capsules

5.2.1 Performance Tests with $MgCl_2$-NaCl Capsules

Concentrating solar plants focus the solar radiation to heat a heat transfer fluid and produce steam and generate electricity. Since the efficiency of the turbine increase with increasing operating temperatures, a lot of attentions have been put in to operation of solar plants at high temperatures. these efforts include but not limited to developthe technology to enhance solar concentration, to develop high temperature storage materials and heat

transfer fluids., It has been reported that the annular solar-to-electricity efficiency can increase to 20% from 16% when the operating temperature of the solar field increase from 550 °C to 650 °C [18]. Therefore in this research, $MgCl_2$ – NaCl eutectic is chosen as a storage medium with a higher melting temperature at 444 °C, and encapsulated in individual capsules. Earlier research in the calorimetry tests has found that $MgCl_2$ - NaCl eutectic is a promising storage medium that can be operated in high temperature range 250 °C – 550 °C, and the storage performance of the encapsulated eutectic is shown to be sustained after long-term high temperature exposure. Followed the calorimetry tests for the $MgCl_2$ – NaCl eutectic, the eutectic is encapsulated and stainless steel capsules are fabricated as shown in Figure 4-28. Ten $MgCl_2$ – NaCl eutectic capsules are loaded in the test section for performance test to demonstrate the energy storage and retrieval of the EPCM with phase change at high temperature 444 °C, and the details are described below.

Figure 5-16 shows the temperature history of the air at the inlet and at the outlet of the T/S, as well as the temperature trace of the #1 $MgCl_2$ – NaCl eutectic near the inlet of T/S and #10 $MgCl_2$ – NaCl eutectic near the outlet of the T/S in a typical thermal cycle. It is seen that during the heating process, the air is quickly heated by the external heater to 540 °C to charge the eutectic capsules, while during the discharging process, the heater is turned off and the cool air is sent to the test section to extract the energy from the capsules. After a short transition, the inlet air temperature approaches 540 °C in the charging process and about 25 °C in the discharging process. The temperature of the air at the outlet shows a similar trend. During the charging test run, the temperature increases of the $MgCl_2$ – NaCl

133

eutectics both near the inlet and near the outlet of the test section have a similar trend – the temperature of the capsules increase fast while the PCM is in solid phase. Temperature increase significantly slows down when the PCM is approaching to the melting point, 444 °C; after the eutectic completely melts, the eutectic is superheated quickly in the liquid phase to ~ 500 °C at the end of this charging process. And during the discharging process, the eutectic cools down quickly with a sharp turn as its temperature decreases below the freezing point. One of the reasons for the appearance of the longer melting process is because the cold solid PCM sinks and touches the thermocouple as discussed previously in Figure 5-3.
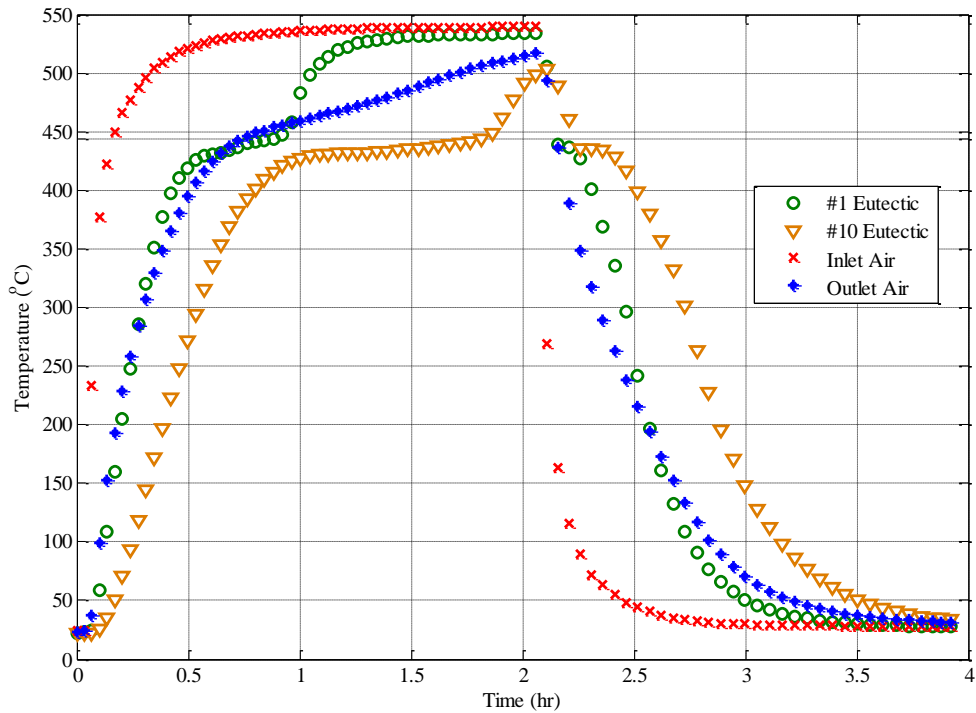
Figure 5-16. Temperature history of the air and eutectic in a typical thermal cycle.

134

Figure 5-17 shows the total energy stored in 10 $MgCl_2$-NaCl capsules in a thermal cycle. All the energy values are referred to the initial state of the $MgCl_2$-NaCl capsules at t=0. It is seen that the 10 $MgCl_2$-NaCl capsules successfully capture the energy from the air during the charging process with an accumulated 18.9 MJ energy stored by the capsules at the end of the experiment. Then in the continued discharging process, the stored energy in the capsules decreases, which indicates the air is effectively extracting the energy from the capsules. At the end of the discharging process, there is still approximately 1.7 MJ residual energy in the $MgCl_2$-NaCl capsules since they are slightly warmer than their own initial state, as shown by the temperature of the $MgCl_2$-NaCl eutectic mixture in Figure 5-16. In other words, at the end of the discharging process, the total energy retrieved from the capsules is about 17.2 MJ with the $MgCl_2$-NaCl eutectic capsules changing from ~ 510 °C – ~ 30 °C. If we assume the temperature of the shell of the #1 and #10 capsules are the same with the air at the inlet and at the outlet of the test section respectively, a linear temperature change from the #1 to #10 shells of the capsules, and a uniform temperature distribution in every capsule, the total energy stored into the capsules themselves can be estimated, and this value should be close to the real but would be somewhat overestimated since the shell temperature should be lower than its surrounding air. Subtracting this estimated energy stored by the capsule shells, there is about 13.6 MJ energy stored in the 14.2 kg $MgCl_2$-NaCl eutectic mixture at the end of the charging process, which accounts for 79% of the energy stored by the EPCM capsules. If we assume that the PCM is completely melted based on the temperature profile of the #10 eutectic salts in Figure 5-16, the latent heat of the phase change contributes about 27% of the total energy stored by the

135

encapsulated MgCl$_2$-NaCl eutectic salts. The storage capacity (kJ/kg) of encapsulated MgCl$_2$-NaCl eutectic salts is expected to be higher for a larger size capsule and larger scale storage units without the penalties from current limited test facility.
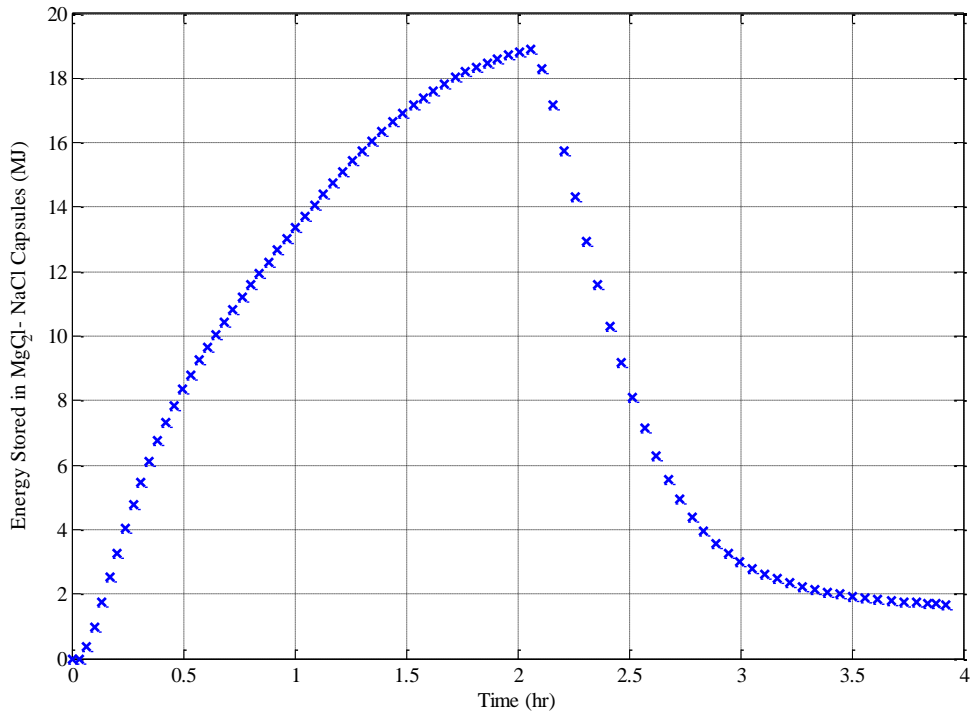
Figure 5-17. The energy stored in the ten MgCl$_2$-NaCl capsules in a typical charging and discharging process.

Besides the storage capacity of the EPCM capsules, the rate of energy storage and removal is another key parameter for evaluation of the storage performance EPCM capsules. The rate of storage is related to: the thermal properties of the storage materials, the heat transfer rates from the HTF to the capsules, the properties of the heat transfer fluid, and EPCM capsules and capsules' geometry. For the current experiment, the rate of the energy storage

and removal is obtained by calculating the derivative of the energy stored in the $MgCl_2$ -

NaCl capsules over the time of thermal testing, which are shown in Figure 5-17.

As shown in Figure 5-17., the rate of the energy storage increases quickly first and reaches

to a maximum of 6.2 kW, and then slows down and decreases to ~ 0.3 kW at the end of the

charging process. In the discharging process, since the energy left in the capsules decreases,

the rate of the energy storage for the capsules is negative, as depicted in Figure 5-17. It is

seen that the absolute value of the rate of the energy storage in the cooling process has a

similar trend. It increases quickly to its maximum of ~ 8.0 kW and then decreases to zero

at the end of the discharging process as the temperature of eutectic drops. It is shown that

the maximum of the rate of the energy storage or removal does not occur at the very

beginning of the process. The maximum temperature difference between the air and the

capsules occurs after the transient as the air temperature settles. With the current test

facility, the average of the energy storage and removal is about 3 kW, which corresponding

to a ~ 50 °C temperature difference between the air and capsules with the capsules surface

area ~ 1 m^2 and an estimated 60 $W/m^2 \cdot °C$ for the convective heat transfer coefficient. It

has been expected based on the simulation work that the rate of the energy storage and

removal would be greater by using liquid HTF with which the convective heat transfer

coefficient to the EPCM capsules would be significantly larger.
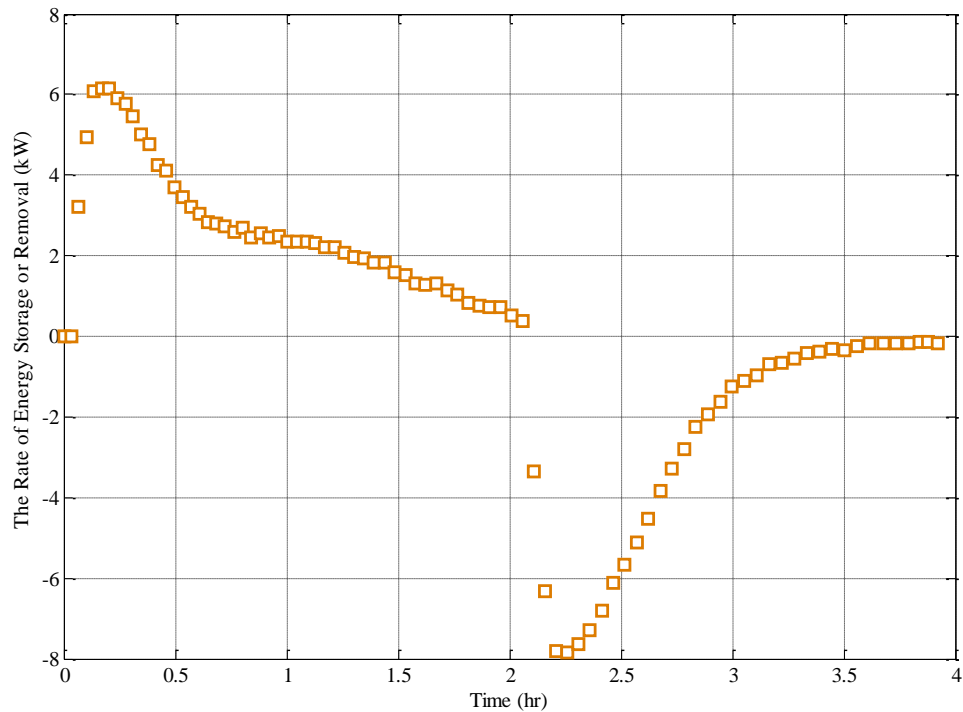
Figure 5-18. The rate of energy storage and retrieval of ten $MgCl_2$ – NaCl capsules in the T/S in a typical thermal charging and discharging process.

From this first thermal cycle test for the $MgCl_2$ – NaCl capsules, it has been well demonstrated that the $MgCl_2$ – NaCl capsules based test section can successfully store and retrieve thermal energy at the temperature up to 540 °C, with eutectic mixture melted at its melting point 444 °C in the charging process, and solidified in the discharging process.

This test section with 10 encapsulated $MgCl_2$ - NaCl has been tested three times in 12 days with ~ 4 hours thermal cycles every time just as shown in Figure 5-17. After the 12 days, a thermal cycle test is conducted with the same operating conditions (inlet air temperature and mass flow of the air) as its first charging and discharging process for the $MgCl_2$ – NaCl

capsules as shown in Figure 5-19(a), to repeat the experiment and investigate whether or not the energy storage is sustained after the $MgCl_2$ – NaCl is encapsulated in the stainless steel capsule for 12 days and subject to occasional thermal test with ~ 12 hours in thermal charging and discharging. In Figure 5-19, it has been found that the temperature trace and the energy storage performance of the $MgCl_2$ – NaCl capsules are consistent with ones in first thermal cycle test. And for the energy storage and retrieval of the 10 $MgCl_2$ – NaCl capsules, the discrepancy between the two tests is ~ 1.0% within the accuracy of the measurements in current test facility. It can be concluded that the encapsulated $MgCl_2$ – NaCl capsules have sustained storage performance without the deterioration in their storage performance in current test range.
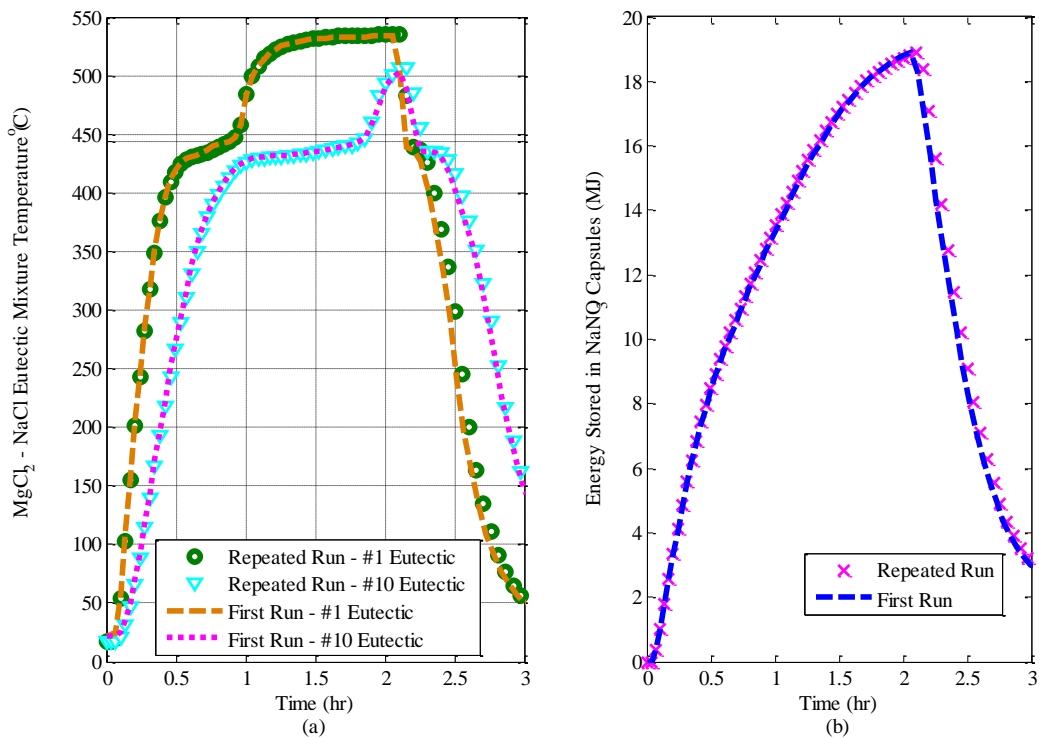
Figure 5-19. The storage performance of the $MgCl_2 - NaCl$ capsules in the repeated thermal cycle. (a) temperature of $MgCl_2 - NaCl$ eutectic salts; (b). energy stored in the $MgCl_2 - NaCl$ capsules.

5.2.2 Comparison with Predicted Results for $MgCl_2 - NaCl$ Tests

Simulations have been conducted for charging and discharging processes with $MgCl_2 - NaCl$ capsules. This is aimed to compare the experimental data with the simulation results, to investigate the capability of the model, and to improve performance the model if necessary for more accurate predictions. The mathematical model is also used to investigate the dynamics of the encapsulated $MgCl_2 - NaCl$ in the T/S during thermal cycles.

140

The model uses the measured mass flow rates of the air, and the temperature of the air at the inlet as inputs. Thermal properties of the $MgCl_2$ – NaCl eutectic mixture is tabulated in Table 5-2 and the properties of the insulation and T/S chamber has been shown previously in Table 5-1. The temperature profiles of the $MgCl_2$ – NaCl and insulation at various locations and the air temperature at the outlet are predicted.

Table 5-2. Thermal properties of the $MgCl_2$ – NaCl eutectic salts [30,45,68].

	Thermal Conductivity (W/m·°C)		Heat Capacity (J/kg·°C)		Latent Heat (kJ/kg)	Density (kg/m³)
	Solid	Liquid	Solid	Liquid		
$MgCl_2$ - NaCl	0.43	0.57	890.8	1724.6	261.2	1610[*]

*density of the eutectic has been adjusted in the model to ensure the same mass as the one in experiment.

Figure 5-20 shows the predicted and measured air temperature in a typical thermal cycle. For the temperature of air at the outlet of the T/S, there is a very good agreement between the experimental data and simulation results during the thermal cycle as shown in the figure. This indicates a good prediction for the overall thermal energy storage and retrieval of the test section during this thermal cycle based on the current simulation model.
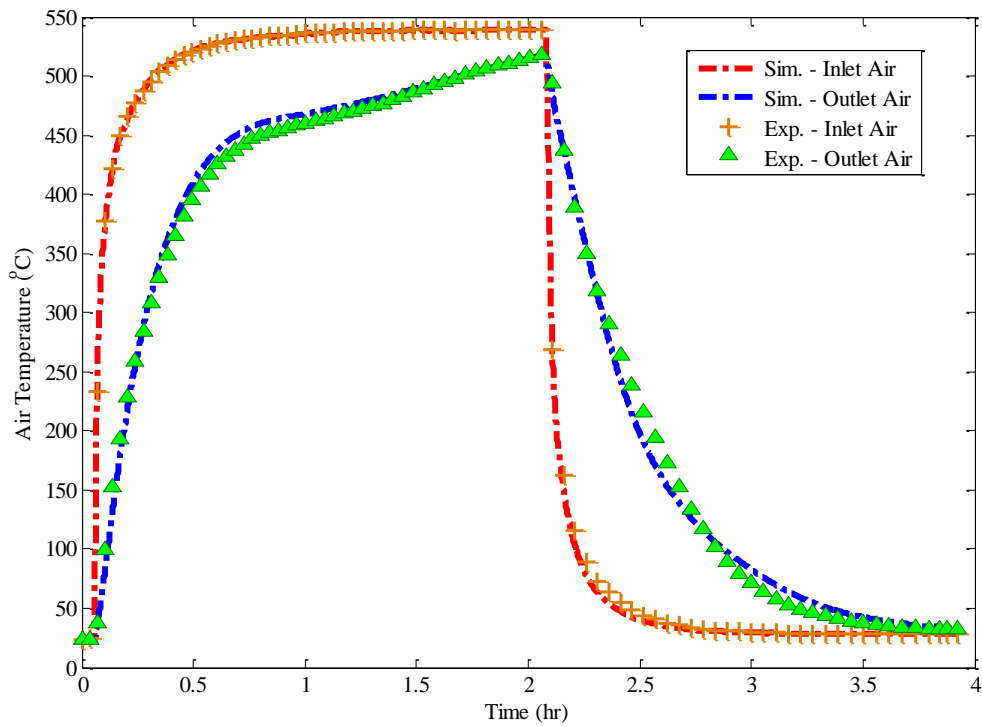
Figure 5-20. Comparison of the simulation results with the experimental data for the air at the outlet of the T/S in testing $MgCl_2 - NaCl$ eutectic mixture in a thermal cycle.

For the temperature of $MgCl_2 - NaCl$ eutectic at the specific measurement point, Figure 5-21 shows the measured temperature and simulation predicted value for the #1 capsule near the inlet and #10 capsule near the outlet of the T/S in the thermal cycle. It is seen that there is a very good agreement between the experimental data and simulation results before the melting point of the $MgCl_2 - NaCl$ eutectic in the charging process, but a considerable difference is shown as the temperature is approaching the melting point. This difference is reasonable considering that in the experiment, thermocouple contacts with the colder solid $MgCl_2 - NaCl$ eutectic which is sinking to the TC location as PCM melts. The model makes the unrealistic but computationally efficient and practical assumption that the solid $MgCl_2$

142

– NaCl eutectic stays in the center without sinking. Therefore, the simulation shows higher

values than the experimental measurements when the melting process starts.
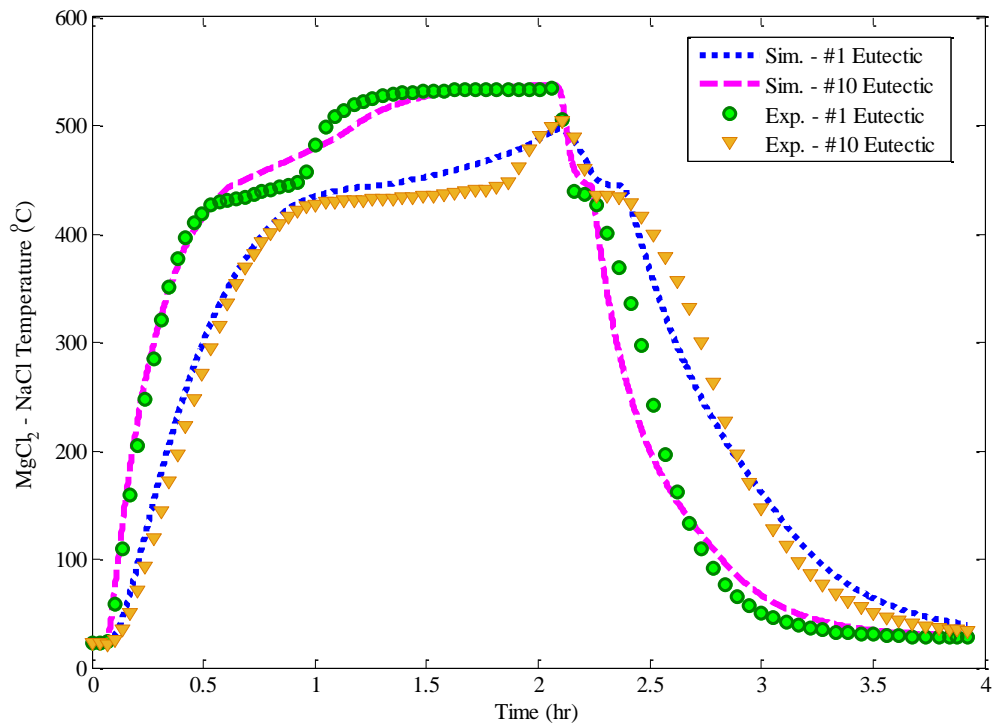
Figure 5-21. Comparison of the predicted temperature for the $MgCl_2$ – NaCl eutectic mixture with the experimental measurements for the capsules near the inlet and near the outlet of the test section.

This is confirmed with the temperature profiles at other radial locations in the EPCM

capsules. Here we take the #10 $MgCl_2$ - NaCl capsule for example, of which the

temperatures in the capsule are predicted by the model, as shown in Figure 5-22. The black

dash line shows the temperature history of the PCM at the inside surface of the capsule r

$= R_{PCM}$. It is seen that the deviation between the experimental measurements and simulation

results for the measurement points appears at the time of $t = t_1$ when the $MgCl_2$ – NaCl

eutectic at the r = R_{PCM} starts melting; while with the liquid eutectic formed at this time from the outside shell, the solid $MgCl_2$ – NaCl eutectic sinks to the bottom in the realistic operating system, therefore a lower temperature is sensed in the experiment. At the end of the charging process t = t_2, the measured temperature for the $MgCl_2$ - NaCl eutectic agrees with the predicted temperature at the inside surface of the capsule. This implies that a well-mixed $MgCl_2$ – NaCl eutectic bulk is present during the melting process due to the natural convection.
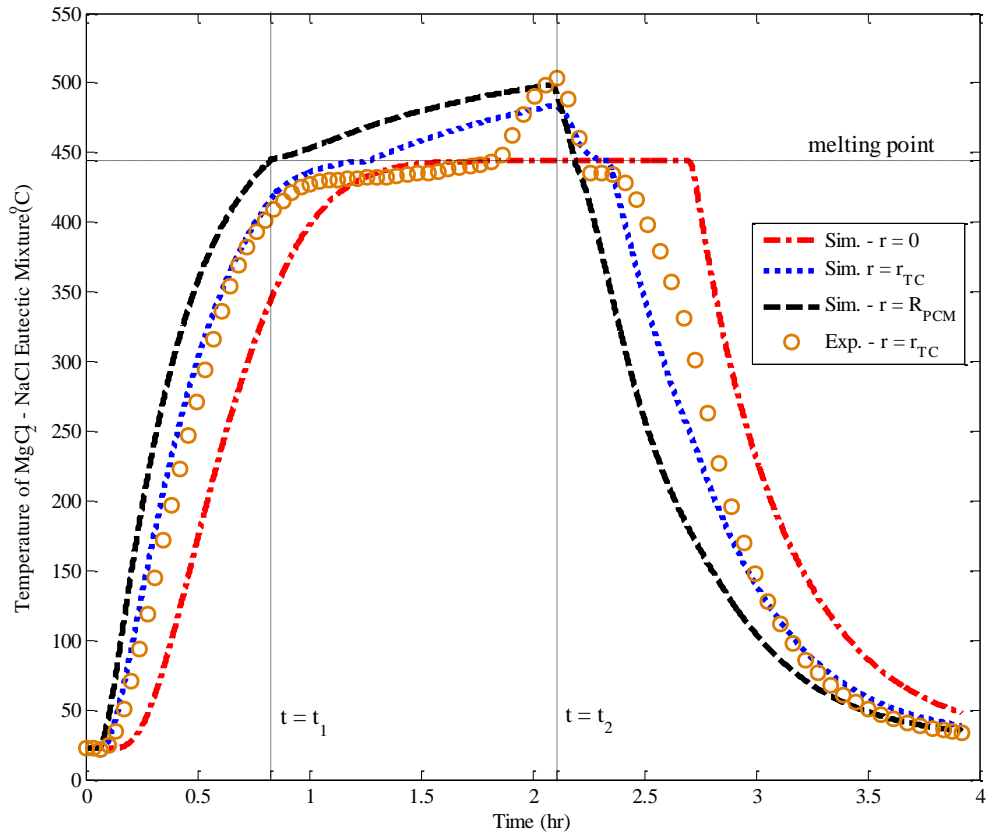
Figure 5-22. Temperature of the $MgCl_2 - NaCl$ eutectic salts of the #10 capsule in the radial directions in a thermal charging and discharging process.

In order to investigate the heat conduction in the encapsulated $MgCl_2 - NaCl$ eutectic mixture, the temperature distribution in the $MgCl_2 - NaCl$ capsule is plotted along the radial direction and shown in Figure 5-23 for the #1 capsule near the T/S inlet, and #10 capsule near the T/S outlet with the progress of time during the thermal cycle. Figure 5-23 (a) and (c) show variation of temperature in the cross section for four different times during the charging process, while Figure 5-22 (b) and (d) are for the ones during in discharging process. In the two figures Figure 5-22 (a) and (c), it is seen that the $MgCl_2 - NaCl$ eutectic

salts has been charged from room temperature to high temperature up to 530 °C with thermal resistances from the conduction and the "heat sink" due to phase change at its melting point 440 °C. As seen in Figure 5-22, the eutectic mixture in the inside surface of #1 capsule has already been heated up to ~ 475 °C, higher than its melting point of 444 °C at t =0.8 hr during the charging process, while at the center of the capsule, the eutectic mixture is ~ 50 °C lower than the temperature at the inside surface of the capsule. At this time, the inside surface of the #10 $NaNO_3$ capsule is about 420 °C at the radius with the center at ~ 330 °C. A sharp turn on temperature profile has been observed when the $MgCl_2$ – NaCl is melting. Take the #1 capsule at t = t_1 for example. The slopes of the temperature curves before and after the melting point is significantly different – the heat transfer in the liquid phase of the $MgCl_2$ – NaCl seems quicker than the heat transfer in its solid phase. This indicates the thermal resistance of the phase change is more important than the one from conduction, which has been greatly hampered the heat conduction further to the center of the solid $MgCl_2$ – NaCl eutectic mixture in this case. While compared with the case in $NaNO_3$ tests shown in Figure 5-11, the temperature difference is smaller from the center of the capsule to the inside surface of the capsule, which is due to the higher charging temperature in testing the $MgCl_2$ – NaCl capsules.

For the discharging process, effect of heat sink at the interface is again observed. The temperature of the #1 capsule drop very quickly, with the surface temperature cooled down to 200 °C from 530 °C within 0.2 hrs after the cooling starts. And at the end of the discharging process, the encapsulated $MgCl_2$ – NaCl eutectic mixture is cooled down to ~

40 °C. For the #10 capsule, because the surrounding air temperature is warmer than the upper section during the discharging process as shown in Figure 5-16, the temperature of the encapsulated $MgCl_2 - NaCl$ is cooled down slowly compared with the #1 capsule. As shown in this figure at t = 2.3 hrs (0.2 hr of discharging), its surface is still ~ 400 °C, ~ 200 °C hotter than the #1 capsule near the inlet of the test section.
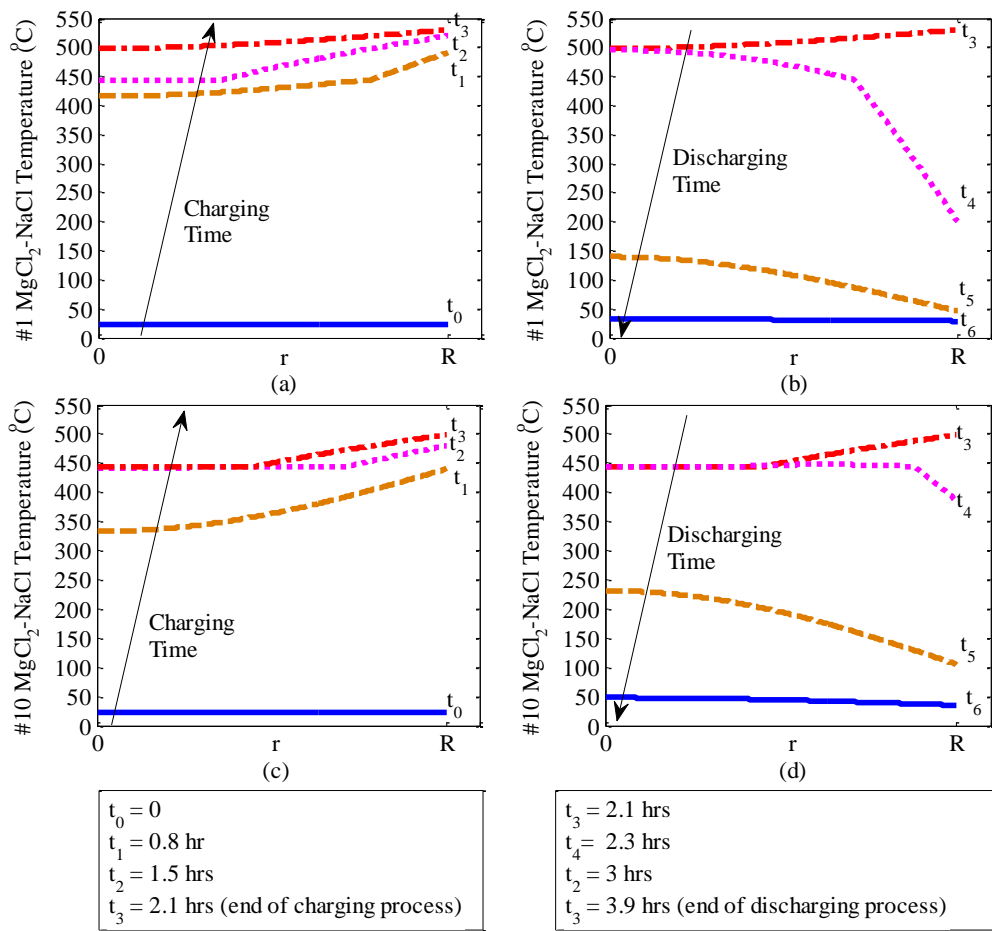
Figure 5-23. The temperature distribution in the $MgCl_2 - NaCl$ eutectic mixture in the radial direction at various times in a thermal cycle. (a). charging #1 $MgCl_2 - NaCl$ capsule; (b). discharging #1 $MgCl_2 - NaCl$ capsule; (c). charging #10 $MgCl_2 - Na$ capsule. (d). discharging #10 MgCl2 – NaCl capsule.
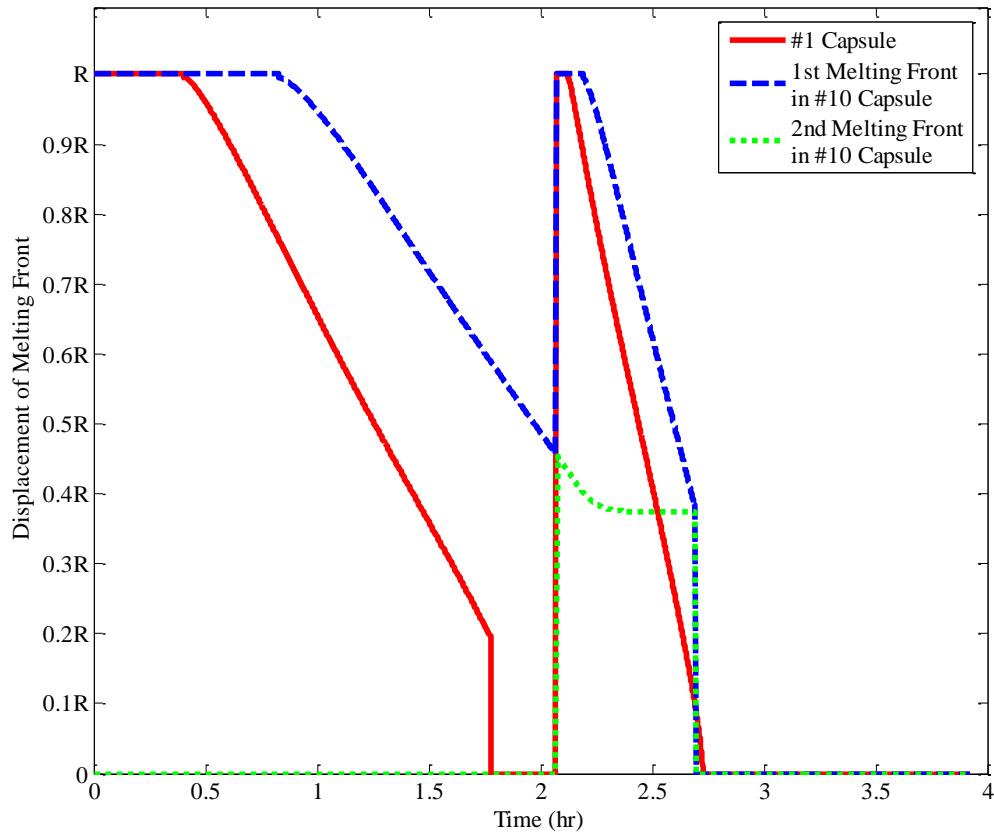
Figure 5-24. Displacement of the melting front in the #1 MgCl$_2$ - NaCl capsule and # 10 MgCl$_2$ - NaCl capsule.

If tracking the radial location and the time where and when phase change is happening during the thermal cycle, it will be easily to identify the progress of the phase change, of which the information is also used to calculate the energy storage contributed by phase change. Such information for the displacement of the melting front is shown in Figure 5-24 for the #1 MgCl$_2$ - NaCl capsule and #10 MgCl$_2$ – NaCl capsules from the simulation. During either charging or discharging process, when the value of the displacement of the melting front is equal to the inside radius of the capsule, it means that the PCM MgCl$_2$ –

NaCl eutectic mixture is in its single phase (either solid or liquid). When this value drops down to zero, it means that the $MgCl_2$ – NaCl eutectic mixture in the capsule has completely melted or solidified.

In Figure 5-24 it is seen that the $MgCl_2$ – NaCl eutectic mixture in the #1 capsule starts to melt at ~ 0.4 hr, it takes totally ~ 1.3 hours to complete the phase change. For the #10 $MgCl_2$ – NaCl capsule, it starts to melt about ~ 0.4 hour later than the #1 capsule, and at the end of the charging process t = 2.1 hrs, it is partially melted with the melting front at r = 0.45 R_{PCM}. With the partially melted $MgCl_2$ – NaCl, there are two melting fronts in the capsule when the discharging process starts. Solid phase of $MgCl_2$ – NaCl eutectic exists in the center of the capsule, which has not yet been melted, and forms from the inside surface of the capsule during the discharging process. And a liquid phase is between these two solid layers of the eutectic salts. Because there is still more energy conducted towards to the center of the capsule, the second melting front is still moving to the center, that is, the solid phase in the center is still melting during the charging process. And at ~ 2.7 hrs, the two boundaries become one as shown in Figure 5-24 and the $MgCl_2$ – NaCl eutectic salts complete solidification in the #10 capsule. With current operating conditions, i.e., ~ 540 °C hot air for charging process and ~ 25 °C cool air for discharging process, the overall solidification process is quicker in the discharging process as shown in Figure 5-23 and Figure 5-24 because of an overall higher temperature difference between the surface of the EPCM capsules and the HTF air.

In this simulation model, with the temperature history of $MgCl_2$ – $NaCl$ eutectic mixture shown in Figure 5-23 for every capsule, and the locations of the melting fronts shown in Figure 5-24, the energy stored in each of the $MgCl_2$ – $NaCl$ capsule can be calculated at any time during the thermal cycle with its phase change. Figure 5-25 shows the energy stored in each of the $MgCl_2$ – $NaCl$ capsule along the test section at various times. In this thermal cycle, the energy stored in the single capsule would be change from zero which is referred to its own initial state at time $t_1 = 0$, to the theoretical value Q^*, with the temperature of the capsule at the inlet hot air temperature 540 °C if the experiment is run infinitely. It is seen that the capsule close to the top section stores and releases the energy more quickly compared with the capsule in the bottom section, considering that in current test facility, the temperature drive for the #1 capsules is the largest both in thermal charging and discharging process. In the charging process, the variation of the stored energy between $MgCl_2$ – $NaCl$ capsules is large at the beginning along the test section since the top section is cold and the temperature drive between the air and capsule is large. Then this variation become smaller with the top section heated up during the charging process. At the beginning of the discharging process, the energy stored in #1 capsule drops significantly by 0.7 MJ in ~ 0.3 hr, while the energy stored in #10 capsule barely changes because its surrounding air is warm after extracting the heat from the capsules in its upper section. At the end of the discharging process $t = 3.9$ hrs, there are still very few energy residue in the $MgCl_2$ – $NaCl$ capsules shown in Figure 5-25.
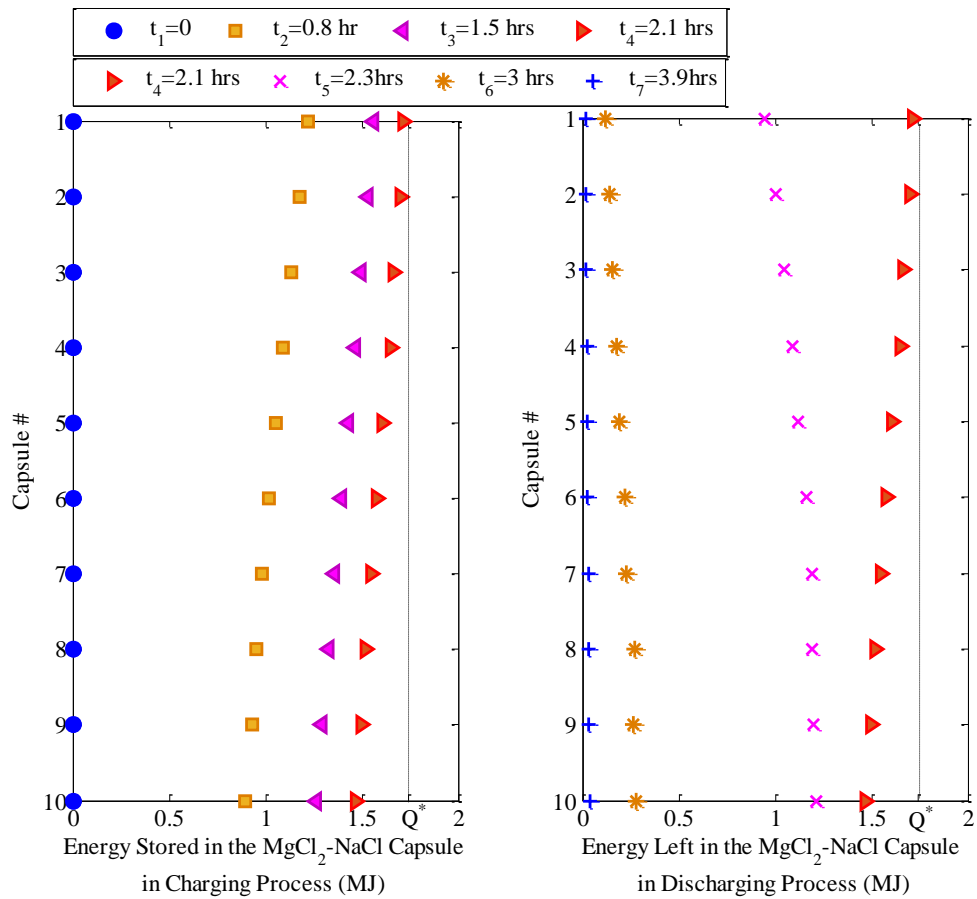
Figure 5-25. Energy stored in the $MgCl_2 - NaCl$ capsule at different variation in the test section.

When summing up the energy stored in each single capsule shown in Figure 5-25, the total energy stored in the 10 $MgCl_2 - NaCl$ capsules can be obtained as shown in Figure 5-14 by blue dash line. It is seen that the experimental measurements for the energy stored in $MgCl_2 - NaCl$ capsules have been well predicted at the beginning of the charging, when the $MgCl_2 - NaCl$ is mostly in solid phase. Then the difference appear especially after 0.5 hr when the encapsulated $MgCl_2 - NaCl$ in the #1 capsule starts to melt as discussed previously in Figure 5-24. At the end of the charging process, the difference between the

151

estimate and experimental measurement is approximately 8.7% for the energy stored in the 10 $MgCl_2$ – NaCl capsule. As discussed previously for the results of $NaNO_3$ testing, the difference might due to the natural convection in the liquid phase of the $MgCl_2$ – NaCl eutectic mixture, which enhances the heat transfer during its melting process.
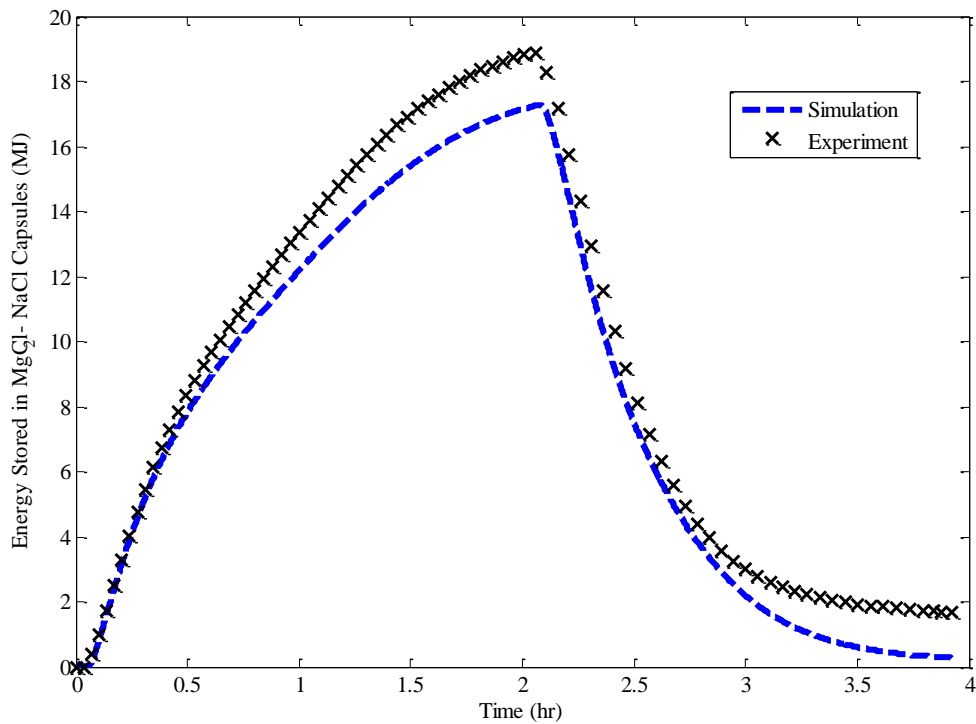
Figure 5-26. The comparison of the energy stored in the overall 10 $MgCl_2$ – NaCl capsules in a thermal cycle between the simulation model and experimental measurements.

5.3   Performance Tests with Encapsulated $NaNO_3$ Capsules and Encapsulated $MgCl_2$-

NaCl Capsules

5.3.1   Performance Tests with Cascaded Encapsulated PCM Capsules

Latent heat storage offers a theoretical potential of significant reduction in storage material by utilizing PCM's latent heat. To realize a high utilization of the PCM and a high efficiency of the turbine in the downstream, a configuration of multiple PCMs can be used. Proposal for cascaded latent heat storage can be found in server publications for application in parabolic through solar power plants [37,38,69]. In these proposals, salts or salts mixture with different melting temperatures are combined and tested in a TES system, where PCM with a lower melting temperature is placed in the "cold end" (bottom of the storage system), and PCM with a higher melting point is placed in the "hot end" (top of the storage system). In this way, during the charging process, when HTF flows from "hot end" to "cold end", the temperature drive can be maintain in a desired temperature range with judicious choice of the operating conditions and PCM in the bottom of the storage system.

In this project, the two salts – $NaNO_3$, and $MgCl_2$ – NaCl eutectic salts have been selected as promising PCMs for energy storage, and tested in the pilot-scale system and shown the technical feasibility in storage and retrieval of the thermal energy in thermal cycles. After the $NaNO_3$ tests, and eutectic salts tests, the test section is tested with 5 $MgCl_2$ – NaCl capsules and 5 $NaNO_3$ capsules, with the encapsulated $MgCl_2$ – NaCl (melting point, 444 °C) at the top of the T/S, and the encapsulated $NaNO_3$ (melting point 308°C) at the bottom of the T/S.

Figure 5-27 shows the temperature history of the air at the inlet and at the outlet of the T/S, as well as the temperature trace of the #1 $MgCl_2$ – NaCl eutectic and #10 $NaNO_3$ eutectic

153

near the outlet of the T/S in a typical thermal cycle. It is seen that in the heating process, the air is quickly heated by the external heater to 540 °C to charge the cascaded EPCM capsules, while in the discharging process, the heater is turned off and the cool air is sent to the test section to extract the energy from the capsules. As shown in this figure, with a short transition, the inlet air temperature is about 540 °C in the charging process and about 28 °C in the discharging process.

For the temperature of encapsulated $MgCl_2$ - $NaCl$ and encapsulated $NaNO_3$, the temperature increase of the salts significantly slows down when it is approaching to their melting points respectively. For the #1 $MgCl_2$ - $NaCl$ capsule near the inlet of the T/S, after the eutectic mixture completely melts, it is superheated quickly in the liquid phase with ~ 535 °C at the end of this charging process. For the #10 $NaNO_3$ capsule near the outlet of the T/S, after the nitrate completely melts, it is superheated quickly in the liquid phase with ~ 475 °C at the end of the charging process. In the charging process with cascaded PCMs, it is seen that #1 encapsulated $MgCl_2$ - $NaCl$ and #10 encapsulated $NaNO_3$ starts to melt about the same time, and all the PCMs complete phase change in one hour. This test results are compared with the test results with 10 $MgCl_2$ - $NaCl$ capsules and the results are shown in Figure 5-28 for the temperature of outlet air and #10 EPCM capsule near the outlet of T/S in a charging process. It is obvious that the temperature difference between the air and the PCM at measurement location is higher in the lower section with two cascaded EPCM in the test section, which implies one of the advantages in utilizing cascaded EPCM in the test section − obtain high temperature in heat transfer from the HTF air to the storage

154

medium. And in the discharging process, both of the $MgCl_2 - NaCl$ eutectic salts and encapsulated $NaNO_3$ cool down quickly with sharp turns when they decreases to their solidification points respectively, and the comparison with the discharging test results with $10\ MgCl_2 - NaCl$ capsules will be elaborated later with the simulation results.
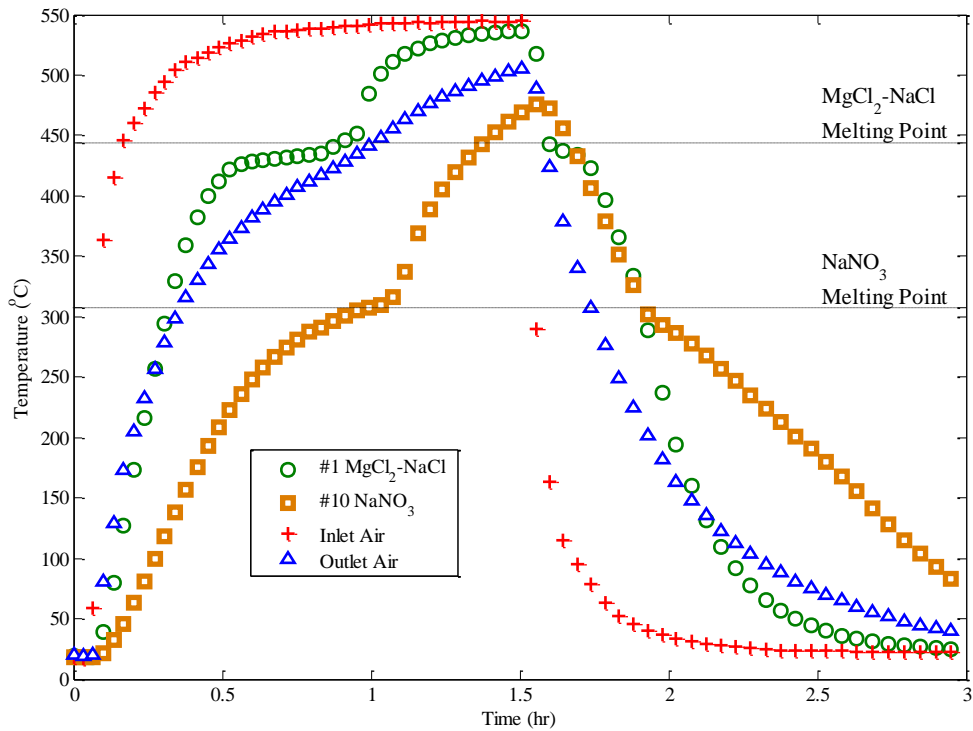
Figure 5-27. Temperature history of the air and PCMs in the test section with cascaded PCMs in a thermal cycle.
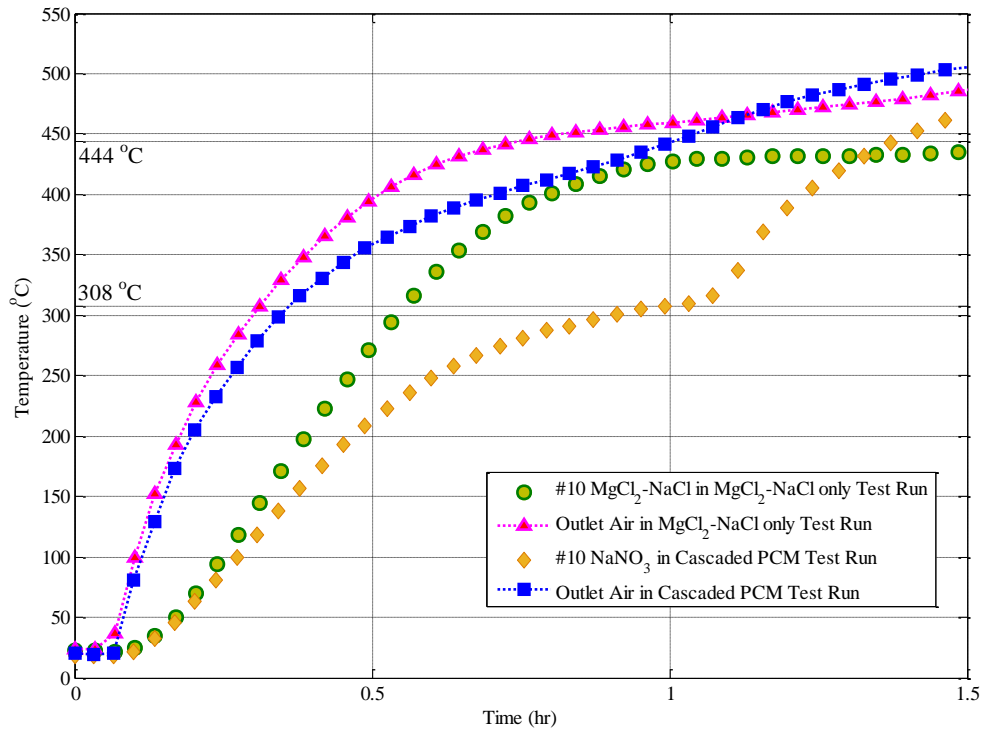
Figure 5-28. Comparison of the temperature history of the air and PCM for the test section with $MgCl_2$ – NaCl eutectic salts only, and the test section with cascaded PCMs in the charging process.

Figure 5-17 shows the total energy stored in the 5 $MgCl_2$-NaCl capsules and 5 $NaNO_3$ capsules in a thermal cycle. All the energy values are referred to initial state of the EPCM capsules at t=0. It is seen that the cascaded EPCM capsules successfully capture the energy from the air during the charging process with an accumulated 20 MJ energy stored at the end of the experiment. Then in the continued discharging process, the energy stored energy in the capsules decreases with the cool air, which indicates the air is effectively extracting the energy from the capsules. At the end of the discharging process, there is still approximately 2 MJ energy residue in the EPCM capsules since they are slightly warmer

156

than their own initial state, as shown in Figure 5-27. In other words, at the end of the discharging process, the total energy retrieved from the capsules is ~ 18 MJ with the cascaded EPCM capsules changing from ~ 535 °C – 45 °C. If we assume the temperature of the shell of the #1 and #10 capsules are the same with the air at the inlet and at the outlet of the test section respectively, and a linear temperature change from the #1 to #10 capsule shells, the total energy stored into the capsules themselves can be estimated, and this value is close to the real but would be slightly overestimated since the shell temperature should be lower than its surrounding air. Subtracting this estimated energy stored by the capsule shells, there is about 16.2 MJ energy stored in the 17.2 kg salts at the end of the charging process. If we assume that the PCM is completely melted based on the temperature profiles shown in Figure 5-27, the latent heat of the phase change contributes ~ 23% of the total energy stored by the EPCM.
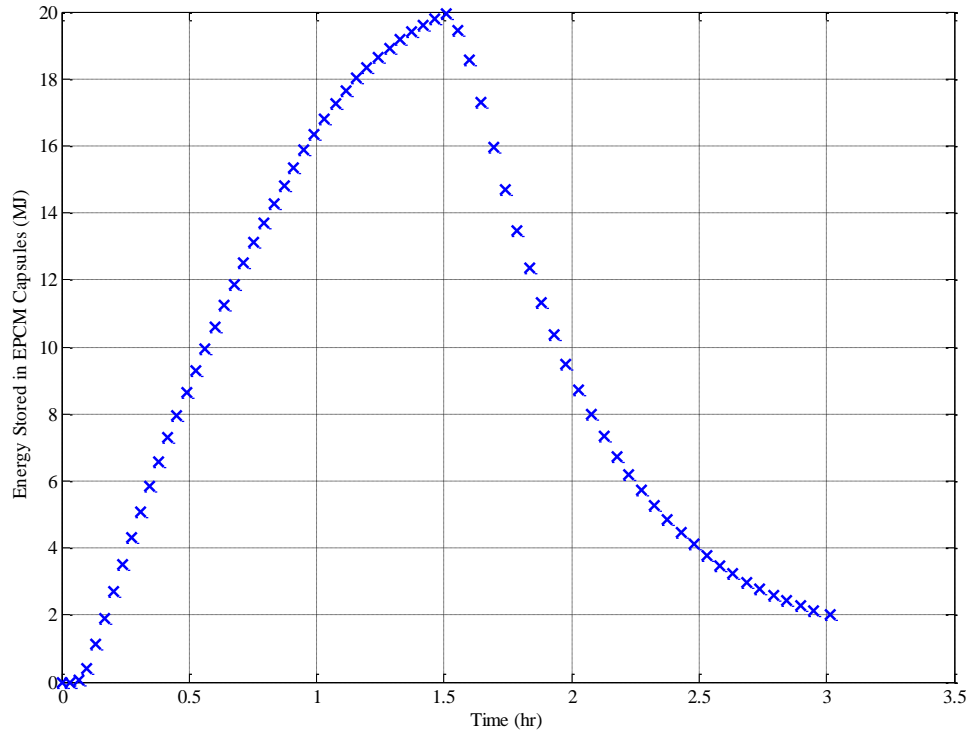
Figure 5-29. The energy stored in the cascaded EPCM capsules in a typical charging and discharging process.

As discussed previously and shown in Figure 5-17, when the test section is loaded with $MgCl_2 - NaCl$ capsules only, the encapsulated $MgCl_2 - NaCl$ eutectic mixture store ~ 18.9 MJ in a two-hour charging process. If we compare the energy storage performance in the duration of 1.5 hours as shown in Figure 5-30, the test section with cascaded EPCM is seen to store more energy after 0.5 hour in a charging process, since in its lower section, the encapsulated NaNO3 starts to melt and the latent heat contributes to the total energy stored by the EPCM.
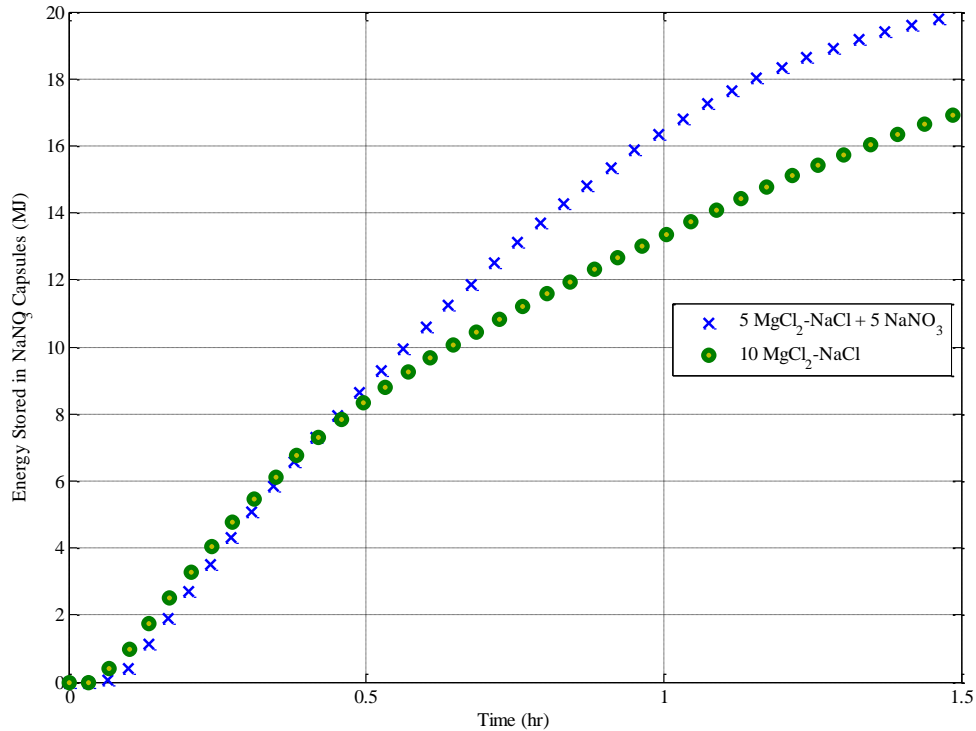
Figure 5-30. The comparison of the total energy stored in EPCM capsules in two different test section configurations − with cascaded EPCMs and with $MgCl_2$ − $NaCl$ only.

Besides the total energy stored in the cascaded EPCM capsules, their thermal response, that is, the rate of energy storage and removal is another key parameter for evaluation of the storage performance the cascaded EPCM capsules in the test section, while it indicate the overall heat transfer between the HTF and EPCM capsules in the thermal charging and discharging process. In the experiment, the rate of the energy storage and removal is obtained by calculating the derivative of the energy stored in the 5 $MgCl_2$ − $NaCl$ capsules and 5 $NaNO_3$ capsules over the time of thermal testing and the results are shown in Figure 5-31 for rate of the energy storage and retrieval for the cascaded capsules in the typical thermal cycle. As seen in the figure, the rate of the energy storage increases quickly first

and reaches to a maximum of ~ 6.5 kW, and then slows down and decreases to ~ 1 kW at the end of this charging process. In the discharging process, since the energy left in the capsules is decreasing with the experimental time, therefore the rate of the energy storage for the capsules is negative as shown in the figure. It is seen that the rate of energy removal, the absolute value of the rate of the energy stored into the capsules in this cooling process, is with a similar trend as the rate of energy storage in the charging process. It increases quickly to its maximum of ~ 6 kW and then decreases to ~ 0.5 kW at the end of this discharging process.
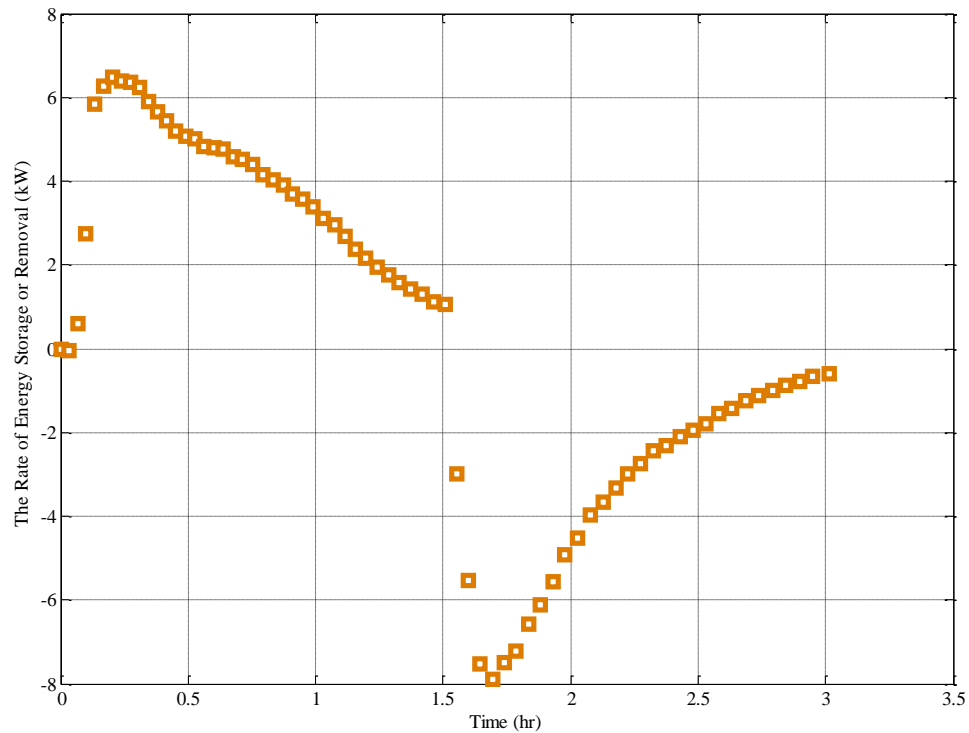
Figure 5-31. The rate of energy storage and retrieval of the cascaded EPCM capsules in the T/S in a typical thermal charging and discharging process.

160

From this thermal cycle test for the test section with 5 $MgCl_2 - NaCl$ capsules and 5 $NaNO_3$ capsules, it has been well demonstrated that the cascaded EPCM based test section can successfully store and retrieve thermal energy at the temperature up to 540 °C, with the $MgCl_2 - NaCl$ eutectic mixture melted at 444 °C in the charging process, and solidified in the discharging process, and with the $NaNO_3$ melted at 308 °C in the charging process and then solidified in the discharging process.

Compared of the performance of the cascaded EPCM with the test section with $MgCl_2 - NaCl$ capsules only, it has been shown that with the cascaded EPCM configuration, it will enhance the heat transfer from the HTF air to the EPCM capsules with a lower melting point in the lower section of the test section with a higher temperature drive between them. In current test section with the two chosen salts, it is also advantageous to store more energy with cascaded EPCM setup.

5.3.2   Comparison with Predicted Results for Cascaded EPCMs Tests

Followed the experimental testing of the five $MgCl_2 - NaCl$ capsules and five $NaNO_3$ capsules in the T/S, a simulation model has been run for the tests with the cascaded EPCM capsules. This is aimed to compare the experimental data with the simulation results first, such as the temperature of the EPCM in different locations of the test section - the encapsulated $MgCl_2 - NaCl$ eutectic mixture in the top section and the encapsulated $NaNO_3$ in the bottom section, in order to generally investigate the capability of the simulation

161

model and explore further the advantages in using cascaded EPCM capsules in the T/S. In the simulation of the experimental testing with the cascaded EPCM capsules, the experimental mass flow rates of the air, and the temperature of the air at the inlet of the T/S have been fit to a function of time respectively, and used as two inputs in the model. Thermal properties of the materials are tabulated previously in Table 5-1 and Table 5-2.

Figure 5-32 shows the comparison between the simulation predicted value and experimental data for the temperature of the air at the outlet of the test section in a thermal cycle for the test section with cascaded EPCM capsules. As seen in the figure, the air temperature at the inlet has been used as one of the inputs in the simulation, therefore the simulation one is overlapping with the experimental data shown by red crosses. For the temperature of the air at the outlet of the test section, it is seen that it is well predicted by the simulation model in the discharging process, and for the discharging process, it is slightly overestimated in the time period of ~ 0.5 hr – 1.2 hrs. With the temperature information of the salts shown in Figure 5-27, it implies an underestimates in heat transfer from the HTF air to the EPCM capsules during the PCM's melting process during the charging process.
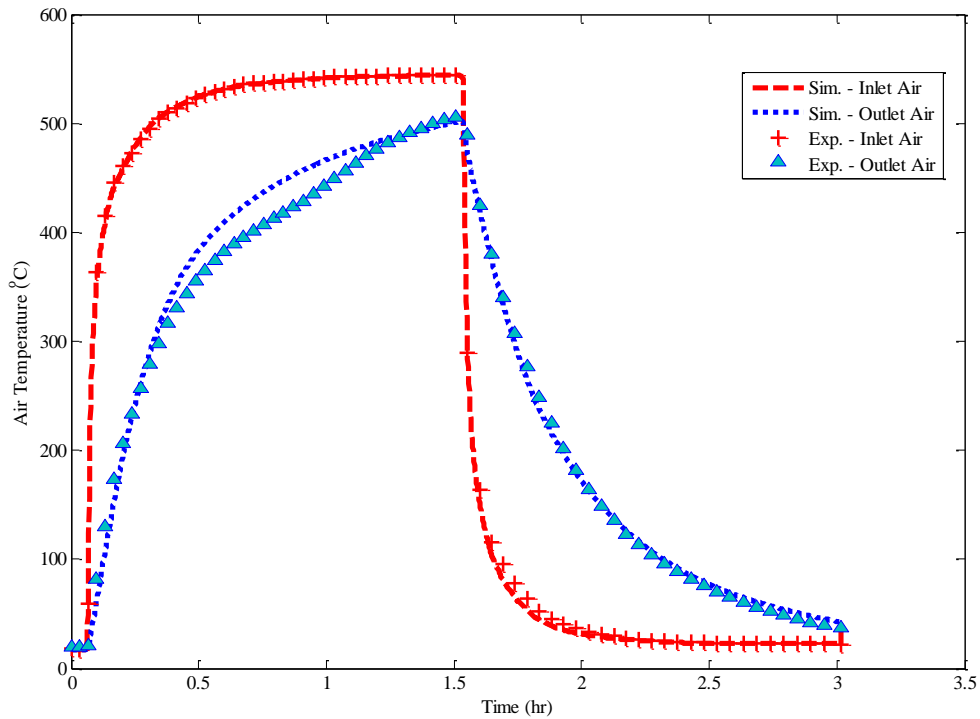
Figure 5-32. Comparison of the simulation results with the experimental data for the air at the outlet of the T/S in testing cascaded EPCM in a thermal cycle.

Figure 5-33 shows the measured temperature and simulation predicted values for the #1 capsule near the inlet and #10 capsule near the outlet in this thermal cycle. It is seen that for both of the capsules, there is a very good agreement between the experimental data and simulation results before their melting points respectively, but a considerable difference is shown in the time when the temperature is approaching the melting point. This difference is reasonable considering as discussed previously, that is, in the experiment, thermocouple contacts with the cold solid PCM which is sinking to the TC location when the liquid is formed from outside shell shown in Figure 5-3. While in the simulation, the solid PCM is assumed to stay in the center without sinking. Therefore, the simulation shows higher

163

values than the experimental measurements when the melting process starts.
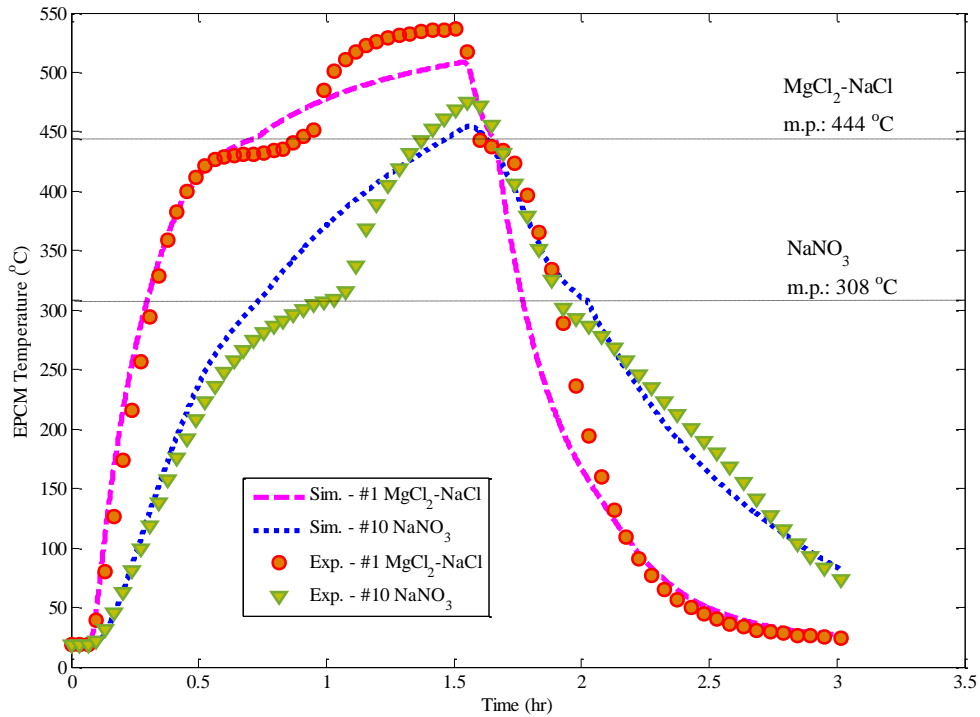
Figure 5-33. Comparison of the predicted EPCM temperature with the experimental measurements for the #1 capsule near the inlet and #10 capsule near the outlet of the test section.

This phenomena and above explanations can be further confirmed with the extra information of the temperature profiles at other radial locations in EPCM capsule. Figure 5-34 shows the temperature of the $MgCl_2 - NaCl$ eutectic salts in various locations in the #1 capsule near the inlet of the test section, while Figure 5-35 shows the predicted temperature information for the $NaNO_3$ in the #10 capsule near the outlet of the test section. It is seen that the temperature of the EPCM is well predicted when it is heated up as a solid phase in the charging process. When the EPCM starts phase change, that is the inside

164

surface (r = R$_{PCM}$) of the capsule reaches the melting point, there appear a deviation between the experiment measurements and simulation results at the measurement point in both of the figures, which due to the natural convection and the sinking of the solid PCM when the liquid PCM is formed at the outside. At the end of the charging process, the measured EPCM temperature agrees with the predicted temperature at the inside surface of the capsule as shown in Figure 5-34 and Figure 5-35, which might indicate a well-mixed EPCM bulk during the melting process because of the natural convection.
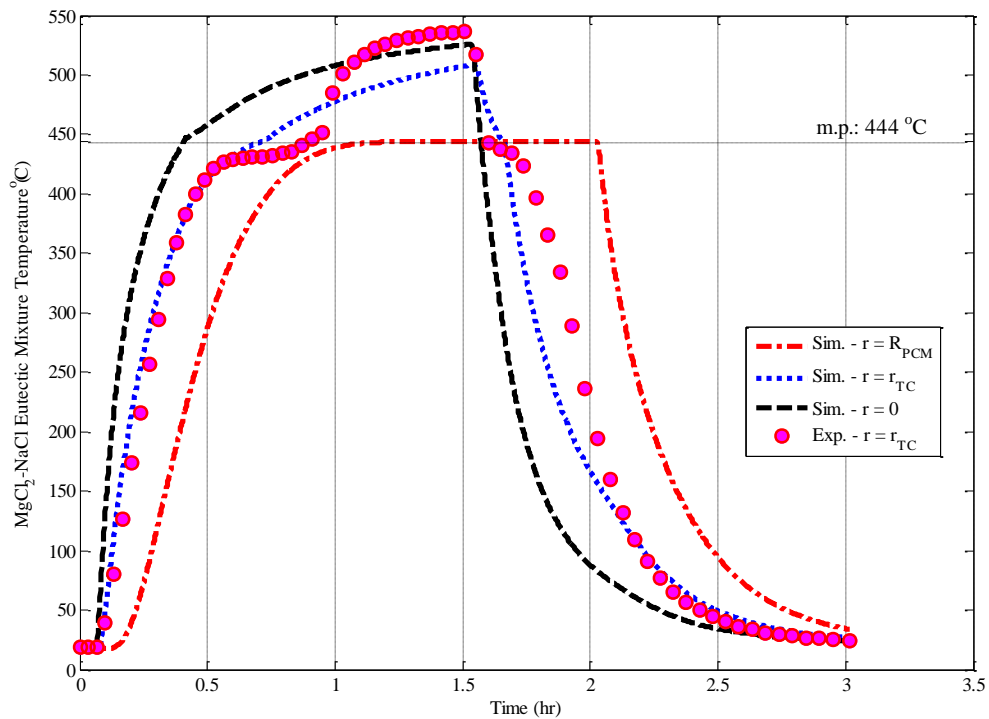
Figure 5-34. Temperature of the MgCl$_2$ – NaCl eutectic salts in the #1 capsule in various radial directions in a thermal test of cascaded EPCM capsules.
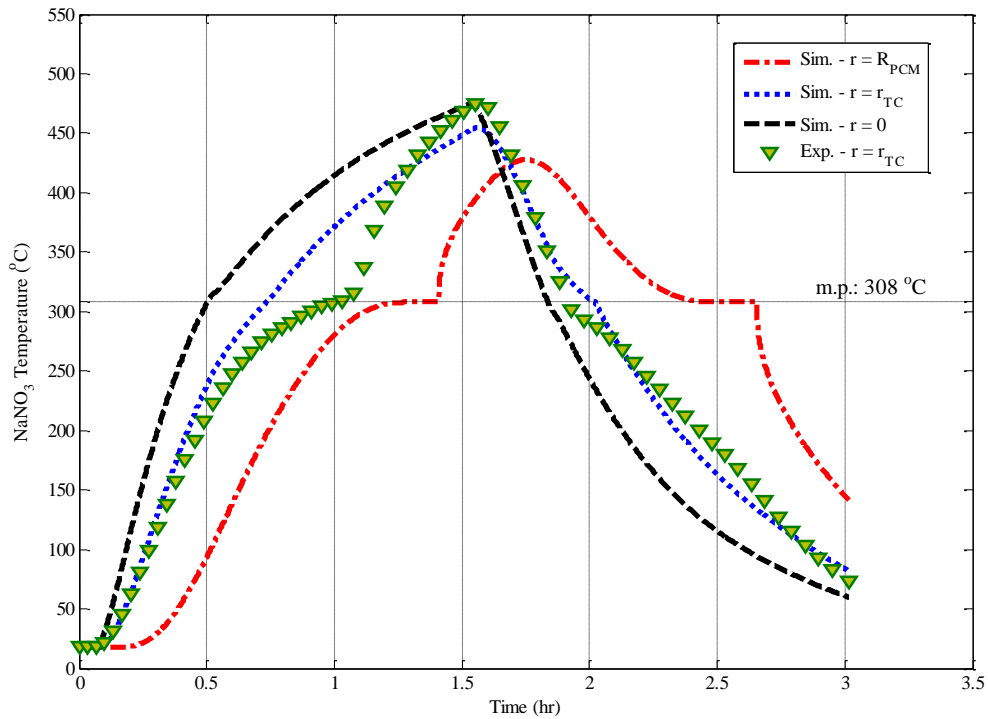
Figure 5-35. Temperature of the NaNO$_3$ in the #10 capsule in various radial directions in a thermal test of cascaded EPCM capsules.

In order to investigate the heat conduction in the encapsulated PCM in the test run with cascaded EPCM capsules, the temperature distribution in the EPCM is plotted along the radial direction and shown in Figure 5-36 for the #1 MgCl$_2$ – NaCl capsule near the T/S inlet, and #10 NaNO$_3$ capsule near the T/S outlet with the progress of time during the thermal cycle. Figure 5-36 (a) and (c) are shown for the temperature information of the EPCM in the charging process, while Figure 5-22 (b) and (d) are for the discharging process. In the two figures

Figure 5-36 (a) and (c), it is seen that the $MgCl_2$ – NaCl eutectic salts has been charged from room temperature to high temperature up to 530 °C with thermal resistances from the conduction and the "heat sink" due to phase change at its melting point 444 °C. As shown in Figure 5-36 (a), the $MgCl_2$ – NaCl eutectic mixture in the inside surface of #1 capsule has already been heated up to ~ 450 °C above its melting point 444 °C at t =0.5 hr in the charging process, while at the center of the capsule, the eutectic mixture is ~ 160 °C lower than the temperature at the inside surface of the capsule. At this time, the inside surface of the #10 $NaNO_3$ capsule is about 250 °C with the center heated up to ~ 100 °C. A sharp turn point has been observed in the temperature curve when the $MgCl_2$ – NaCl is melting.Take #1 $MgCl_2$ – NaCl capsule at t = t_3 for example. The slopes of the temperature curves before and after the melting point is significantly different – the heat transfer in the liquid phase of the $MgCl_2$ – NaCl seems quicker than the heat transfer in its solid phase. This indicates the thermal resistance of the phase change is more important than the one from conduction, which has been greatly hampered the heat conduction further to the center of the solid $MgCl_2$ – NaCl eutectic mixture in this case. And Figure 5-36 (c) shows similar phenomena for the #10 encapsulated $NaNO_3$ during its phase change from solid phase to liquid phase.

For the discharging process, sharp turn points have been also observed during the solidification of the encapsulated PCM in both of the #1 $MgCl_2$ – NaCl capsule and #10 $NaNO_3$ capsule. The temperature of the #1 $MgCl_2$ – NaCl capsule drop very quickly, with the surface temperature cooled down to 100 °C from 530 °C after 0.5 hrs discharging by the cool air. At the end of the discharging process, the encapsulated $MgCl_2$ – NaCl eutectic

mixture is cooled down to ~ 40 °C. For the #10 NaNO₃ capsule, because the surrounding

air temperature is warmer than the upper section during the discharging process as shown

in Figure 5-27, the temperature of the encapsulated NaNO₃ is cooled down slowly

compared with the #1 MgCl₂ – NaCl capsule. As shown in this figure at t = 2 hrs (0.5 hr of

discharging by the cool air), its surface is ~ 250 °C, ~ 150 °C hotter than the #1 MgCl₂ –

NaCl capsule near the inlet of the test section.
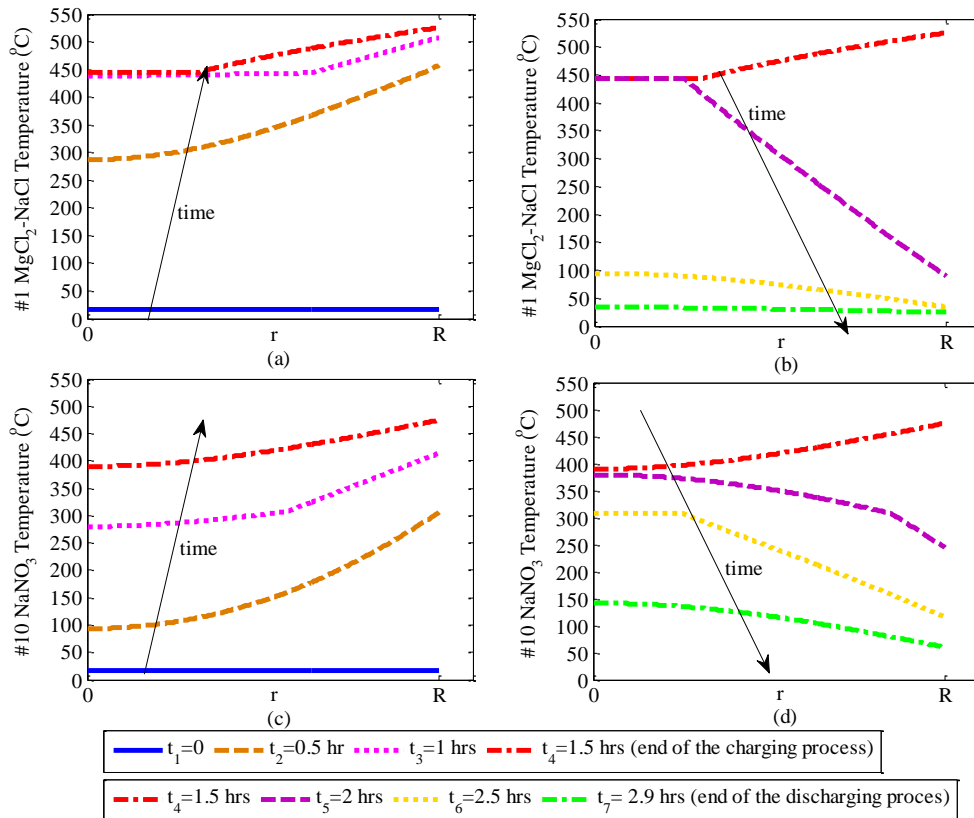
Figure 5-36. The temperature distribution in the EPCM in a thermal cycle test with cascaded EPCM capsules. (a). charging #1 MgCl₂ – NaCl capsule; (b). discharging #1 MgCl₂ – NaCl capsule; (c). charging #10 NaNO₃ capsule. (d). discharging #10 NaNO₃ capsule.

If tracking the radial location and the time where and when phase change is happening

during the thermal cycle, it will be easily to identify the progress of the phase change, of which the information is also used to calculate the energy storage contributed by phase change. Such information for the displacement of the melting front is shown in Figure 5-37 for the #1 $MgCl_2$ - NaCl capsule and #10 $NaNO_3$ capsule from the simulation. In either charging or discharging process, when the value of the displacement of the melting front is equal to the inside radius of the capsule, it means that the encapsulated PCM is in its single phase (either solid or liquid). When this value drops down to zero, it means that the EPCM in the capsule has completely melted or solidified.

In Figure 5-37 it is seen that the $MgCl_2$ – NaCl eutectic mixture in the #1 capsule starts to melt at ~ 0.4 hr, and at the end of the charging process, it is partially melted with the melting front at r = 0.3R away from the center of the capsule. For the #10 $NaNO_3$ capsule, it starts to melt about ~ 0.5 hour, slightly later than the #1 capsule, and completes melting at the end of the charging process.

With the partially melted $MgCl_2$ – NaCl in the #1 capsule, there are two melting fronts in the capsule when the discharging process starts. Solid phase of $MgCl_2$ – NaCl eutectic exists in the center of the capsule, which has not yet been melted, and forms from the inside surface of the capsule during the discharging process. And a liquid phase is between these two solid layers of the eutectic salts. It is seen that the second melting front is still moving to the center, that is, the solid phase in the center is still melting during the charging process. At time = ~ 2.05 hrs, the two boundaries become one as shown in the figure and the $MgCl_2$

169

– NaCl eutectic salts complete solidification in the #1 capsule at that time. For the #10 NaNO$_3$ capsule, the PCM NaNO$_3$, it starts to solidify at time = ~ 1.7 hrs, and complete the phase change in ~ 1 hr. With current operating conditions, i.e., ~ 540 °C hot air for charging process and ~ 25 °C cool air for discharging process, the overall solidification process is quicker in the discharging process because of an overall higher temperature difference between the surface of the EPCM capsules and the HTF air.
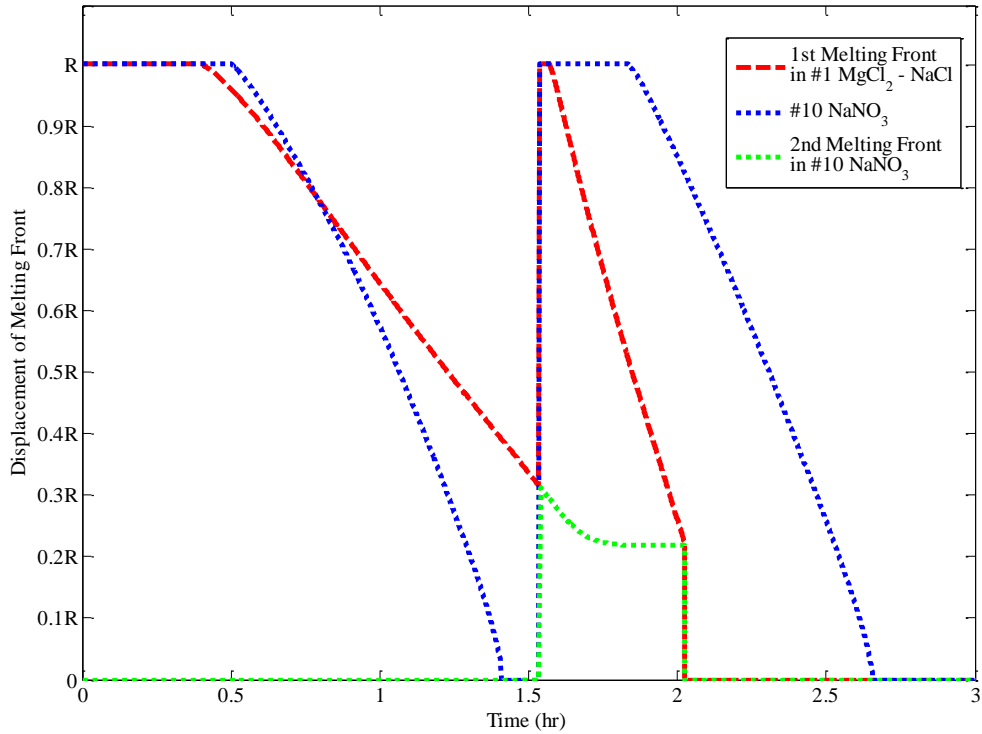

Figure 5-37. Displacement of the melting front in the cascaded EPCM capsules in a thermal cycle.

In this simulation model, with the temperature history of MgCl$_2$ – NaCl eutectic mixture and NaNO$_3$ shown in Figure 5-27 and Figure 5-36 for every capsule, and the locations of

170

the melting fronts shown in Figure 5-37, the energy stored in each cascaded EPCM capsule can be calculated at any time during the thermal cycle with its phase change. Figure 5-38 shows the energy stored in each of the capsule along the test section at various times. In this thermal cycle, the energy stored in the single capsule would be change from zero which is referred to its own initial state at time $t_1 = 0$, to the theoretical value Q^*, with the temperature of the capsule at the inlet hot air temperature 540 °C if the experiment is run infinitely. For the top section, the $MgCl_2 - NaCl$ eutectic mixture is encapsulated in the capsule from #1 and #5, and the theoretical value of each of the capsule is denoted as $Q_{MgCl2-NaCl}^*$, and for the bottom section, $NaNO_3$ is encapsulated in the capsule from #6 to #10, and the theoretical value of each of the $NaNO_3$ capsule is denoted as Q_{NaNO3}^*.

In Figure 5-38, it is seen that the capsule close to the inlet stores and releases the energy more quickly compared with the capsule far from the inlet of the T/S in the top and bottom section respectively, considering that in current test facility, the temperature drive is larger in the upper section both in thermal charging and discharging process. In the charging process for the top and bottom section of the T/S, the variation of the stored energy between EPCM capsules is large at the beginning and decrease with the proceeding time. In Figure 5-38, it is also seen that the average energy stored in the $NaNO_3$ capsule is higher than the energy stored in the $MgCl_2 - NaCl$ capsule. Take the energy storage at time $t_4=1.5$ hr in the charging process for example. This is because the storage capacity of the $NaNO_3$ is higher than the $MgCl_2 - NaCl$ eutectic in the solid phase, and at that time, all of the $NaNO_3$ has completed melting as shown in with additional heat stored by its phase change.

171
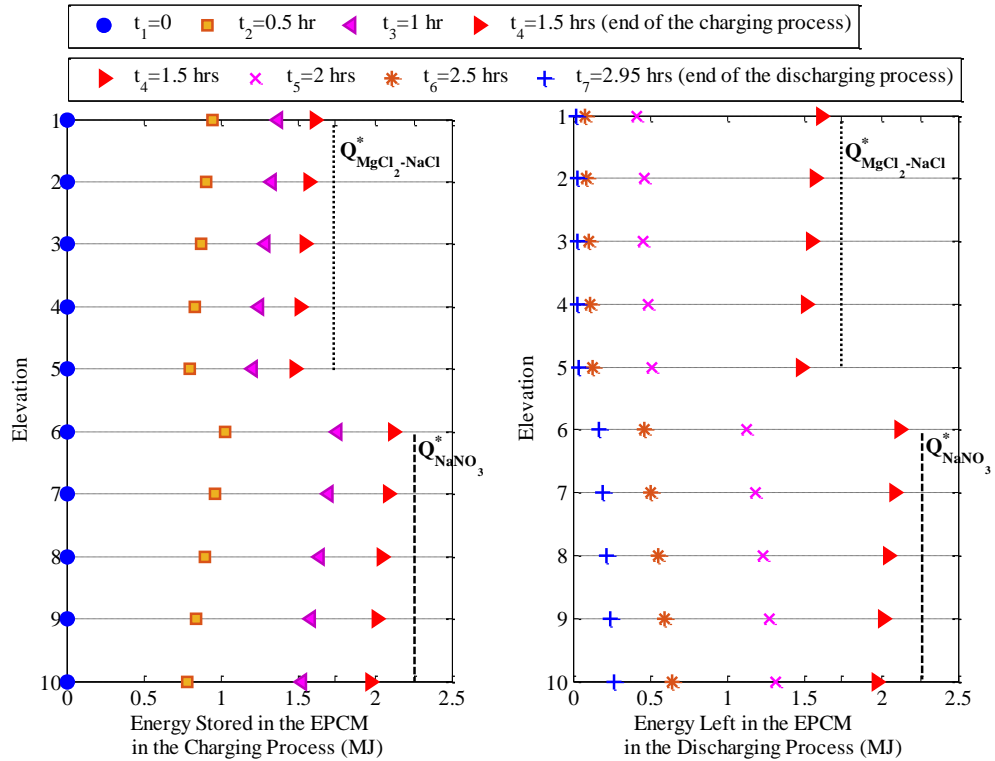
Figure 5-38. Energy stored in the cascaded EPCM capsule at different variation in the test section in a thermal cycle.

When summing up the energy stored in each single capsule shown in Figure 5-38, the total energy stored in the 5 $MgCl_2 - NaCl$ capsules and 5 $NaNO_3$ capsules can be obtained as shown in Figure 5-39 by purple solid line. It is seen that the experimental measurements for the energy stored in the ten cascaded capsules have been well predicted at the beginning of the charging, when the encapsulated PCM is mostly in solid phase. Then the difference appears especially after 0.7 hr when the encapsulated PCMs in the capsules start to melt as shown in Figure 5-37. At the end of the charging process, the difference between the estimate and experimental measurement is approximately 7.1 % for the energy stored in the ten capsules. As discussed previously for the results of $NaNO_3$ testing and $MgCl_2 -$

NaCl eutectic testing, the difference might due to the natural convection in the liquid phase

of the PCM, which enhances the heat transfer during its melting process. Therefore the

measured energy storage is higher than the predictions from the simulation model.
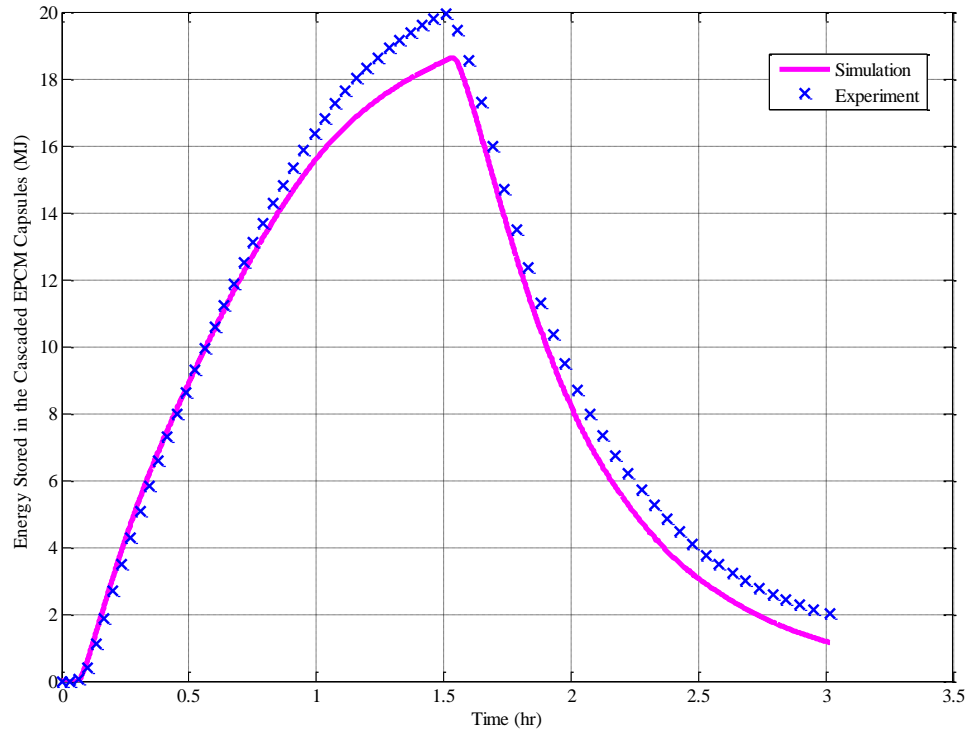
Figure 5-39. The comparison of the energy stored in the cascaded capsules in a thermal
cycle between the numerical predicts and experimental measurements.

5.4   Summary of the Performance Tests of EPCM-Based TES System

In this research, a pilot-scale test section is designed and built to demonstrate latent heat

based thermal energy storage using EPCM at temperatures up to 540 °C. $NaNO_3$ and $MgCl_2$

– NaCl eutectic salts are selected and used as storage media and are encapsulated in

stainless steel cylinders. Compressed air is used as the heat transfer fluid. Multiple EPCM capsules are installed in the test section for the demonstrations of the energy storage and retrieval with phase change in thermal cycles. The test facility and measurement methodology have been initially qualified using solid copper capsules and then loaded with EPCM capsules for performance test. A numerical model is developed to investigate the dynamic performance of the charging and discharging of the test section with phase change in the EPCM capsule.

The experimental and the numerical investigations indicate that:

- The test section with the EPCM capsules successfully demonstrated its ability to transfer thermal energy to and from a transport fluid, achieving energy storage and retrieval in multiple charging and discharging cycles.

- For the test section with $NaNO_3$ capsules, in a given storage – retrieval cycle where $NaNO_3$ capsule temperatures varied from ~ 50 °C - ~ 400 °C, the test section has been found to store significant amount of thermal energy per EPCM capsule (~ 451 kJ/kg), with the $NaNO_3$ material (PCM) accounting for ~ 76% of the energy stored in the capsules. The latent heat of phase change of the $NaNO_3$ contributed to ~ 17% of the energy stored in the capsules due to the very large changes of the fluid temperature. A thermal energy storage test has been conducted after the $NaNO_3$ capsules have been tested ~ 40 hours in 45 days. It has been found that the encapsulated $NaNO_3$ capsules have sustained

174

storage performance without deterioration in their storage capacity.

- For the test section with $MgCl_2$ - NaCl eutectic capsules, in a given storage – retrieval cycle where $MgCl_2$ - NaCl capsule temperatures varied from ~ 30 °C - ~ 510 °C, the test section has been found to store significant amount of thermal energy per EPCM capsule (~ 560 kJ/kg), with $MgCl_2$ - NaCl material (PCM) accounting for ~ 80% of the energy stored in the capsules. The latent heat of phase change of the $MgCl_2$ - NaCl eutectic contributed to ~ 25% of the energy stored in the capsules due to the very large changes of the fluid temperature.

- A configuration of cascaded EPCM capsules is proposed to be used in the test section, with five $MgCl_2$ – NaCl capsules at the top section and five $NaNO_3$ capsules at the bottom section of the T/S. It has been found that under similar operating conditions when the test section is charged by 540 °C air, the cascaded EPCM capsules store ~ 15% more thermal energy within 1.5 hours in a charging process compared with the test section with $MgCl_2$ – NaCl capsules only. It is shown that use of five $MgCl_2$ – NaCl capsules and five $NaNO_3$ capsules is advantageous with its increased heat storage capacity.

- The results of the numerical simulations of the energy storage are found to agree with experimental measurements within 9%. The dynamic performance of charging and discharging rates were also well predicted by the model, giving confidence for engineering design capabilities for potential larger scale utur

175

applications using encapsulated phase change materials for energy storage.

6   FURTHER WORKS AND SUGGESTIONS

The objective of this project is to establish methods for storage of thermal energy using encapsulated phase change materials at temperatures up to 540 °C, suitable for applications in concentrating solar power plants. First a calorimeter is designed and built to measure the storage capacity of the EPCM candidate as well as investigate its storage performance after long-term thermal cycles. Secondly, a pilot-scale test section is designed, built and tested with multiple EPCM capsules, and successfully demonstrate its ability to transfer and extract energy to and from the EPCM capsules in thermal cycles. Meanwhile, a simulation model has been developed for the engineering design and optimization of the test section before building the test facility, evaluation of the dynamic heat transfer performance comparison of the experimental data with the numerical predictions. Based on the work accomplished in the project, here are what we can do further:

- It is possible to encapsulate these candidate PCMs in stainless steel or carbon steel containers, though possible corrosion of the shell should be further tested under longer exposures for the $MgCl_2$-NaCl salt.

- A test section with liquid heat transfer fluid could help to enhance the heat transfer from the HTF to the EPCM capsule and then increase the storage performance of the EPCM capsule in a given time duration.

- A simulation model work can be extended to include the effects of gravity and

177

natural convection in large EPCM-based thermal energy storage system.

- A system-level simulation model, integrating the solar field, energy storage system and power generation system, would be of great help to design and operate the thermal energy storage applicable to the energy demand

REFERENCE

1. Http://En.wikipedia.org/wiki/phase_transition.

2. http://www.engineeringtoolbox.com/latent-heat-melting-solids-d_96.html.

3. Abhat A. Short term thermal energy storage. *Revue de Physique Appliquée*. 1980;15:477-501.

4. Abhat A. Low temperature latent heat thermal energy storage: Heat storage materials. *Solar Energy*. 1983;30(4):313-332.

5. Farid M, Khudhair A, Razack S, Al-Hallaj S. A review on phase change energy storage: Materials and applications. *Energy Conv Manag*. 2004;45(9-10):1597-1615.

6. Heine D, HEESS F, Groll M. Physical and chemical properties of phase change materials for application in solar tower and solar farm plants. *Sun II*. 1979:1187-1191.

7. Sharma A, Tyagi VV, Chen CR, Buddhi D. Review on thermal energy storage with phase change materials and applications. *Renew Sust Energ Rev*. 2009;13(2):318-345.

8. Zalba B, Marin J, Cabeza L, Mehling H. Review on thermal energy storage with phase change: Materials, heat transfer analysis and applications. *Appl Therm Eng*. 2003;23(3):251-283.

9. Pacheco JE, Showalter SK, Kolb WJ. Development of a molten-salt thermocline thermal storage system for parabolic trough plants. *Journal of Solar Energy Engineering*. 2002;124(2):153-159.

10. Hoshi A, Mills DR, Bittar A, Saitoh TS. Screening of high melting point phase change materials (PCM) in solar thermal concentrating technology based on CLFR. *Solar Energy*. 2005;79(3):332-339.

11. Kotzé JP, von Backström TW, Erens PJ. High temperature thermal energy storage utilizing metallic phase change materials and metallic heat transfer fluids. *Journal of Solar Energy Engineering*. 2013;135(3):035001-1-035001-6.

12. Medrano M, Gil A, Martorell I, Potau X, Cabeza LF. State of the art on high-temperature thermal energy storage for power generation. part 2 - case studies. *Renewable and Sustainable Energy Reviews*. 2010;14(1):56-72.

13. Colvin DP. Enhanced thermal management using encapsulated phase change materials: An overview. *ASME-PUBLICATIONS-HTD*. 1999;363:199-206.

14. Janz GJ, ed. *Thermodynamic and transport properties for molten salts: Correlation equations for critically evaluated density, surface tension, electrical conductance, and viscosity data* . United States. National Bureau of Standards: the American Chemical Society and the American Institute of Physics for the National Bureau of Standards; 1988. http://books.google.com/books?id=qSXxAAAAMAAJ.

15. Nasch PM, Steinemann SG. Density and thermal expansion of molten manganese, iron, nickel, copper, aluminum and tin by means of the gamma-ray attenuation technique . *Physics and Chemistry of Liquids*. 1995;29(1):43-58.

16. IRENA. Thermal energy storage technology brief. . 2013.

17. Neti, S.,Chen, J.C., Tuzla, K., Oztekin, A., Misiolek, W.Z., Zheng, Y., Zhao, W. Novel thermal storage technologies for concentrating solar power generation. .Research Performance Progress Report. DOE EERE SETP CSP subprogram, Award Number: DE-FC36-08GO18015. 2012.

18. Kuravi S, Trahan J, Goswami DY, Rahman MM, Stefanakos EK. Thermal energy storage technologies and systems for concentrating solar power plants. *Progress in Energy and Combustion Science*. 2013;39(4):285-319.

19. http://en.wikipedia.org/wiki/Paraffin_wax.

20. *Encyclopedia of polymer science and technology.* John Wiley & Sons Inc; 1971.

21. Abhat A, Heine D, Heinisch M, Malatidis NA, Neuer G. Development of a modular heat exchanger with integrated latent heat thermal energy store . . 1981;BMFT FB-T 81-050.

22. Lorsch HG, Denton JC, Kauffman KW. Thermal energy storage for solar heating and off-peak air conditioning. *energy production and coversion*. 1975;15:1-8.

23. Buddhi D, Bansal N, Sawhney R, Sodha M. Solar thermal storage-systems using phase-change materials. *Int J Energy Res*. 1988;12(3):547-555.

24. Hasnain SM. Review on sustainable thermal energy storage technologies, part I: Heat storage materials and techniques. *Energy Conversion and Management*. 1998;39(11):1127-1138.

25. Feldman D, Shapiro MM, Banu D, Fuks CJ. Fatty acids and their mixtures as phase-change materials for thermal energy storage. *Solar Energy Materials*. 1989;18(3–4):201-216.

26. Khudhair AM, Farid MM. A review on energy conservation in building applications with thermal storage by latent heat using phase change materials. *Energy Conversion and Management*. 2004;45(2):263-275.

27. Telkes M. Solar house heating: Problem of heat storage. *Heating and Ventilating*. 1947;44:68-75.

28. Telkes M. Nucleation of supersaturated inorganic salt solutions. *Industrial and Engineering Chemistry*. 1952;44(6):1308-1310.

29. Guyer EC. *Handbook of applied thermal design.* New York: Mcgraw-Hill; 1988:1 v. (various pagings) :.

30. Zheng Y, Zhao W, Sabol JC, et al. Encapsulated phase change materials for energy storage - characterization by calorimetry. *Solar Energy*. 2013;87:117-126.

31. Wang X, Liu J, Zhang Y, Di H, Jiang Y. Experimental research on a kind of novel high temperature phase change storage heater. *Energy Conversion and Management*. 2006;47(15-16):2211-2222.

32. Gil A, Medrano M, Martorell I, et al. State of the art on high temperature thermal energy storage for power generation. part 1-concepts, materials and modellization. *Renewable & Sustainable Energy Reviews*. 2010;14(1):31-55.

33. Metz B, Davidson O, Coninck H.D., Loos M., Meyer L. *IPCC special report on carbon dioxide capture and storage.* New York, United States of America: Cambridge University Press; 2005.

34. Energy Information Administration. Electric power monthly. . 2012.

35. Energy Information Administration. Annual energy outlook 2012. . 2012.

36. Dunn RI, Hearps PJ, Wright MN. Molten-salt power towers:Newly commercial concentrating solar storage. . 2012;100.

37. Dinter F, Geyer MA, Tamme R, eds. *Thermal energy storage for commercial applications: A feasibility study on economic storage systems.* 1st ed. Springer; 1991.

38. Michels H, Pitz-Paal R. Cascaded latent heat storage for parabolic trough solar power plants. *Solar Energy*. 2007;81(6):829-837.

39. Luz International Ltd., Solar Energy Research Institute, CBY Associates I. Phase-change thermal energy storage. . 1988;SERI/STR-250-3516.

40. Takahashi K, Sakamoto R, Kamimoto M. Heat capacities and latent heats of LiNO3, NaNO3 and KNO3. *International Journal of Thermophysics*. 1988;9(6):1081-1090.

41. Blaney JJ, Neti S, Misiolek WZ, Oztekin A. Containment capsule stresses for encapsulated phase change materials. *Appl Therm Eng*. 2013;50(1):555-561.

42. Goods SH, Bradshaw RW, Prairie MR, Chavez JM. Corrosion of stainless steel and carbon steel in molten mixtures of industrial nitrates. . 1994;SAND94-8211 UC-404.

43. Goods SH, Bradshaw RW. Corrosion of stainless steels and carbon steel by molten mixtures of commerical nitrate salts. *Journal of Materials Engineering and Performance*. 2004;13(1):78-87.

44. Corrosion: Fundamentals, teesting, and protection. In: Cramer SD, Covino BSJ, eds. *ASM handbook.* 1st ed. US: ASM International; 2003.

45. Williams DF. Assessment of candidate molten salt coolants for the NGNP/NHI heat-transfer loop. . 2006.

46. Zhao W, Elmozughi AF, Oztekin A, Neti S. Heat transfer analysis of encapsulated phase change material for thermal energy storage. *Int J Heat Mass Transfer*. 2013;63:323-335.

47. Zhukauskas A. Heat transfer from tubes in cross flow. In: Hartnett JP, Irvine TF, eds. *Advances in heat transfer.* New York: Academic Press; 1972.

48. Tufeu R, Petitet J, Deniellou L, Leneindre B. Experimental determination of the thermal conductivity of molten pure salts and salt mixtures. *Int J Thermophys*. 1985;6(4):315-330.

49. Bauer T, Laing D, Tamme R. Characterization of sodium nitrate as phase change material. *Int J Thermophys*. 2012;33(1):91-104.

50. Southard JC. A modified calorimeter for high temperatures. the heat content of silica, wollastonite and thorium dioxide above 25C. *Journal of the American Chemical Society*. 1941;63:3142-3146.

51. Yamaguchi K, Itagaki K. Measurement of high temperature heat content of silicon by drop calorimetry. *Journal of Thermal Analysis and Calorimetry*. 2002;69(3):1059-1066.

52. Incropera FP, DeWitt DP, eds. *Foundamentals of heat and mass transfer.* 5th ed. Wiley; 2001.

53. Gronvold F, Stolen S. Heat capacity of solid zinc from 298.15 to 692.68 K and of liquid zinc from 692.68 to 940 K: Thermodynamic function values. *Thermochimica Acta*. 2003;395(1-2):127-131.

54. Jriri T, Rogez J, Bergman C, Mathieu J. Thermodynamic study of the condensed phases of NaNO3, KNO3 and CsNO3 and their transitions. *Thermochimica Acta*. 1995;266:147-161.

55. Churchill SW, Chu HHS. Correlating equations for laminar and turbulent free convection from a vertical plate. *Int J Heat Mass Transfer*. 1975;18(11):1323-1329.

56. Lane GA. Encapsulation of heat of fusion storage materials. . 1976:442-445.

57. Dutil Y, Rousse DR, Ben Salah N, Lassue S, Zalewski L. A review on phase-change materials: Mathematical modeling and simulations. *Renew Sust Energ Rev*. 2011;15(1):112-130.

58. Nallusamy N, Velraj R. Numerical and experimental investigation on a combined sensible and latent heat storage unit integrated with solar water heating system. *Journal of Solar Energy Engineering-Transactions of the ASME*. 2009;131(4):041002-1-041002-8.

59. Regin AF, Solanki SC, Saini JS. Heat transfer characteristics of thermal energy storage system using PCM capsules: A review. *Renew Sust Energ Rev*. 2008;12(9):2438-2458.

60. Verma P, Varun, Singal SK. Review of mathematical modeling on latent heat thermal energy storage systems using phase-change material. *Renew Sust Energ Rev*. 2008;12(4):999-1031.

61. Ergun S. Fluid flow through packed columns. *Chemical Engineering Progress*. 1952;48(48):89-94.

62. Bauer T, Laing D, Kröner U, Tamme R. Sodium nitrate for high temperature latent heat storage. . 2009.

63. Zheng Y. *Thermal energy storage with encapsulated phase change materials for high temperature aplications.* [PhD]. Lehigh University; 2015.

64. White LR, Davis HT. Thermal conductivity of molten alkali nitrates. *Journal of Chemical Physics*. 1967;47(12):5433-5439.

65. Zhang X, Fujii M. Simultaneous measurements of the thermal conductivity and thermal diffusivity of molten salts with a transient short-hot-wire method. *Int J Thermophys*. 2000;21(1):71-84.

66. Zhao W. *Characterization of encapsulated phase change materials for thermal energy storage.* [Doctor of Philosophy]. Lehigh University; 2013.

67. Elmozughi A, Zheng Y. Computational models of EPCM based thermal energy storage system. (under preparation)

68. Cornwell K. Thermal conductivity of molten salts. *Journal of Physics D: Applied Physics*. 1971;4(3):441-445.

69. Haslett RA, Kosson RL, Ferrara AA, Roukis JG. Thermal energy storage heat exchanger design. . 1978.

VITA

Ying Zheng was born on June 9th, 1986 in Fujian, China. She is the first child of Tianting Zheng (Father) and Jianrong Huang (Mother), and has a brother and a sister in the happy family. When Ying was in her high school, she found great interest in Chemistry, and then chose Chemistry as her major in her undergraduate studies at Nankai University in Tianjin, China. After two-year studies, she fulfilled all the classes in Chemistry at Nankai, then she was transferred to Tianjin University spent another two years in Chemical Engineering. Ying was graduated in 2008 with a B.S. degree in Chemistry at Nankai University and a B.E. degree in Chemical Engineering at Tianjin University. After graduation, Ying came to Lehigh University and joined the PhD program in the Department of Chemical Engineering in 2008. In her PhD project, she is working with Dr. Kemal Tuzla and Dr. John C. Chen in the area of thermal energy storage with encapsulated phase change materials for high temperature applications. During her stay at Lehigh, she has also been a teaching assistant for Chemical Engineering Laboratories, Fluid Dynamics and Heat and Mass Transfer. Ying enjoy the life and studies at Lehigh very much.